TECHNISCHE UNIVERSITÄT MÜNCHEN

Lehrstuhl für Biofunktionalität der Lebensmittel

Malignancy and metastatic spread of Ewing Tumors explored based on the identification of angiogenic target structures

Annette Martina Fasan

Vollständiger Abdruck der von der Fakultät Wissenschaftszentrum Weihenstephan für Ernährung, Landnutzung und Umwelt der Technischen Universität München zur Erlangung des akademischen Grades eines

Doktors der Naturwissenschaften

genehmigten Dissertation.

Vorsitzender: Univ.-Prof. Dr. S. Scherer
Prüfer der Dissertation:
1. Univ.-Prof. Dr. D. Haller
2. Univ.-Prof. Dr. St. Burdach

Die Dissertation wurde am 30.06.2010 bei der Technischen Universität München eingereicht und durch die Fakultät Wissenschaftszentrum Weihenstephan für Ernährung, Landnutzung und Umwelt am 23.11.2010 angenommen.

Table of Contents

1 Introduction

1.1 Primary tumor growth and metastasis

Tumorigenesis is considered to be a multistep process of genetic and epigenetic alterations including growth signal autonomy, insensitivity to antigrowth signals and resistance to apoptosis, which lead to a deregulated proliferation program [1]. However, in addition to the genetic and epigenetic changes that occur during transformation, another discrete step is required to allow tumor-propagation and progression - the induction of a tumor vasculature.

1.1.1 The role of angiogenesis

It is well understood that tumor growth and metastasis strongly depend on angiogenesis. As soon as tumor size reaches 1-2 mm in diameter passive diffusion from the preexisting vasculature fails to provide the essential nutrients and oxygen supply for sustained growth of the tumor cells [2]. To exceed this size, the tumor requires the formation of new blood vessels to provide the rapidly proliferating cells with an adequate amount of oxygen and metabolites. Tumors employ multiple mechanisms to develop and maintain their vascular supply including angiogenesis, vasculogenesis and tumor cell vascular mimicry [3].

Tumor angiogenesis is a multistep process including the degradation of the extracellular matrix, migration and proliferation of endothelial cells from postcapillary venules, and, finally, tube formation [4]. The initiation of angiogenesis - the 'angiogenic switch' - is an important step in tumor progression, as the tumor switches from an avascular to a vascular phenotype [5]. This is due to an alteration in the expression of angiogenic and anti-angiogenic factors tilting the strictly controlled balance in favor of angiogenesis. The imbalance of pro-angiogenic and anti-angiogenic factors promotes endothelial cell sprouting, migration and proliferation.

In contrast to normal vessels, tumor vasculature is highly disorganized. Vessels are irregularly shaped, dilated and tortuous and can have dead ends. They are not organized into definitive venules, arterioles and capillaries like their normal counterparts, but rather share chaotic features. The vascular network that forms in

tumors is often leaky and hemorrhagic, partly due to the overproduction of vascular endothelial growth factor (VEGF) [5]. Thus, tumor-induced angiogenesis creates numerous blood vessels with structural abnormalities and functional defects [4].

Accumulating evidence indicates that, in addition to the sprouting of neighboring pre-existing vessels, tumor angiogenesis is supported by the mobilization and functional incorporation of other cells, including circulating endothelial progenitor cells (CEPs), highly proliferative cells that are derived from the bone marrow [6]. They are suggested to participate in formation of new tumor blood vessels, a process called vasculogenesis.

In contrast, vasculogenic mimicry describes the process in which tumor cells gain features of endothelial cells, thus contributing to blood supply by forming vasculature-like structures [7]. This phenomenon was first described in melanomas, where periodic acid-Schiff's reagent (PAS) staining of cutaneous melanoma sections revealed patterned networks of interconnected loops of extracellular matrix [8]. Moreover, the presence of PAS patterns was associated with poor prognosis indicating that aggressive melanoma cells may generate vascular channels that facilitate tumor perfusion independent of tumor angiogenesis. After these initial observations in melanoma, vasculogenic mimicry has been described in several other tumor entities, including breast [9], ovarian [10] and prostate carcinoma [11], osteosarcoma [12] and Ewing Family Tumors (EFT) [13].

Tumor-induced blood vessels are crucial for the growth and persistence of primary solid tumors, as they guarantee the supply with nutrients and oxygen. Furthermore, they may support metastatic dissemination, since the tumor cells can employ the newly formed vessels as entry sites into the circulatory system. Induction of angiogenesis precedes the formation of malignant tumors, and increased vascularization seems to correlate with the invasive properties of tumors and thus with the malignant tumor phenotype [14].

The tumor mass consists of rapidly proliferating cells, which need increasing amounts of nutrients and oxygen for sustained growth. Close proximity to blood vessels fulfills these requirements, but with ongoing growth, areas within the tumor develop that are deprived of oxygen and become hypoxic. As oxygen is necessary for maintenance of cellular structure and function, limited supply can lead to

irreversible cellular damages. Thus, the response to hypoxia plays an important pathophysiological role in carcinogenesis.

1.1.2 The role of hypoxia

Hypoxia has emerged as a major factor that influences tumor proliferation and malignant progression. Up to 50-60 percent of advanced solid tumors exhibit hypoxic tissue areas heterogeneously distributed throughout the tumor mass [15]. Tumor hypoxia arises due to increased metabolic activity and oxygen consumption of rapidly proliferating tumor cells leading to alterations of local pH levels and resulting in oxidative stress in the surrounding microenvironment. Additionally decreasing O_2 levels within the cell mass lead to a hypoxic environment. These microenvironmental stresses are mainly the result of poorly formed tumor vasculature, which fails to provide the essential nutrients and oxygen supply for sustained growth of the tumor cells [16].

Hypoxic conditions are further amplified as diffusion distances within the tumor mass increase and cells that spread beyond the distance that guarantees optimal O_2 supply (>70µm) do not get enough oxygen [16].

As a result, in areas of the tumor distant from the supporting blood vessels, nutrient supply decreases whereas metabolic products accumulate. To overcome this oxygen- and nutrient deprivation state and to be able to survive, tumor cells respond with proteomic and transcriptomic changes, which are mediated e.g. by the transcription factor hypoxia-inducible factor-1α (HIF-1α) [17]. This transcription factor binds to the hypoxia responsive element (HRE) in the promoter of hypoxia-responsive genes such as *VEGF*, *PDGF* and *TGFα* and induces their expression. HIF-1α regulated genes play critical roles in pathways controlling angiogenesis, metabolism, proliferation, metastasis and differentiation. In addition, specific mutagenic properties are attributed to the hypoxic environment, accounting to genomic instability of malignant tumors [18]. Under hypoxia, cells are committed to an enormous selective pressure resulting in the fact that the dominant population within a tumor mass will be derived from those cells that develop proteomic or genomic alterations, which enable survival under hypoxic conditions. For example, tumor cells that develop a mutation within the apoptosis associated gene p53 are insusceptible for hypoxia-induced apoptosis and thus have a selective advantage

over non-mutated cells [19]. Similarly, with genomic alterations increasing the angiogenic potential or decreasing the capacity for cell cycle arrest tumor cells gain an advantage to survive under hypoxic conditions. Furthermore, these cells are more likely to acquire features that promote invasiveness and metastatic potential leading to an enhanced aggressive phenotype.

This demonstrates clearly, why tumor hypoxia has become a critical indicator for the prognosis of malignant diseases. It has been observed in various tumor entities, e.g. soft tissue sarcoma, head and neck cancers and cervical cancers that the presence of hypoxia is associated with a poor patient outcome [20-22]. This was also shown for EFT [23].

Furthermore, the effects of tumor hypoxia also entail therapeutic problems. Hypoxia describes a condition where the tumor mass is deprived of oxygen, which is not only essential for the survival and progression of the tumor entity but also essential for the cytotoxic activities of radiation therapy agents, which are directed at the tumor mass. In addition, it may indirectly support resistance to chemotherapy, since hypoxic cells lack the blood vessels supplying them with oxygen, and therefore stop proliferating. Many chemotherapeutic drugs however, are only effective against rapidly proliferating cells and depend on blood vessels to reach the tumor [15, 24]. Therefore, this may also increase the poor prognosis for patients with malignant cancers.

Bone and soft tissue tumors constitute some of the most aggressive adult and childhood malignant cancers in that they have a high metastatic potential and are typically refractory to conventional chemo- and radiation therapy [25]. The EFT represents the second most common solid bone and soft tissue malignancy of children and young adults after osteosarcoma. Although EFT has been intensively studied, they are still correlated with poor prognosis.

1.2 Ewing Family Tumors (EFT)

EFT is characterized by an aggressive osteolytic behavior and a tendency towards early hematogenous metastasis mainly to the lung, bone and bone marrow [25]. Morphologically, EFT consists of uniformly bland, undifferentiated small round cells and is part of a heterogeneous family of pediatric small round cell neoplasms that include neuroblastoma, rhabdomyosarcoma and lymphoma [26]. Since its first

description by James Ewing in 1921, who referred to it as *diffuse endothelioma of the bone* [27], classification of EFT was rather difficult due to the rather primitive morphology and the lack of characteristic differentiation markers. But a rapid and precise diagnosis is essential for therapeutic cure. This task was finally accomplished with the identification of characteristic chromosomal translocations that cause the expression of specific fusion genes. In 85% of cases, EFT are associated with a reciprocal t(11;22)(q24;q12) chromosome translocation, which leads to the formation of the *EWS/FLI-1* fusion gene [28, 29]. Alternatively, in 10-15% of EFT the translocation t(21;12)(22;12) results in the *EWS/ERG* fusion [30]. The remaining 1-5 % of cases carry one of several translocations, each resulting in a fusion of the 5-prime *EWS* gene to a member of the ets family of transcription factors [25]. The identification of the *EWS/ETS* fusion genes enabled a more exact classification of the EFT, containing classical Ewing Tumors, malignant peripheral neuroectodermal tumors (MPNT) and the Askin tumor of the thoracic wall [26].

The development of multimodal therapeutic approaches improved the prognosis of patients with localized EFT. The survival rate for patients treated with a combination of surgery, radiation and multiagent chemotherapy is at a ratio of about 65 - 70 percent [31]. But patients with detectable metastases at diagnosis (25 percent of cases), patients not responding to therapy and patients with disease relapse have a significantly poorer prognosis. The survival rate for those patients as well as for patients with multifocal primary tumors and disease relapse is only at about 27 percent [31]. This emphasizes the urgent need of new therapeutic approaches to improve the prognosis for patients with metastatic and recurrent disease. Furthermore, the current treatment strategies, consisting of a combination of chemotherapy, radiation therapy and surgery, have to be improved, as they still are associated with mutilation and severe side effects.

One innovative strategy targeting solid tumors is the inhibition of angiogenesis, as it theoretically offers the perspective of long-term control of tumor-progression. Anti-angiogenic therapy has a number of potential benefits including lack of resistance to some agents, lack of significant toxicity compared to conventional agents and a potent antitumor effect. Administration of angiogenesis inhibitors might keep the tumor and its metastases dormant and co-administration of cytotoxic drugs might kill it. Early clinical data suggest that anti-angiogenic and anti-vascular strategies may be beneficial in the treatment of patients with EFT.

1.3 Vascularization mechanisms in EFT

EFT have been described as employing multiple mechanisms to develop and maintain their vascular supply including angiogenesis, vasculogenesis and tumor cell vascular mimicry. Endothelial cells in EFT show a high proliferation rate, indicating active angiogenesis of this tumor [13]. Several studies have shown the importance of VEGF in this process in EFT. For example, EFT cells that are deficient in a certain VEGF isoform - $VEGF_{165}$ - have been shown to form smaller tumors with reduced microvessel density (MVD), whereas re-expression of $VEGF_{165}$ restored MVD [32].

Furthermore, there are several lines of evidence that VEGF also appears to be important in vasculogenesis of EFT. It is responsible for the recruitment of bone marrow derived cells, which can differentiate into pericytes and tumor-associated endothelial cells [33]. $VEGF_{165}$ deficient EFT cells have been shown to recruit significantly fewer bone marrow derived cells into xenograft tumors compared to $VEGF_{165}$ expressing cells [32]. Furthermore, the inhibition of VEGF receptor 2 (VEGFR-2) has been demonstrated to cause decreased migration of bone marrow cells into the tumor in a bone marrow transplant EFT mouse model [34].

Given the central role of VEGF in both angiogenic and vasculogenic processes in EFT, several interesting studies addressed the question, whether VEGF might actually be a direct target of EWS/FLI-1. First evidence was given by a study showing that EFT-specific EWS/ETS oncoproteins were capable of activating the *VEGF* promoter in transient transfections of tissue culture cells [35]. Further studies revealed that this effect is not due to direct DNA-binding by EWS/ETS oncoproteins and does not require the presence of the hypoxia responsive element of the *VEGF* promoter [35]. Furthermore, one group recently proposed that EWS/FLI-1 is located upstream of *VEGF-A* and up-regulates its mRNA and protein levels and concluded that EWS/FLI-1 has a tumorigenic effect on EFT by causing over-expression of VEGF-A [36].

Another vascularization mechanism of EFT is vasculogenic mimicry, which may not be driven by VEGF. Here so called blood lakes, pools of red blood cells lined by tumor cells, were observed in 92% of human EFT samples in one study [13]. The cells surrounding these blood lakes were found to be tumor cells mimicking features of endothelial cells expressing Tissue pathway factor inhibitor 1/2 (TPFI-1/2), VE-cadherin and Ephrin receptor A2 (EphA2), which are essential proteins in

vascular mimicry [13]. Further results demonstrated that EFT cell lines were able to form vascular-like structures *in vitro* and that the formation of these structures was not enhanced by VEGF or inhibited by VEGF blocking antibody [13].
Due to the relatively low MVD and the highly aggressive phenotype of EFT, these blood lakes have been suggested to contribute to the blood supply of EFT.

1.4 Angiogenic markers as prognostic tools for EFT patients

Studies investigating the prognostic impact of angiogenesis biomarkers in patients with EFT are still relatively scarce and inconsistent despite the fact that there is urgent need for new therapeutic approaches.
There are conflicting investigations concerning MVD as prognostic factor in EFT. One group demonstrated a correlation between MVD and overall and event-free survival. They stained 29 sections of primary EFT with the endothelial cell marker CD31 and correlated the results with the clinical outcome of the patients. They found a significant association between high MVD and poor event free survival, whereas patients with lower MVD had better prognosis [37].
In contrast, two other groups screening sections of 40 and 27 patients, respectively, could not correlate a high MVD with event free or long-term survival [38, 39].
Other studies focused on prognostic relevance of VEGF levels in the tumor or in blood serum, again with conflicting results. One group investigated VEGF expression in sections of 40 EFT patients and found that a high VEGF expression in the tumor significantly correlated with a better prognosis for 10-year relapse-free and overall survival [38]. In contrast, another group analyzed tissue samples from 31 EFT patients for VEGF expression and found high VEGF levels in the tumor to be a negative predictor for overall survival [35].
As VEGF serum levels are elevated in several cancer types, VEGF cannot be used as specific EFT marker, even though EFT patients have higher mean serum levels compared to healthy controls [40, 41]. To date, there are no studies evaluating the effect of blood serum levels of VEGF on clinical prognosis for patients with EFT. The only study concerning this issue investigated VEGF and basic fibroblast growth factor (bFGF) serum levels of a cohort of 40 patients with solid malignancies, including 5 patients with EFT [42]. They observed that patients

with high serum levels of VEGF had an inferior 3-year event-free survival prognosis compared to patients with lower VEGF serum levels.

Our group focused on investigating the prognostic impact of intratumoral necrosis in EFT [23]. Hypoxia has been shown to correlate with poor prognosis in various solid tumors, including head and neck cancers, gliomas and adult soft tissue sarcomas [20, 43, 44]. As long-lasting hypoxia results in necrosis, we evaluated, whether the presence of necrosis within EFT has prognostic impact in EFT. We prospectively screened 79 patients with EFT for the presence and the amount of necrotic areas within their tumors and monitored their survival rate over 3 years. Necrosis was measured using contrast-enhanced magnetic resonance (MR) images. All patients with non-necrotic tumors survived event-free during the observation period, whereas only 55 percent of patients with necrotic tumors had a 3-year event-free survival. Therefore we concluded that the presence of non-perfused areas on pretreatment contrast-enhanced MR-images is associated with an increased risk of metastases, especially with an unfavorable pattern of metastatic spread at diagnosis. This observation may be explained by a more aggressive biological behavior of hypoxic tumor cells, as described above. The group of patients with non-necrotic tumors had an excellent prognosis suggesting that the absence of necrosis might be helpful in identifying a very favorable prognostic subgroup in EFT.

Nevertheless, larger studies that specifically include patients with EFT will be required to further assess the utility of angiogenic biomarkers for prognostic and therapeutic guidance. At the same time, new therapeutic approaches have to be evaluated in preclinical studies to develop individual treatment strategies for patients diagnosed with EFT.

1.5 Preclinical approaches targeting EFT vasculature

Several preclinical studies deal with the evaluation of anti-angiogenic and anti-vascular strategies in preclinical EFT xenograft mouse models.

Since VEGF seems to play an important role in EFT pathogenesis, inhibiting the expression or function of VEGF may lead to improvements in disease outcome. Several studies therefore focused on examining the effects of VEGF inhibitors on EFT growth in mouse models.

In one study, the VEGF inhibitors bevacizumab and VEGF-Trap were investigated for their anti-angiogenic ability in an EFT xenograft mouse model [45]. Bevacizumab is a humanized monoclonal antibody that recognizes and blocks VEGF-A. VEGF-Trap is a composite receptor based on VEGF receptors VEGFR-1 and VEGFR-2, fused to an Fc segment of IgG1 [46]. Both agents showed the ability to reduce growth of EFT xenografts in mice and even transiently regress established tumors compared to vehicle controls [45]. However, regressed tumors uniformly recurred after the abortion of treatment and furthermore, the xenograft tumors derived from one EFT cell line appeared to be more sensitive to these therapies than those derived from another EFT cell line. These data indicate that anti-VEGF monotherapy is not suitable for clinical efficiency and that tumor heterogeneity has the potential to influence clinical response.

Strategies to suppress VEGF-mediated angiogenesis in mouse models of EFT have also included the use of an *adenovirus early region 1A* (*E1A*) gene. This tumor suppressor gene was shown to suppress VEGF expression *in vitro* and *in vivo*. EFT xenografts injected with adenoviral vector containing the *E1A* gene showed decreased tumor growth and increased survival rates, compared with those treated with control injections [47].

Small molecule inhibitors of VEGF-R, which all have tyrosine kinase inhibitory activity, have also been studied as potential anti-vascular agents for EFT. The receptor tyrosine kinase inhibitors SU6668 and SU5416 are ATP site-directed compounds that inhibit growth factor–stimulated receptor tyrosine phosphorylation of VEGF-R2 alone (SU5416) [48] or VEGF-R2, FGF receptor 1 and PDGF receptor (PDGFR)-β (SU6668) [45]. Rate of tumor growth was significantly reduced in EFT mouse xenografts after SU6668 and SU5416 treatment [45]. The Pediatric Preclinical Testing Program (PPTP) screened the VEGF-R inhibitors AZD2171 (cedirinib), an antibody targeting VEGFR-1, VEGFR-2, VEGFR-3, c-kit and PDGFR-β, and sunitinib an orally bioavailable multi-targeted tyrosine kinase inhibitor with selectivity for PDGF receptors, VEGF receptors, FLT3 and KIT, for tumor growth inhibitory effects [49, 50]. Both agents displayed a relatively low *in vitro* effect on EFT cell growth. In contrast, both inhibitors induced decreased tumor growth rates without tumor regression in human xenograft mouse models indicating an anti-angiogenic rather than a direct tumor effect of both agents.

In addition to strategies directly targeting VEGF, some studies focus on targeting endogenous anti-angiogenic proteins. One study investigated the role of thrombospondins, a family of angiogenic inhbitors, in EFT and the effect of forced expression on tumor formation [51]. They observed that the increase of thrombospondin expression in EFT cell lines inhibited tumor vascularization and lead to a decrease of tumor formation in a mouse xenograft model.

Another group focused on the investigation of the anti-angiogenic isoform of VEGF, $VEGF_{165}b$ [52]. $VEGF_{165}b$ is known to inhibit VEGF- and hypoxia-induced angiogenesis as well as VEGF-induced cell migration and proliferation in vitro. The study shows that forced over-expression of $VEGF_{165}b$ in tumor cells inhibits the growth of prostate carcinoma, EFT and renal cell carcinoma in xenograft mouse tumor models. Moreover, $VEGF_{165}b$ over-expression inhibited tumor cell-mediated migration and proliferation of endothelial cells. Taken together, these data indicate that targeting endogenous anti-angiogenic pathways may be of therapeutic importance in EFT treatment.

Another approach under investigation is the targeted disruption of tumor vasculature, as the majority of EFT patients present with a tumor with established vasculature at diagnosis. A class of vascular disrupting agents (VDA) that cause a rapid and selective shutdown of the tumor vascular by damaging in the tumor vessel endothelium through binding to tubulin have been identified [53]. Treatment with such agents results in the arrest of the blood flow, which in turn acts to starve the tumor of the oxygen and nutrients it needs to survive. Recently, the effects of VDA OXi4503 (CA1P) has been investigated alone and in combination with doxorubicin in subcutaneous mouse models of EFT [54]. Treatment with multiple doses of OXi4503 caused significant growth delay in subcutaneous mouse xenograft models. A single dose of OXi4503 caused complete shutdown of vasculature and extensive hemorrhagic necrosis. However, this study revealed that VDAs alone are unlikely to be curative, as a viable rim of proliferating cells remained, which repopulated the tumor soon after the end of treatment. Combined treatment with doxorubicin enhanced the effects of OXi4503 causing a synergistic delay in tumor growth. This study demonstrates that VDA in combination with conventional cytotoxic agents represent a promising treatment strategy for EFT.

Taken together, preclinical studies have revealed multiple approaches for inhibiting EFT growth *in vivo* by antivascular and anti-angiogenic strategies, indicating that targeting these mechanisms is a valid approach for EFT therapy.

Another anti-angiogenic approach is targeting VEGF by small interfering RNA (siRNA). One study inhibited VEGF expression in EFT cells *in vitro* and subsequently investigated the effects *in vivo* [55]. They found that the inhibition of VEGF expression resulted in impaired development of EFT xenograft tumors and reduced growth. Furthermore, tumors derived from VEGF siRNA treated cells showed reduced MVD and diminished osteolysis compared to wt EFT cells. RNA interference (RNAi) has gained growing attention as new promising pharmacological advance since the advent of protein therapeutics. The implications are profound, as disease-associated targets can easily be selected and proteins that had remained intractable to inhibition by conventional methods, such as small molecules, can be suppressed.

1.6 RNAi therapeutics

RNA interference (RNAi) is an evolutionary conserved endogenous post-translational regulatory mechanism, which controls gene expression and enables degradation of a specific mRNA. RNAi has been discovered as a mechanism that can be exploited as a valuable experimental tool, leading to efficient sequence-specific gene silencing, thus allowing functional gene analysis. Furthermore, it has gained increasing interest as a novel pharmacological approach to human disease over the past years.

In the RNAi process, double-stranded RNA (dsRNA), homologous to the target locus, can specifically inactivate gene function [56]. RNA interference can be experimentally achieved by delivery of a synthetic small interfering RNA (siRNA) [57] or by a plasmid DNA vector containing sequence coding for a small hairpin RNA (shRNA) [58-60].

Many studies have used siRNAs as an experimental tool to dissect the cellular pathways that lead to uncontrolled cell proliferation and cancer. To develop siRNAs for cancer therapy, several researchers have investigated them in animal models. Experimentally tested, effective targets are genes involved in cancer-associated cellular pathways, either oncogenes, particularly fusion oncogenes due

to their unique link with certain tumor cells, or anti-apoptotic genes. In addition, genes that play a role in tumor-host interactions, such as factors involved in angiogenesis or innate immunity, and those that mediate resistance to chemo- or radiotherapy are targets for interference.

To date, there are several ongoing preclinical studies investigating the use of siRNA based therapeutic molecules.

ALN-VSP is designed to target two genes critical in the growth and development of cancer: kinesin spindle protein (KSP) required for tumor proliferation and VEGF. ALN-VSP treatment led to mitotic arrest and to marked reductions in tumor MVD and intratumoral hemorrhage in orthotopic liver tumor models. Moreover, multi-dose administration of ALN-VSP significantly prolonged survival in the orthotopic hepatoma tumor model [61].

The second therapeutic molecule currently under development for the treatment of advanced solid cancer is Atu027, a siRNA-lipoplex directed against protein kinase N3 (PKN3). *In vitro* studies revealed that Atu027- mediated inhibition of PKN3 function in primary endothelial cells impaired tube formation on extracellular matrix and cell migration, but is not essential for proliferation. Systemic administration of Atu027 in orthotopic mouse models for prostate and pancreatic cancers resulted in significant inhibition of tumor growth and lymph node metastasis formation. The tumor vasculature of Atu027-treated animals showed a specific reduction in lymph vessel density but no significant changes in microvascular density [62].

An approach for treatment of ovarian cancer is targeting focal adhesion kinase (FAK), which plays a critical role in ovarian cancer cell survival and in various steps in the metastatic cascade. Treatment with FAK siRNA reduced mean tumor weight and when combined with docetaxel chemotherapy there was even greater reduction in mean tumor weight, decreased MVD, decreased expression of vascular endothelial growth factor and matrix metalloproteinase-9, and increased apoptosis of tumor-associated endothelial cells and tumor cells [63].

However, to date, there are no preclinical data concerning the use of RNAi therapeutics in EFT treatment.

1.7 Preliminary work

To identify new therapeutic targets and to get new insights into the biology of EFTs, we analyzed the EFT-specific gene expression on DNA microarrays which initially have been introduced for molecular discrimination between members of the "small round blue cell tumor" family (EFTs, neuroblastomas, rhabdomyosarcomas and lymphomas). We identified 37 genes specifically or highly over-expressed in EFTs when compared with a wide spectrum of normal tissues [64]. The identified EFT-specific gene expression profile molecularly supports the concept of a neural crest and endothelial origin of the EFT stem cell. In addition, the results of the DNA microarray analysis presumably identify new diagnostic and therapeutic targets for the development of new treatment strategies.

1.8 Aim of the study and overview of the experimental approach

The goal of the present study was to identify new potential targets for anti-vascular and anti-angiogenic therapeutic approaches in EFT. As a first step, the most promising candidate genes with presumable roles in EFT angiogenesis and invasive growth had to be identified. A pool of targets was provided by the DNA microarray analysis mentioned in 1.7. This screening revealed two potential targets, Chondromodulin-1 and the G-protein coupled receptor 64, which the present study focuses on.

Chondromodulin-1 (CHM1) is a glycoprotein that was first discovered as a functional matrix component with phenotypic expression in chondrocytes stimulating cartilage growth [64].

The G-protein coupled receptor 64 (GPR64) is an orphan receptor with high expression in the epithelia of *ductulus efferentes* and proximal epididymis, but in no other tissues of the adult [65].

The aim of this work was to assess the function of CHM1 and GPR64 and their potential down-stream targets in the biology and pathology of EFT. As a first step, the over-expression of the selected genes had to be verified *in vitro.* Subsequently, the expression of GPR64 and CHM1 was down-regulated in different EFT cell lines by RNA-interference and their influence on proliferation, angiogenesis and invasiveness was analyzed *in vitro*. Furthermore their potential

contribution to tumor pathology was investigated in a xeno-transplant model. Therefore, local and metastatic growth of siRNA treated EFT cells was assessed in immunodeficient $Rag2^{-/-}\gamma_c^{-/-}$ mice. Local tumor growth was studied by injecting the cells subcutaneously into the inguinal region of mice. Potential differences in vascularization between tumors of siRNA treated EFT cells and tumors of control EFT cells were assessed by immunohistochemistry. The metastatic potential was investigated by tail vein assay, where EFT cells were injected intravenously into the tail vein of mice and organ colonization was quantitated. This procedure permits analyses of the step of metastasis that occur during and after the extravasation of tumor cells from blood vessels into target organs and provides valuable insights into the mechanism of metastasis and a system for testing candidate anti-metastatic drugs.

2 Materials

2.1 List of manufacturers

AEG	Frankfurt, Germany
Agilent (Stratagene)	Waldbronn, Germany
Ambion	Darmstadt, Germany
ATCC	Wesel, Germany
B. Braun Biotech Int.	Melsungen, Germany
Bayer HealthCare Pharmaceuticals	Leverkusen, Germany
BD Biosciences	Heidelberg, Germany
Beckman Coulter	Krefeld, Germany
Becton Dickinson	Heidelberg, Germany
Biochrom	Berlin, Germany
BioRad	München, Germany
Biowhittaker (Lonza)	Köln, Germany
Biozym	Hess. Olendorf, Germany
Brand	Wertheim, Germany
DSMZ	Braunschweig, Germany
Eppendorf	Hamburg, Germany
Falcon (BD)	Oxnard, California, USA
Feather	Osaka, Japan
Fermentas	St. Leon-Rot, Germany
GE Healthcare	München, Germany
Genomed	St. Louis, Missouri, USA
Greiner	Nürtingen, Germany
Heraeus	Hanau, Germany
ImaGenes GmbH	Berlin, Germany
Invitrogen	Karlsruhe, Germany
Kern	Balingen-Frommern, Germany
Leica	Wetzlar, Germany
Lonza	Köln, Germany
Macherey-Nagel	Düren, Germany
Merck	Darmstadt, Germany
Millipore	Billerica, Massachusetts, USA

Miltenyi Biotec GmbH	Bergisch Gladbach, Germany
Molecular BioProducts, MbP	San Diego, California, USA
Nalgene (Thermo Fisher Scientific)	Rochester, New York, USA
New England BioLabs	Frankfurt am Main, Germany
Nunc (Thermo Fisher Scientific)	Wiesbaden, Germany
Pan Biotech GmbH	Aidenbach, Germany
Pechiney Plastic Packaging	Chicago, Illinois, USA
Peske OHG	München, Germany
Promega	Mannheim, Germany
Qiagen	Hilden, Germany
R&D Systems	Wiesbaden-Nordenstadt, Germany
Roche	Mannheim, Germany
(Carl) ROTH	Karlsruhe, Germany
Sartorius	Göttingen, Germany
Schleicher und Schüll	Dassel, Germany
Scientific Industries	Bohemia, New York, USA
Scotsman	Vernon Hills, Illinois, USA
Sempermed	Wien, Austria
Sigma-Aldrich	Hamburg, Germany
Syngene	Cambridge, UK
Taylor-Wharton	Husum, Germany
TKA GmbH	Niederelbert, Germany
TPP	Trasadingen, Switzerland
Thermo Fisher Scientific	Wiesbaden, Germany
Zeiss	Göttingen, Germany

2.2 General material

Cryovials	Nunc
Filters for cells, Cell Strainer	Falcon
Filters for solutions (0.2 µm and 0.45 µm)	Sartorius
Flasks for cell culture (75 cm^2 and 175 cm^2)	TPP
Flasks for cell culture (75 cm^2 and 175 cm^2)	Falcon
Gloves (nitrile, latex)	Sempermed
Parafilm	Pechiney Plastic Packaging

Pasteur pipettes	Peske OHG
Petri dishes	Falcon
Pipettes (2, 5, 10 and 25 ml)	Falcon
Pipette tips (10, 200 and 1000 µl)	MbP
Pipette tips (10, 200 and 1000 µl with a filter)	Biozym
Plates for cell culture (6-well, 24-well and 96-well)	TPP
Scalpels (Nr. 12, 15, 20)	Feather
Tubes for cell culture (polystyrene, 15 ml)	Falcon
Tubes for cell culture (polypropylene, 15 ml and 50 ml)	Falcon
Tubes for molecular biology, Safelock (1.5 ml and 2 ml)	Eppendorf
Tubes for FACS™ (5 ml)	Falcon

2.3 Instruments and Equipment

Type of device		**Manufacturer**
Bacteria shaker	Certomat BS-T	Sartorius
Ice machine	AF 100	Scotsman
Balance	EW 300-LM	Kern
Balance (analytical)	770	Kern
Cell counting chamber	Neubauer	Brand
Centrifuge	Multifuge 3 S-R	Heraeus
Centrifuge	Biofuge fresco	Heraeus
Controlled-freezing box		Nalgene
Electrophoresis chamber		BioRAD
Freezer (-80 °C)	Hera freeze	Heraeus
Freezer (-20 °C)	cool vario	Siemens
Fridge (+4 °C)	cool vario	Siemens
Gel documentation	Gene Genius	Syngene
Incubator	Hera cell 150	Heraeus
Liquid Nitrogen Tank	L-240 K series	Taylor-Wharton
Multichannel pipette	(10 -100 µl)	Eppendorf

Heating block	Thermomixer Comfort	Eppendorf
Micropipettes	(0.5-10 µl, 10-100 µl, 20-200 µl, 100-1000 µl)	Eppendorf
Microscope (fluorescence)	AxioVert 100	Zeiss
Microscope		Leica
Microwave oven		Siemens, AEG
Pipetting assistant	Easypet	Eppendorf
Spectrophotometer	GeneQuant II	Amersham Biosciences
Sterile Bench		Heraeus
Water bath		GFL
Electroporator	Gene Pulser Xcell™	BioRad
Real Time PCR	7300 Real-Time PCR	Applied Biosystems
Vortexer	Vortex-Genie 2	Scientific Industries
Water purification system	TKA GenPure	TKA GmbH

2.4 Chemical and biological reagents

Agar	Sigma
Agarose	Invitrogen
Ampicillin	Merck
β-Mercaptoethanol	Sigma
BenchMark™ Prestained Protein Ladder	Invitrogen
Blue Juice Gel Loading Buffer	Invitrogen
Chloroform	Merck
DEPC (diethyl pyrocarbonate)	Sigma
DMEM medium	Invitrogen
DMSO (dimethyl sulfoxide)	Merck
Dimethylformamide	ROTH
Ethidium bromide	BioRad
Ethanol	Merck
FBS (fetal bovine serum)	Biochrom

Gentamicin	Biochrom
Glycerol	Merck
HiPerFect Transfection Reagent	Qiagen
Isopropanol	Sigma
LB Broth Base	Invitrogen
L-glutamine	Invitrogen
Matrigel Matrix	BD Biocoat
Na-pyruvate	Invitrogen
100 x non-essential amino acids	Invitrogen
One Shot® TOP10F´ competent cells	Invitrogen
PBS 10 x (phosphate buffered saline)	Invitrogen
Peptone	Invitrogen
Penicillin / streptomycin	Invitrogen
Propidium iodide	Sigma
*Pst*I restriction enzyme	Roche
RNase A (ribonuclease A)	Roche
RPMI 1640 medium	Invitrogen
Sodium chloride	Merck
*Spe*I restriction enzyme	New England BioLabs
TAE (tris acetate EDTA) buffer	Invitrogen
TBE (tris borate EDTA) buffer	Ambion
TEMED (N,N,N′,N′-Tetramethylethan-1,2-diamin)	Sigma
Trypan blue	Sigma
Trypsin / EDTA	Invitrogen
Tween 20	Sigma
*Xba*I restriction enzyme	Fermentas

2.5 Commercial Reagent Kits

Table 1: Commercial reagent kits

Name	Manufacturer
Cell proliferation ELISA	Roche
ECL Plus™ Western Blotting Detection System	GE Helthcare
JETstar 2.0 Maxiprep Kit	Genomed
MycoAlert Mycoplasma Detection Kit	Lonza
NucleoSpin® Plasmid Kit	Macherey-Nagel
QIAEX II Gel Extraction Kit	Qiagen
RNeasy® Mini Kit	Qiagen
TaqMan® Gene Expression Assays	Applied Biosystems

2.6 Media, Buffers and Solutions

2.6.1 Universal solutions

10 x TBS

Tris-HCl pH 7.4	0.5 M
NaCl	1.5 M

3 % paraformaldehyde pH 7.4 (PFA)

PFA	30 g
1 M NaOH	a few drops
10 x PBS	10 %

2.6.2 Cell culture media and solutions

Standard medium:

RPMI 1640	500 ml
Fetal calf serum (FCS)	10 %
L-glutamine (200 mM)	2 mM
Pen / Strep (10^4 U / ml)	100 U / ml

Freezing Medium:

FCS	90 %
DMSO	10 %

2.6.3 Media and solutions for bacterial cultivation

LB medium:

peptone	10 g
Yeast extract	5 g
sodium chloride	10 g
distilled water	ad 1 l

LB agar medium:

LB Broth Base	10 g
Agar	7.5 g
distilled water	ad 500 ml

2.6.4 Buffers, Solutions and Gels

APS

ammonium persulfate in Aq. bidest	10 % (w/v)

DNA electrophoresis gel:

TAE buffer	200 ml
agarose	1.5 g
ethidium bromide	3 µl

DNA electrophoresis running buffer:

TAE buffer (10 x)	20 ml
distilled water	180 ml

Laemmli buffer (3 x)

Tris/HCl pH 6.8	100 mM
SDS	3.0 %
Glycerol	45.0 %
Bromphenol blue	0.01 %
ß-Mercaptoethanol	7.5 %

SDS running buffer (10 x):

Tris base	0.25 M
Glycine	1.92 M
Glycerol	45.0 %
SDS solution	0.01 %
ß-Mercaptoethanol	1 %

Transfer buffer (10 x):

Tris	3 g
Glycine	11,3 g
Methanol	100 ml
distilled water	ad 1000 ml

TBST (1 x)

1 x TBS with 1 % (v/v)Tween 20

Separating buffer (4 x) pH 8.8

Tris-HCl (1.5 M), pH 8.8	6.06 g
SDS (0.4 %)	0.4 g
distilled water	ad 100 ml

Stacking buffer (4 x) pH 6.8

Tris-HCl (1.5 M), pH 6.8	18.17 g
SDS (0.4 %)	0.4 g
distilled water	ad 100 ml

Stacking Gel (2.5 %)

30 % Acrylamide / Bis	0.75 ml
4 x Stacking buffer	1.25 ml
distilled water	3.0 ml
APS (10 %)	35 µl
TEMED	3 µl

Separating Gel (10 %)

30 % Acrylamide / Bis	3.33 ml
4 x Separating buffer	2.5 ml
distilled water	4.17 ml
APS (10 %)	50 µl
TEMED	5 µl

2.7 Antibodies

2.7.1 Antibodies for Western Blot Analysis

Table 2: Primary Antibodies for Western Blot

Antibody	Species	Dilution	Manufacturer
FLI-1	rabbit	1 : 500	Santa Cruz
HPRT	rabbit	1 : 500	Santa Cruz

Table 3: Secondary Antibodies for Western Blot

Antibody	Species	Dilution	Manufacturer
anti rabbit HRPT	bovine	1 : 500	Santa Cruz

2.7.2 Antibodies for Immunohistochemistry

Table 4: Antibodies for Immunohistochemistry

Antibody	Species	Dilution	Manufacturer
CD31	rat	1: 500	Abcam
Mac-3	rat	1:500	BD Pharmingen

2.8 Short interfering RNA

Table 5: Small interfering RNA used for transient transfection

siRNA Name	Target Sequence (5'-3')	Manufacturer
Hs_CHM1_1	CAGAAGGAATCTGTTGTATA	Qiagen
Hs_CHM1_4	CCAGAACTTTAGTATATGCAA	Qiagen
Control (non-silencing) siRNA	AATTCTCCGAACGTGTCACGT	Qiagen
EWS/FLI-1_1	AGCTACGGGCAGCAGAACCCTT	MWG
EWS/FLI-1_2	AGCAGAACCCTTCTTATGACTT	MWG
Hs_GPR64_1	CCCAGTAGTCAGATTATAGAA	Qiagen
Hs_GPR64_4	ATGGTACATTGTTGATTGTTA	Qiagen
Hs_MMP-1_7	AAGCTAACCTTTGATGCTATA	Qiagen
Hs_MMP-1_12	ATGATGAATATAAACGATCTA	Qiagen
Hs_PGF_1	ACCCGGCTCGTGTATTTATTA	Qiagen
Hs_PGF_2	TGCCCTCTATTTATTAGCCAA	Qiagen

2.9 Expression Vector

Table 6: Utilized expression vector

Name	Source
pSIREN RetroQ	Clontech

2.10 Oligonucleotides for Retroviral Gene-Transfer

Table 7: Oligonucleotides used for retroviral gene transfer

Name	Sequence (5'-3')
CHM1-for	gatccgcgaaggaatctgttgtatattcaagagatatacaacagattccttcgctttttttctagag
CHM1-rev	aattctctagaaaaaagcgaaggaatctgttgtatatctcttgaatatacaacagattccttcgcg
GPR64-for	gatccgggtacattgttgattgttattcaagagataacaatcaacaatgtacccttttttctagag
GPR64-	aattctctagaaaaaagggtacattgttgattgttatctcttgaataacaatcaacaatgtacccg

rev	
PGF-for	gatccgccctctatttattagccaattcaagagattggctaataaatagagggctttttctagag
PGF-rev	
MMP-1-for	gatccggatgaatataaacgatctattcaagagatagatcgtttatattcatccttttttctagag
MMP-1-rev	aattctctagaaaaaaggatgaatataaacgatctatctcttgaatagatcgtttatattcatccg

2.11 Cell lines, mouse strains and Bacterial Strains

2.11.1 Cell lines

Table 8: Cell lines and sources

Cell Line	Description	Origin
697	cALL cell line	DSMZ
(MHH)-cALL2	cALL cell line	DSMZ [66]
A673	EFT cell line	ATCC [75]
CHP126	Neuroblastoma cell line	DSMZ
MHH-ES1	EFT cell line	DSMZ
MHH-NB11	Neuroblastoma cell line	DSMZ
Nalm6	cALL cell line	DSMZ
RD-ES	EFT cell line	DSMZ
SBSR-AKS	EFT cell line	generated in the laboratory
SH-SY5Y	Neuroblastoma cell line	DSMZ
SIMA	Neuroblastoma cell line	DSMZ
SK-ES1	EFT cell line	DSMZ
SK-N-MC	EFT cell line Established as neuroblastoma cell line, erroneously	DSMZ
TC-71	EFT cell line	DSMZ

2.11.2 Mouse Strain

Table 9: Utilized mouse strain

Mouse strain	Characteristics	Reference	Origin
BALB/c $Rag2^{-/-}\gamma_c^{-/-}$	Absence of all T lymphocyte, B lymphocyte and NK cell function	[68]	Central Institute for Experimental Animals (Kawasaki, Japan).

2.11.3 Bacterial strain

Table 10: Utilized Bacterial strain

E. Coli strain	Genotype Description	Origin
One Shot® TOP10 Chemically Competent	F- *mcr*A Δ(*mrr-hsd*RMS-*mcr*BC) φ80*lac*ZΔM15 Δ*lac*X74 *rec*A1 *ara*D139 Δ(*ara- leu*)7697 *gal*U *gal*K *rps*L (Str^R) *end*A1 *nup*G	Invitrogen

3 Methods

3.1 Cell culture methods

3.1.1 Cultivation of adherent tumor cell lines

EFT cell lines and the neuroblastoma cell lines SH-S5Y5 and SIMA were cultured in the standard tumor medium. Volume of the medium in a middle-sized culture flask (75 cm^2 adherence surface) was 20 ml. Volume of the medium in a large-sized flask (175 cm^2 adherence surface) was 40 ml. Approximately every 3 - 4 days cells grew to confluence. At that time point, their medium was exchanged and they were split 1 : 2 to 1 : 10, depending on the growth rate of individual cell lines. The medium was removed; cells were washed once with warm PBS and then incubated with up to 5 ml trypsin / EDTA at room temperature. Degree of detachment was controlled microscopically. Detached cells were resuspended in fresh standard tumor medium and spread in new culture flasks. Cultured cells were routinely tested for Mycoplasma using a commercial kit (Lonza).

3.1.2 Cultivation of suspension tumor cell lines

cALL tumor cell lines and the neuroblastoma cell line CHP126 were cultured in the corresponding medium. Volume of the medium was 30 ml in a middle-sized culture flask. Approximately every 4 days, half of the cell suspension was removed and the same volume of fresh medium was added.

3.1.3 Cryopreservation of cells

Tumor cell lines were frozen at concentrations between 1×10^6 and 1×10^7 / ml in 1 ml volumes respectively. Pelleted cells were first resuspended in an appropriate volume of FCS. The same volume of pre-cooled 20 % DMSO was then gradually added to the cell suspension. After thorough mixing, 1 ml aliquots of the cell suspension were transferred into pre-cooled cryovials. The cryovials were placed into controlled freezing boxes and stored at –80 °C overnight. The following day, the cryovials were transferred into the liquid nitrogen freezer for long-term storage at –196 °C.

3.1.4 Thawing of cryopreserved cells

The cryovials were retrieved from the liquid nitrogen freezer and thawed rapidly in a water bath at 37 °C. As soon as only small ice crystals were seen floating inside the cryovial, the contents of a vial were transferred into a 15 ml Falcon tube containing 1 ml of medium. The tube was immediately centrifuged at 1500 rpm for 5 minutes. Pelleted cells were then resuspended in the corresponding culture medium pre-warmed to 37 °C.

3.1.5 Cell counting

The cell count and viability was assessed by trypan blue exclusion. Formulas used to calculate cell concentrations and total cell numbers are shown in **Table 11**.

Table 11: Determining the cell number using a Neubauer hematocytometer

$$\frac{\text{cell concentration}}{\text{ml}} = \text{average number of counted cells per square} \times CF \times DF$$

CF: chamber factor $= \dfrac{1}{\text{volume of chamber counted}}$

The volume of one big square of an improved Neubauer hemocytometer is 0.1 µl.

The chamber factor is 10^4.

DF: dilution factor $= \dfrac{\text{final volume}}{\text{initial volume}}$

total number of cells = cell concentration × volume of cell suspension

3.2 Transformation of competent bacteria

Transformation of TOP10 chemically competent *E. coli* was performed following the Protocol One Shot® TOP10 Competent Cells (Invitrogen). Briefly, one 50 µl vial of One Shot® cells was thawed on ice for each transformation. 2 µl of each ligation reaction (see 3.3.3) was added directly into the vial of competent cells and gently mixed. After an incubation time of 5 minutes on ice the vials were heat-shocked for 30 seconds at 42°C without shaking and instantly put on ice for

another 2 minutes. Subsequently, 250 µl of pre-warmed S.O.C medium was added and the vials were shaken for 1 hour at 37°C at 225 rpm in a shaking incubator. 80 µl from each transformation vial were spread on separate LB agar plates containing ampicilin and incubated at 37°C overnight. Colonies were selected and analyzed by plasmid isolation and sequencing.

3.3 DNA and RNA methods

3.3.1 Electrophoresis of DNA on agarose gel

Separation of DNA fragments was performed in 1 % agarose gel at 5 - 10 V / cm. 2 g agarose was dissolved in 200 ml TAE buffer by boiling. To the melted solution 4 µl ethidium bromide was added before casting the gel.
The solution containing the DNA was loaded into the gel-pockets in a volume of 25 µl. At least 0.5 µg of DNA - diluted with H_2O if necessary - was used. 4 µl of 6 × Blue Juice Gel Loading Buffer was added. A 1 Kb DNA ladder was included as a size standard in electrophoresis. For extraction of DNA fragments from agarose gels, the desired fragments were cut from the gel after electrophoresis and purified using the QIAEX II Gel Extraction Kit according to manufacturer's instructions.

3.3.2 Annealing of Oligonucleotides

For annealing, the purified oligonucleotides were resuspended in 1 x TE Buffer to a final concentration of 100 µM. The oligonucleotides for the top strand and bottom strand were mixed at a 1 : 1 ratio, resulting in 50 µM of ds oligonucleotides in a volume of 10 µl.
The following annealing program was run:

95°C	30 sec
72°C	2 min
37°C	2 min
25°C	2 min
4°C	∞

The annealed oligonucleotides were diluted with TE buffer to a final concentration of 0.5 µM and used for ligation into an expression vector (see 3.3.3).

3.3.3 Ligation of DNA Fragments

To ligate ds oligonucleotides (see 3.3.1) into expression vectors, the annealed oligonucleotides were diluted with TE buffer to obtain a concentration of 0.5 µM. The following ligation reaction was assembled:

1 µl	linearized expression vector (50 ng / ml)
1 µl	diluted, annealed oligonucleotide (0.5 µM)
1.5 µl	10 x T4 DNA Ligase Buffer
0.5 µl	BSA (10 mg / ml)
10.5 µl	DEPC H_2O
0.5 µl	T4 DNA Ligase (400 U / µl)

The reaction was incubated for 3 hours at 22°C and instantly used for transformation of competent bacteria (see 3.2).

3.3.4 Mini-preparation of Plasmid DNA

Isolation of plasmid DNA from *Escherichia coli* was performed with the NucleoSpin® Plasmid Kit from Macherey-Nagel according to manufacturer's instructions.

Briefly, a single colony from a freshly streaked bacterial plate was picked and used to inoculate 2.5 ml of LB medium supplemented with an appropriate antibiotic. The culture was incubated overnight with shaking. Bacteria were harvested and centrifuged at 11.000 x g for 30 seconds at 4 °C to pellet the bacterial cells, the supernatant was discarded. The pellet was resuspended in 250 µl of resuspension buffer supplemented with RNase A. After vigorous vortexing 250 µl lysis buffer containing sodium hydroxide was added and mixed gently by inverting the tube. After five minutes of incubation at room temperature 300 µl neutralization buffer containing guanidine hydrochloride was added and the tube was mixed by inverting. The suspension was then centrifuged at 11.000

x g in a microcentrifuge for 10 minutes at 4 °C. The supernatant was loaded into a NucleoSpin® column which was placed in a 2 ml collection tube and centrifuged at 11.000 x g for one minute at room temperature. The flow-through was discarded. The NucleoSpin® column was washed with 500 µl of preheated (50 °C) wash buffer containing guanidine hydrochloride and isopropanol, centrifuged as before and the flow-through discarded. The plasmid DNA bound to the silica membrane in the NucleoSpin® column was then eluted with 50 µl elution buffer. The flow-through containing the plasmid DNA was collected in a tube, the concentration measured via spectrophotometry, and the plasmid was analyzed be restriction enzymes. Bacterial stocks containing correct plasmids were frozen after the addition of 15 % glycerol. Those stocks were used to inoculate LB medium for Maxi prep (see 3.3.5).

3.3.5 Maxi-preparation of Plasmid DNA

Isolation of plasmid DNA from *E. coli* was performed with the EndoFree Plasmid Purification Kit from Qiagen according to manufacturer's instructions.
The isolation method was very similar to the miniprep method (see 3.3.4), only differing in scope. This method was used to obtain a large amount of known correct plasmid DNA.

3.3.6 Restriction analysis

To determine whether the correct plasmid was obtained by the cloning strategy, plasmid DNA was analyzed by digesting it with restriction enzymes. The pattern of DNA fragments of different size present after agarose gel electrophoresis was compared to the pattern expected of the correct plasmid.

3.3.7 Isolation of RNA from cells

Total cellular RNA was isolated from tumor cells using the RNeasy® Mini Kit. The isolation procedure was performed with up to 10^7 cells per column according to manufacturer's instructions. Cellular plasma membranes and organelles were first disrupted by vortexing cells in a buffer containing guanidine isothiocyanate. The lysate was passed at least five times through a blunt 20-gauge needle (0.9

mm diameter) fitted to an RNase-free syringe to fragment DNA and obtain a homogeneous lysate. The lysate was mixed with an ethanol containing buffer and transferred onto an RNeasy® column. Ethanol provided conditions that promoted selective binding of RNA to a silica-gel membrane during centrifugation of the solution through the column. Washing buffers were then used to eliminate contaminants while RNA remained attached to the membrane inside the column. Finally, DEPC-treated water was used to elute the RNA from the column. Isolated and purified RNA was stored at –80 °C.

3.3.8 Isolation of RNA from tissue using TriReagent

For isolation of RNA from tissue, frozen organ pieces (50-100 mg) were mechanically crushed. The tissue-powder was then homogenized in 2 ml TriReagent and incubated for 5 minutes at room temperature (RT). The homogenate was supplemented with 200 µl BCP and vigorously vortexed for 20 seconds. After incubation for 2-3 minutes at RT, where aqueous and organic phases were separated, the mixture was centrifuged at 4000 rpm for 60 minutes at 4°C. After centrifugation the aqueous upper RNA phase was transferred into a separate reaction tube. RNA was precipitated by adding 500 µl isopropanol and the sample was vortexed rigorously. After incubation at RT for 5 minutes, the sample was centrifuged at 4000 rpm for 30 minutes at 4°C, the supernatant was removed and the RNA pellet washed with 1 ml 75 % cold ethanol. After centrifugation at 4000 rpm for 10 minutes at 4°C, ethanol was removed and the pellet air-dried for 2-5 minutes. The RNA was dissolved in RNase- free water and stored at -80°C.

3.3.9 cDNA synthesis

Reverse Transcription (RT reaction) is a process in which single-stranded RNA is reverse transcribed into complementary DNA (cDNA) by using total cellular RNA or poly(A) RNA, a reverse transcriptase enzyme, in this case MultiScribe™ Reverse Transcriptase, derived from Moloney murine leukemia virus (rMoMuLV), primers and dNTPs. The resulting cDNA can be used in RT-PCR reaction. RT reaction is also called first strand cDNA synthesis. As primers for RT reaction random primers were used.

1) Preparation of the RT master mix

Component	Volume (µl)
10 x RT Buffer	2.0
25 x dNTP Mix (100 mM)	0.8
10 x RT Random Primers	2.0
Multiscribe™ Reverse Transcriptase	1.0
Nuclease-free H_2O	9.2
Total per Reaction	**15.0**

2) Addition of 5 µl of RNA sample

3) cDNA synthesis using the conditions shown in table 12

Table 12: Thermal cycler conditions

	Step 1	Step 2	Step 3	Step 4
Temperature	25°C	37°C	85°C	4°C
Time	10 min	120 min	5 sec	∞

3.3.10 Quantitative Real time PCR

Quantification of synthesized cDNA by quantitative real-time PCR allows examination of differential gene expression, as the amount of cDNA correspond to the amount of cellular mRNA. Quantitative real-time PCR was performed by use of TaqMan® Universal PCR Master Mix and fluorescence detection with an AB 7300 Real-Time PCR System. Gene-specific primers and probes were obtained as TaqMan® Gene Expression Assays from Applied Biosystems which consisted of a FAM™ dye-labeled TaqMan® MGB probe and two unlabeled PCR primers. 1.25 µl of these primer assays were added to the TaqMan® Universal PCR Master Mix (12.5 µl) with cDNA (0.5 µl; synthesized as described in 3.3.9) and adjusted to a final volume of 25 µl with water. The final concentration of primers and probe were 0.9 and 0.25 µM respectively. Assays were performed in duplicate following the manufacturer's instructions.

For EWS/FLI-1 detection the following primers were designed:

sense 5’-TAGTTACCCACCCAAACTGGAT-3’
antisense 5’-GGGCCGTTGCTCTGTATTCTTAC-3’
probe 5’-FAM-CAGCTACGGGCAGCAGAACCCTTCTT-TAMRA -3’

Inventoried TaqMan® Gene Expression Assays were used for other genes (Tab. 13):

Table 13: List of TaqMan® primer assays

Gene	**Assay ID**
GPR64	Hs00971391_g1
CHM1	Hs00170877_m1
GAPDH	Hs99999905_m1
PGF	Hs00182176_m1
IFITM1	Hs01652522_g1
ISG15	Hs00192713_m1
MMP-1	Hs00899658_m1

For all assays the same program was used (Tab. 14):

Table 14: Temperature profile and repetitions of real time PCR in 7300 Real-Time PCR System

Stage 1	**Stage 2**	**Stage 3**	
Repetition: 1	Repetition: 1	Repetition: 40	
50.0 °C	95.0 °C	95.0 °C	60.0 °C
2:00 min	10:00 min	0:15 min	1:00 min

Gene expression profiles were normalized to the mRNA levels of the housekeeping gene GAPDH and standard deviation of duplicates was calculated as described in 3.7.

3.4 Protein methods

3.4.1 Generation of whole protein lysates

Cells were trypsinized, counted and washed 2 x with PBS. 2 - 3 x 10^6 cells were resuspended in 200 µl 3x Laemmli-buffer and incubated at 70°C for 10 minutes to denature proteins. Lysates were then homogenized through a 23 gauge needle and centrifuged for 5 minutes at 14000 rpm. Supernatants were transferred to a new reaction tube and either stored at -80°C or immediately processed for SDS-PAGE.

3.4.2 Sodium Dodecyl Sulfate Polyacrylamide Gel Electrophoresis (SDS-PAGE)

Protein samples were separated using SDS -polyacrylamide gel electrophoresis. Therefore, 25 - 30 µl of protein sample were applied to SDS -polyacrylamide gel and electrophoresis was carried out at 100-120 V for 1.5 to 2.5 hours. Molecular weight of the separated proteins was determined by comparison with a prestained molecular weight standard.

3.4.3 Western Blotting

For immunoblot analysis proteins were transferred to Hybond-P PVDF membranes for 2 hours at 0.8 mA / cm^2 using a "Semidry"-Blot device in the presence of Transblot-SD buffer.

3.4.4 Immunoblotting of immobilized protein

After electroblotting the transferred proteins are bound to the surface of the PVDF membrane, providing access for reaction with immunodetection reagents. Unspecific binding sites were blocked by immersing the membrane in 5 % skim milk / 0,05 % Tween for 1 hour at RT. The membrane was then probed with primary antibody over night at 4°C. Antibodies were diluted according to the manufacturers instructions in 5 % skim milk, 0,05 % Tween. The membrane was washed 3 x 5 minutes in 1 x TBST, incubated for 1 hour with horseradish

peroxidase (HRP) coupled secondary antibody and washed again as before. Antibody-antigen complexes were detected using the ECL-Plus Western Blotting Detection System (#RPN2132, GE Healthcare). This detection system is based on the oxidation of a Luminogen by HRP and peroxide resulting in a chemiluminescent signal detectable by a CCD camera. Signals were detected with the Gel Logic 1500 imaging system and analyzed with Kodak Molecular Imaging Software (Version 5.0).

3.4.5 Transient transfection of EFT cell lines

Target gene silencing was achieved by transient transfection of appropriate siRNA into EFT cells using HiPerFect (Qiagen) according to manufacturer's instructions. Briefly, for silencing 2 - 3 x 10^6 cells were seeded in a 8 cm^2 cell culture dish. 3.6 µl siRNA (20 µM) were mixed with 36 µl HiPerFect reagent in 2 ml serum free RPMI. After an incubation time of 8 minutes, the mixture was added slowly to the target cells. Experiments were conducted after a minimum of 48 hours to allow reduction of target gene expression. Used siRNAs are listed in table 5 (see 2.8).

3.4.6 Electroporation

To generate stable transfected packaging cell lines pT 67, linearized pSIREN Retro Q construct and vector control DNA (20 µg) was mixed with 3 x 10^6 pT67 cells in 0.8 ml of RPMI-1640 medium. Electroporation was performed at the capacitance of 960 µF and 270 V / 0.4 cm. After electroporation, cells were incubated on ice for 10 minutes and seeded in two 175 cm^2 cell culture flasks. Stable transfectants were selected by puromycin selection at a concentration of 2 µg / ml. To gain viral supernatants, stable lines were grown in 175 cm^2 cell culture flasks. After the cells reached confluence, supernatants were harvested, filtered through 0.45-µm filter and stored at -80°C.

3.4.7 Retroviral Infection of EFT cell lines

For retroviral infection of EFT cell lines with pSIREN Retro Q constructs, target cells were seeded 12–18 hours before infection, at a cell density of 1 x 10^5 / well

in a 6 well-plate. Cells were transduced with 1 ml retrovirus supernatant supplemented with polybrene (final concentration 4 µg / ml). Cells were cultivated for 48 hours at 37°C (5 % CO_2) and selected with puromycin (2 µg / ml).

3.5 Assay

3.5.1 Invasion Assay

To study cell invasion the *BioCoat™ Angiogenesis System: Endothelial Cell invasion* was used (BD Biosciences) according to the manufacturers instructions. Briefly, for rehydration the plate was removed from −20° C storage and allowed to adjust to room temperature. Pre-warmed RPMI-Medium was added to the interior of the insert wells and allowed to rehydrate for 2 hours at 37°C / 5 % CO_2. Subsequently, 5 x 10^4 cells (in 250 µl RPMI without supplements) were added to each insert well. As a chemoattractant, diluted bone marrow-derived serum from an EFT patient was added to each of the bottom wells. The plate was incubated for 48 hours at 37°C / 5 % CO_2. Cell invasion was measured by staining and counting the invasive cells at the bottom side of the membranes using Calcein AM solution at a concentration of 4 µg / ml. For each plate 12,5 ml of pre-warmed HBSS was added to 50 µg calcein AM in 20 µl DMSO. The insert plate was transferred into a second BD Falcon 24-well plate containing 0,5 ml / well of 4 µg / ml calcein AM in HBSS and incubated for 90 minutes at 37°C / 5 % CO_2. Cells were imaged by fluorescence microscopy using a Zeiss AxioVert 100 (Jena, Germany) with AxioVision software (Release 4.7.1).

3.5.2 Colony Forming Assay

Cells were seeded in duplicate at a density of 5 x 10^3 cells per 1.1 ml methylcellulose-based media (R&D Systems, Wiesbaden, Germany) into a 35 mm plate according to the manufacturer's instruction and cultured for 14 days at 37°C and 5 % CO_2 in a humidified atmosphere.

3.5.3 Angiogenesis Assay

Cellular tube formation was tested by use of a commercial Matrigel Matrix assay (Biocoat, BD Biosciences) according to the manufacturer's instruction. Briefly, cells were seeded at 50000 cells/well in a 96 well plate and grown at 37°C / 5 % CO_2 in a humidified atmosphere. After 16-18 hours, cells were stained with Calcein AM Fluorescent Dye (BD Biosciences) 1 µg / ml for 30 minutes in the dark. Cells were imaged by fluorescence microscopy using a Zeiss AxioVert 100 (Jena, Germany) with AxioVision (Release 4.7.1) software.

3.6 Animal Experiments

3.6.1 Analysis of local tumor growth

For the analysis of *in vivo* tumor growth 2-4 x 10^6 EFT cells and derivatives were harvested by trypsinization, washed with Dulbecco's phosphate buffered saline, and injected in a volume of 0.2 ml into immunodeficient Rag2$^{-/-}\gamma_C^{-/-}$ mice (see 2.11.2). To monitor local tumor growth cells were injected subcutaneously (s.c.). intra-inguinal and tumor size was determined. Mice bearing a tumor >10 mm in diameter were considered as positive and sacrificed. Tumors were excised for immunohistology and RNA preparation for expression analysis.

3.6.2 Analysis of invasive tumor growth

The principle of the metastasis assay is to investigate a critical process of metastasis, namely the extravasation of tumor cells from blood vessels in target organs. The steps of this process in detail include both cell survival in and escape from circulation, invasion of the endothelial cell lining of blood vessels, degradation of the subendothelial basement membrane and migration out of the vascular compartment [69]. As the tumor cells are applied intravenously, most tumor cells are arrested in the lung tissue, simply because the lung capillary bed is the first to be encountered [70]. Lung capillaries are lined with a continuous basement membrane underlying epithelial and endothelial cells, which build a clear barrier to metastasis [71]. If tumor cells are able to cross this barrier, they colonize the lung and grow to metastases. If they are not able to invade, they recirculate and get trapped in other organs.

For the analysis of in vivo invasive growth 2-4 x 10^6 EFT cells and derivatives were harvested by trypsinization and washed twice with Dulbecco's phosphate buffered saline. Cells were injected in a volume of 0.2 ml intravenously (i.v.) into the tail vein of immunodeficient Rag2$^{-/-}\gamma_C^{-/-}$ mice (see 2.11.2). Four weeks later mice were sacrificed and metastatic spread was monitored in individual organs. Affected organs were excised and fixed with 4 % formaldehyde for immunohistochemistry.

3.6.3 Immunohistochemistry

Organs were fixed in 4 % formaldehyde and paraffin embedded. Three to five micrometer thick sections from all tissues were cut and stained with hematoxylin and eosin (H&E). PD Dr. Irene Esposito from the Institute of Pathology of the Helmholtz Zentrum München reviewed all sections.

3.7 Determination of Standard Deviation

Error bars represent the mean ± standard deviation of duplicates if not stated otherwise. Standard deviation was calculated using the 2^{-ddCt} method. The mean value and standard deviation of duplicates were displayed graphically using Microsoft Excel.

4 Results

4.1 Identification of Ewing Tumor specific expression profiles

To identify EFT specific gene expression, we used customized high density DNA microarrays (EOS-Hu01) containing 35.356 oligonucleotide probe sets to query a total of 25.194 gene clusters. 11 EFT samples were analyzed in comparison to 133 normal tissues of diverse origin. This analysis revealed 37 genes that are highly up-regulated or even specifically expressed in EFT [64]. CHM1 and GPR64 were selected for analysis as potential targets for new anti-angiogenic therapies as they have potential central roles in vascularization mechanisms of EFT.

Chondromodulin-1 (CHM1) is a glycoprotein that was first discovered as a functional matrix component with phenotypic expression in chondrocytes stimulating cartilage growth [72]. It was also described to have anti-angiogenic activity and has been suggested to inhibit endothelial cells from invading cartilage [73, 74]. The over-expression of CHM1 in a malignant tumor is surprising, as one would rather suspect a reduced expression, which enables tumor-angiogenesis, thereby promoting further tumor-growth. In chondrosarcoma, CHM1 expression is down-regulated. Furthermore the ectopic administration of CHM1 to chondrosarcoma bearing mice significantly reduced tumor size and microvessel density [75], emphasizing its role as angiogenesis-inhibitor and tumor-suppressor. In EFT, CHM1 might have a different function. EFT are characterized by the presence of blood lakes and a reduced MVD, indicating that the maintenance of vascular supply functions not only via angiogenesis but also via vasculogenic mimicry [13]. The over expression of CHM1 in EFT might be associated with the reduced microvessel density and thus advance the process of vasculogenic mimicry. Furthermore, it might thereby promote the aggressive phenotype of EFT, as hypoxic tumor cells are discussed to correlate with increased metastasis and inferior prognosis [23].

The G-protein coupled receptor 64 (GPR64) is an orphan receptor with high expression in the epithelia of *ductulus efferentes* and proximal epididymis, but in no other tissues of the adult [65]. GPR64 belongs to the LNB-TM7 (B2) subfamily

of G-Protein-coupled receptors and is assumed to control water balance and fluid re-absorption in the male excurrent ducts [76].

4.1.1 CHM1

CHM1 was found to be considerably over-expressed in EFT tissue samples and cell lines compared to samples derived from normal body tissue (**Figure 1**).

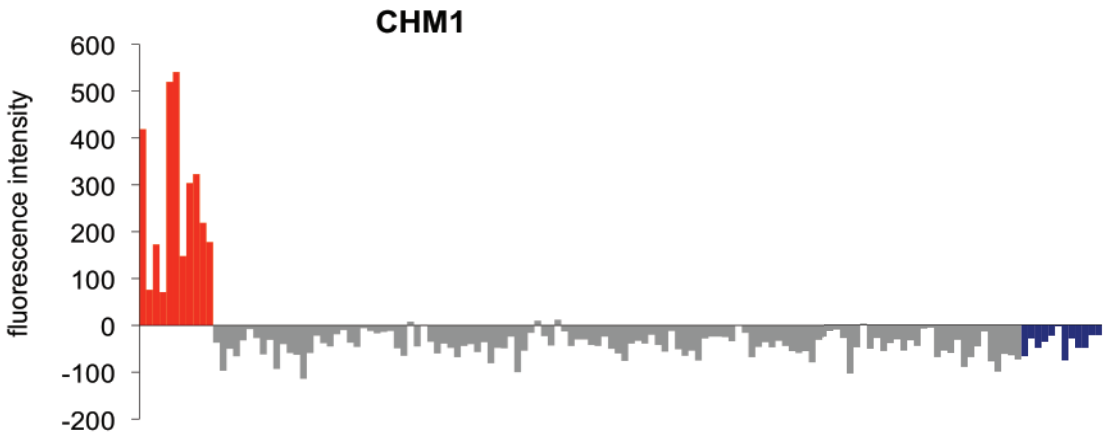

Figure 1: *CHM1* gene expression on mRNA level in EFT tissue samples (red bars), normal body tissue (gray bars) and fetal tissue (blue bars).

To verify the observed expression profile of the microarray data the mRNA expression in EFT cell lines was analyzed compared to other pediatric tumors. I found evidently lower expression of CHM1 in common acute lymphoblastic leukemia (cALL) and neuroblastoma, which display a cytological appearance similar to EFT (small-round-blue) (**Figure 2**).

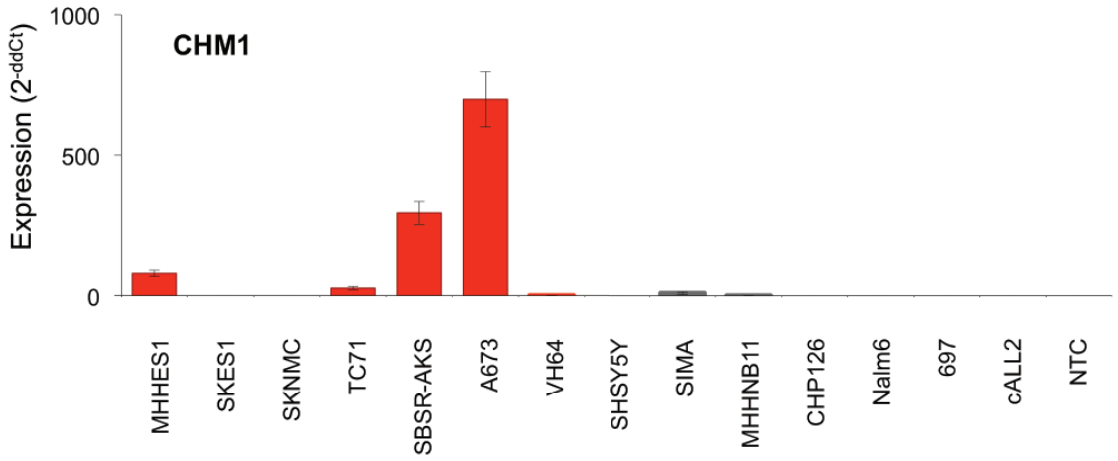

Figure 2: CHM1 mRNA expression in tumor cell lines: EFT cell lines (red bars); neuroblastoma (black bars); cALL (gray bars); NTC: non template control (water); Error bars represent the mean ± standard deviation of duplicates.

4.1.2 GPR64

GPR64 was found to be apparently over-expressed in EFT tissue samples and cell lines compared to samples derived from normal body tissue (**Figure 3**).

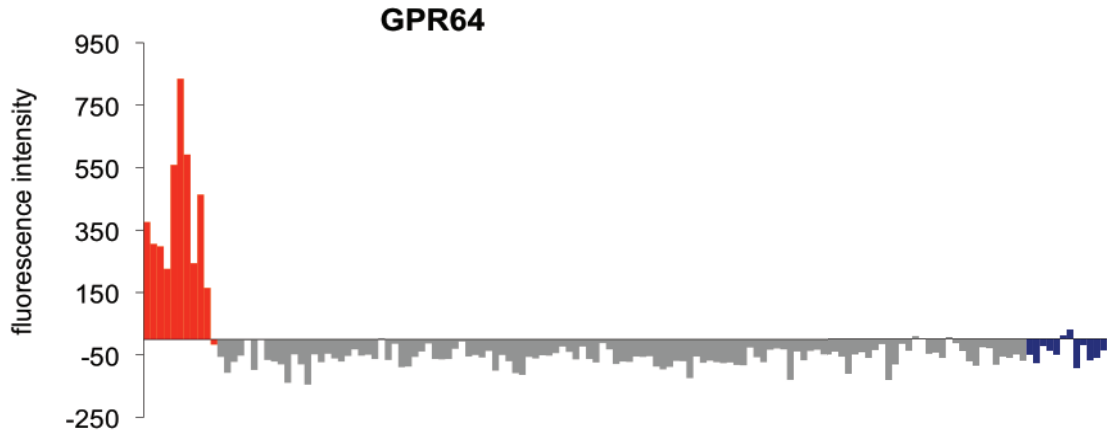

Figure 3: GPR64 gene expression on mRNA level in EFT tissue samples (red bars), normal body tissue (gray bars) and fetal tissue (blue bars).

To verify the observed expression profile of the microarray data the mRNA expression in EFT cell lines was analyzed compared to other pediatric tumors. I found considerably lower expression of GPR64 in cALL and neuroblastoma (**Figure 4**).

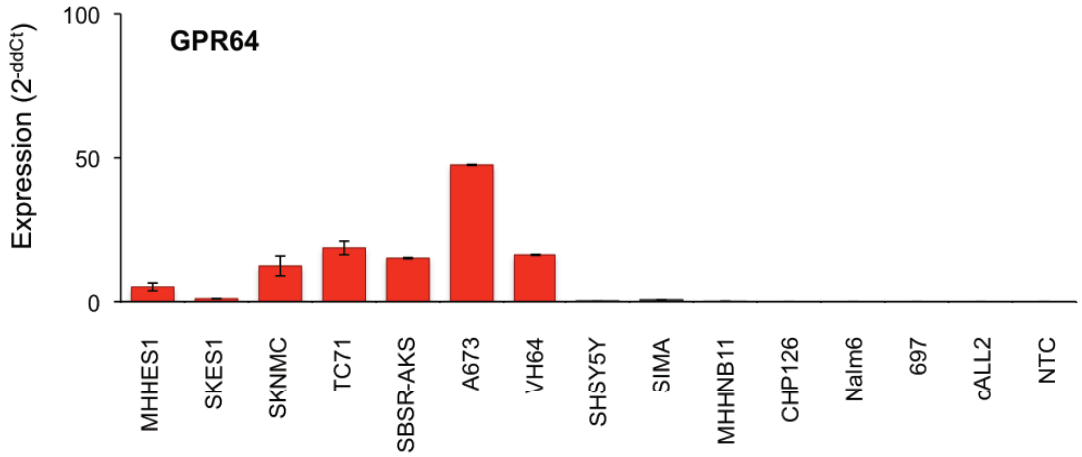

Figure 4: GPR64 mRNA expression in tumor cell lines: EFT cell lines (red bars); neuroblastoma (black bars); cALL (gray bars); NTC: non template control (water); Error bars represent the mean ± standard deviation of duplicates

4.2 Transient down-regulation of target gene expression

To identify appropriate siRNAs for efficient target gene knock down in EFT cell lines A673 and SBSR-AKS, several different siRNAs were tested in transient transfection assays (see Materials and Methods). Expression knock down efficiency was tested by quantitative RT-PCR (qRT-PCR) 48 hours after transfection. To exclude an unspecific down-regulation and induction of an interferon response, expression of the IFN responsive genes G1P2 and IFITM1 was monitored. When expression of one of the genes was induced more than 2-fold by a siRNA, the respective siRNA was not used for further experiments.

4.2.1 CHM1

For expression knock down of CHM1, the siRNAs Hs_CHM1_1 and Hs_CHM1_4 (see Materials and Methods) were used. 48 hours after transfection, CHM1 expression was analyzed by qRT-PCR using specific CHM1 primer assay (**Figure 5**). *CHM1* expression was validated against the expression of the housekeeping gene *GAPDH*.

Transfection with siRNA CHM1_1 enabled a down regulation of CHM1 expression to levels 5-10 % of normal values in siRNA controls in both cell lines.

Transfection with siRNA CHM1_4 enabled a down regulation of CHM1 expression to levels 5 % of normal values in siRNA controls in SBSR-AKS, whereas transfection of A673 resulted in a down-regulation of only about 36 % of normal values in siRNA controls. An unspecific induction of an interferon response was not observed for both siRNAs. The siRNA CHM1_1 was used for the generation of stable shRNA infectants (see 4.3.1).

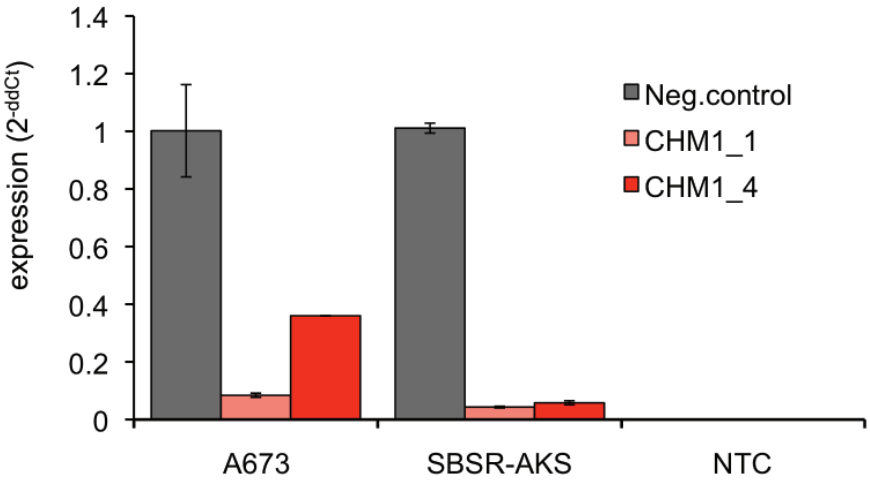

Figure 5: Transient CHM1 siRNA Transfection. Gene expression analysis (qRT-PCR) 48 hours after transfection. CHM1_1 and CHM1_4 are different siRNAs, Neg.control: non-silencing siRNA; NTC: non-template control. Error bars represent the mean ± standard deviation of duplicates

4.2.2 GPR64

For expression knock down of GPR64, the siRNAs Hs_GPR64_1 and Hs_GPR64_4 were used (see Materials and Methods). 48 hours after transfection, GPR64 expression was analyzed by qRT-PCR using specific GPR64 primer assay (**Figure 6**). GPR64 expression was validated against the expression of the housekeeping gene *GAPDH*.

The transfection with siRNA GPR64_1 resulted in a down-regulation of GPR64 expression to levels 18-20 % of normal values of siRNA control transfectants in both cell lines.

Transfection with siRNA GPR64_4 enabled a down regulation of GPR64 expression to levels 5-10 % of normal values in siRNA controls in both cell lines. An unspecific induction of an interferon response was not observed for both

siRNAs. The siRNA GPR64_4 was used for generation of stable shRNA infectants (see 4.3.2).

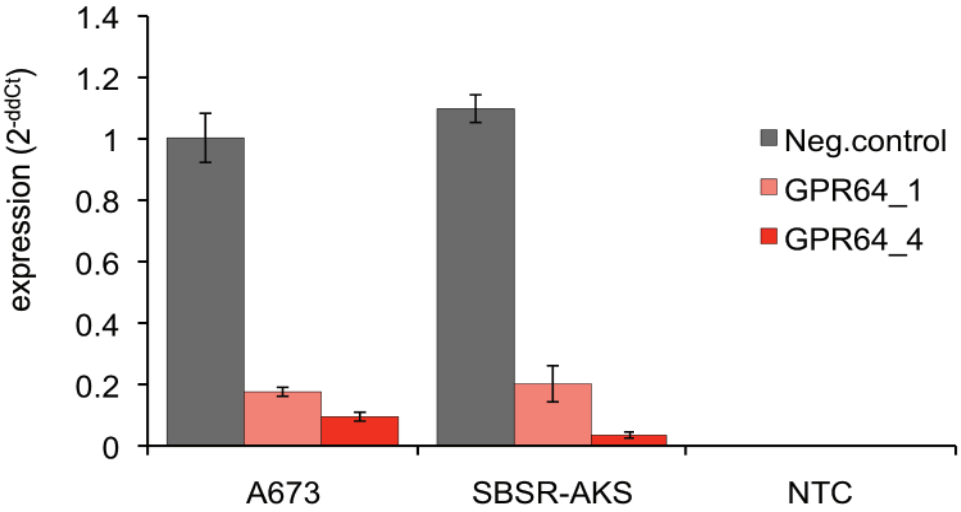

Figure 6: Transient GPR64 siRNA Transfection. Gene expression analysis (qRT-PCR) 48 hours after transfection. GPR64_1 and GPR64_4 are different siRNAs, Neg.control: non-silencing siRNA; NTC: non-template control; Error bars represent the mean ± standard deviation of duplicates.

4.3 Down-regulation of target gene expression by retroviral gene transfer

Stable shRNA infectants were generated by cloning oligonucleotides based on the positive tested siRNA into the expression vector pSIREN RetroQ (see Materials and Methods) and subsequent retroviral gene transfer of pSIREN constructs into A673 and SBSR-AKS EFT cell lines. Expression knock down efficiency was tested by qRT-PCR. To exclude an unspecific down-regulation and induction of an interferon response, again the expression of the IFN responsive genes *G1P2* and *IFITM1* was monitored.

4.3.1 CHM1

The oligonucleotide based on siRNA Chm1_1 was cloned into the expression vector pSIREN RetroQ and the resulting pSIREN^{CHM1} construct introduced into A673 and SBSR-AKS cells by retroviral gene transfer. CHM1 expression was analyzed by qRT-PCR using specific CHM1 primer assay. CHM1 expression was validated against the expression of the housekeeping gene *GAPDH*.

Stable transfection resulted in a down-regulation of CHM1 expression to 2-5 % of normal values of siRNA control infectants in both cell lines (**Figure 7**). An unspecific induction of an interferon response was not observed.

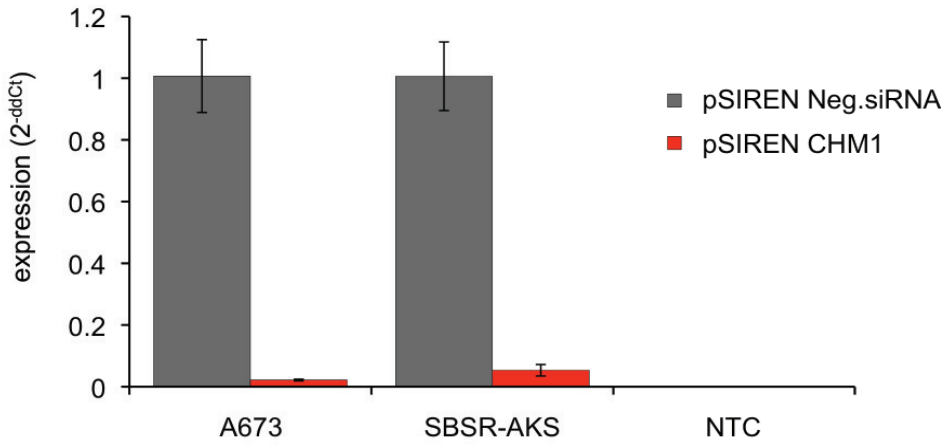

Figure 7: CHM1 mRNA expression in EFT cell lines after constitutive down-regulation assessed by qRT-PCR; NTC: non-template control; Error bars represent the mean ± standard deviation of duplicates

4.3.2 GPR64

The oligonucleotide based on siRNA GPR64_4 was cloned into the expression vector pSIREN RetroQ and the resulting pSIREN^{GPR64} construct introduced into A673 and SBSR-AKS cells by retroviral gene transfer. GPR64 expression was analyzed by qRT-PCR using specific GPR64 primer assay. GPR64 expression was validated against the expression of the housekeeping gene *GAPDH*.

Stable transfection resulted in a down-regulation of GPR64 expression to 7-10 % of normal values of siRNA control infectants in both cell lines (**Figure 8**). An unspecific induction of an interferon response was not observed.

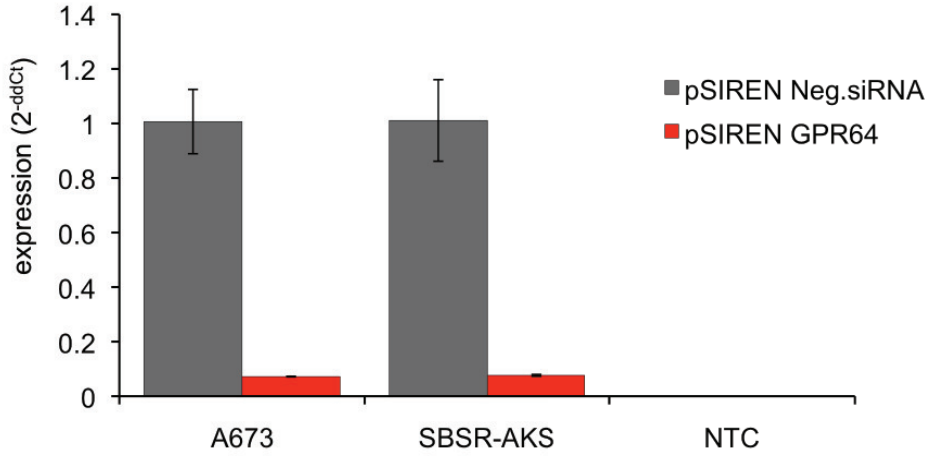

Figure 8: GPR64 mRNA expression in EFT cell lines after constitutive down-regulation assessed by qRT-PCR; NTC: non-template control; Error bars represent the mean ± standard deviation of duplicates.

4.4 Over-expression of EWS/FLI-1 in mesenchymal stem cells

To identify genes, which are induced by the EWS/FLI-1 fusion gene, we over-expressed of EWS/FLI-1 cDNA under the control of a stem cell virus LTR (pMSCVneo, Clontech) in human mesenchymal stem cell (MSC) lines V54.2 and L87. Western-blot analysis identified several MSC lines with a positive EWS/FLI-1 expression (**Figure 9**) [77].

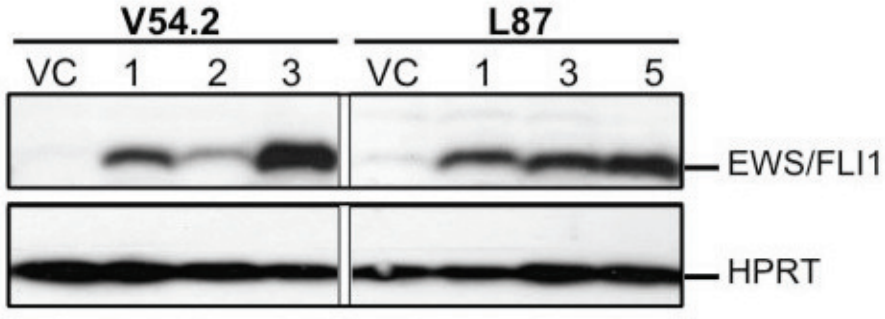

Figure 9: Western Blot of protein lysates of EWS/FLI-1 transfected stem cell lines V54.2 and L87. Retroviral gene transfer of EWS/FLI1 cDNA into MSC lines result in a strong EWS/FLI-1 expression as shown by Western Blot analysis with FLI1 antibody. Numbers for different obtained lines are given; VC vector control. HPRT: loading control.

The induction of EWS/FLI-1 expression was also monitored on RNA level (**Figure 10**).

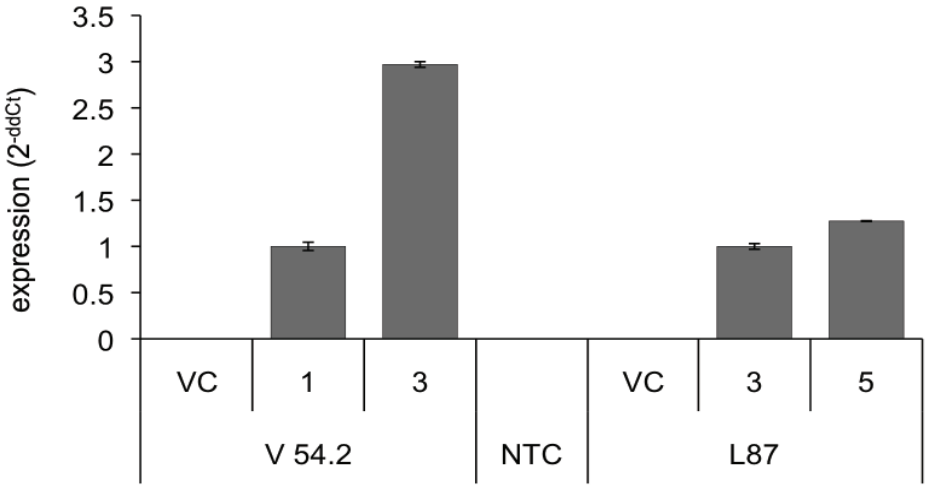

Figure 10: qRT-PCR of EWS/FLI-1 expression in EWS/FLI-1 transfected MSC clones. Numbers for different obtained lines are given; VC vector control; Error bars represent the mean ± standard deviation of duplicates

4.5 Tube formation assay

Endothelial differentiation potential of parental EFT cell lines was evaluated by tube formation assay. The ability to form endothelial tubules on basement membrane is associated with vasculogenic mimicry and allows investigators not only to study factors that regulate this process, but also to define genes and signaling pathways that cannot be studied easily *in vivo*. The formation of tube-like structures is regarded as a first step during the process of the generation of new vessels.

4.5.1 EFT cell lines with Vasculogenic Mimicry Phenotype

SBSR-AKS and RDES show endothelial differentiation potential in Matrigel assay (**Figure 11**).

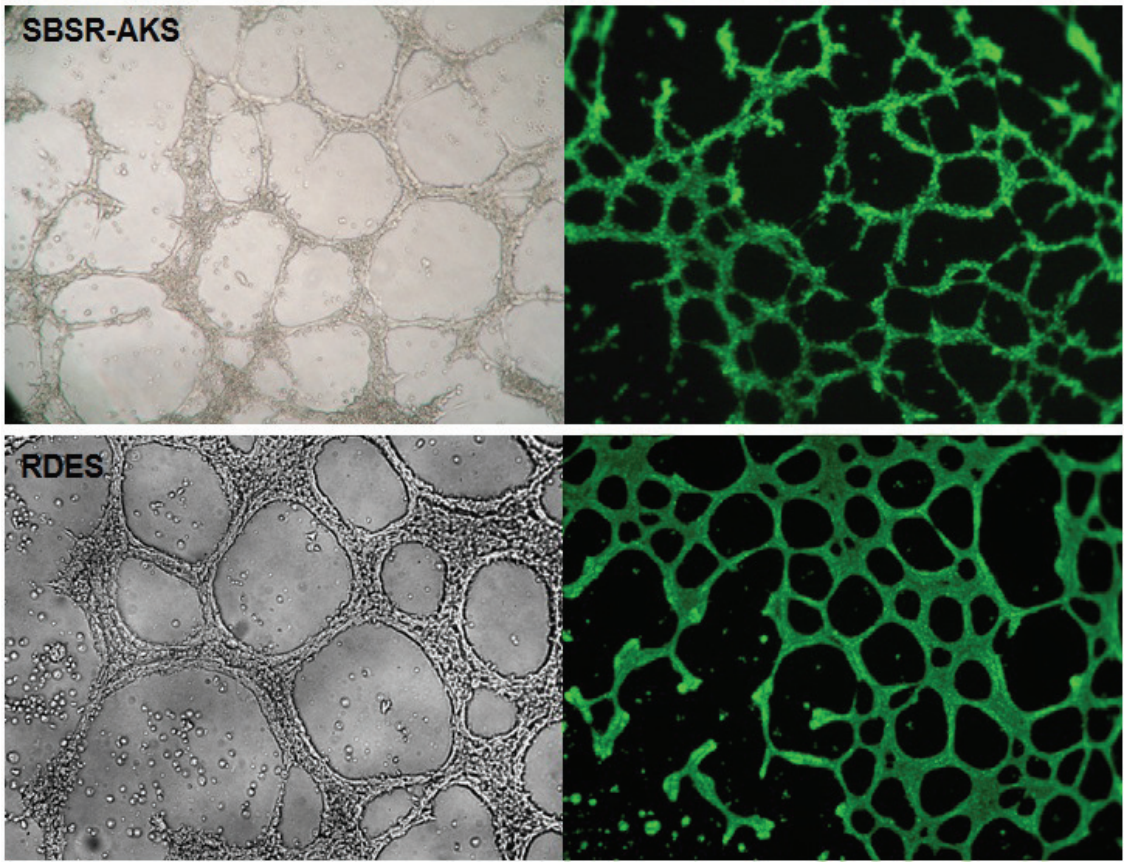

Figure 11: Tube formation assay of parental EFT cell lines with vasculogenic phenotype. *Left*: phase contrast microscopy at 10 x magnification. *Right*: Calcein staining, images at 4 x magnification.

4.5.2 EFT cell lines with Non-Vasculogenic Mimicry phenotype

A673, MHH-ES1, SK-ES1, SK-N-MC, TC71 and VH64 show no endothelial differentiation potential in Matrigel Assay (**Figure 12** and **Figure 13**).

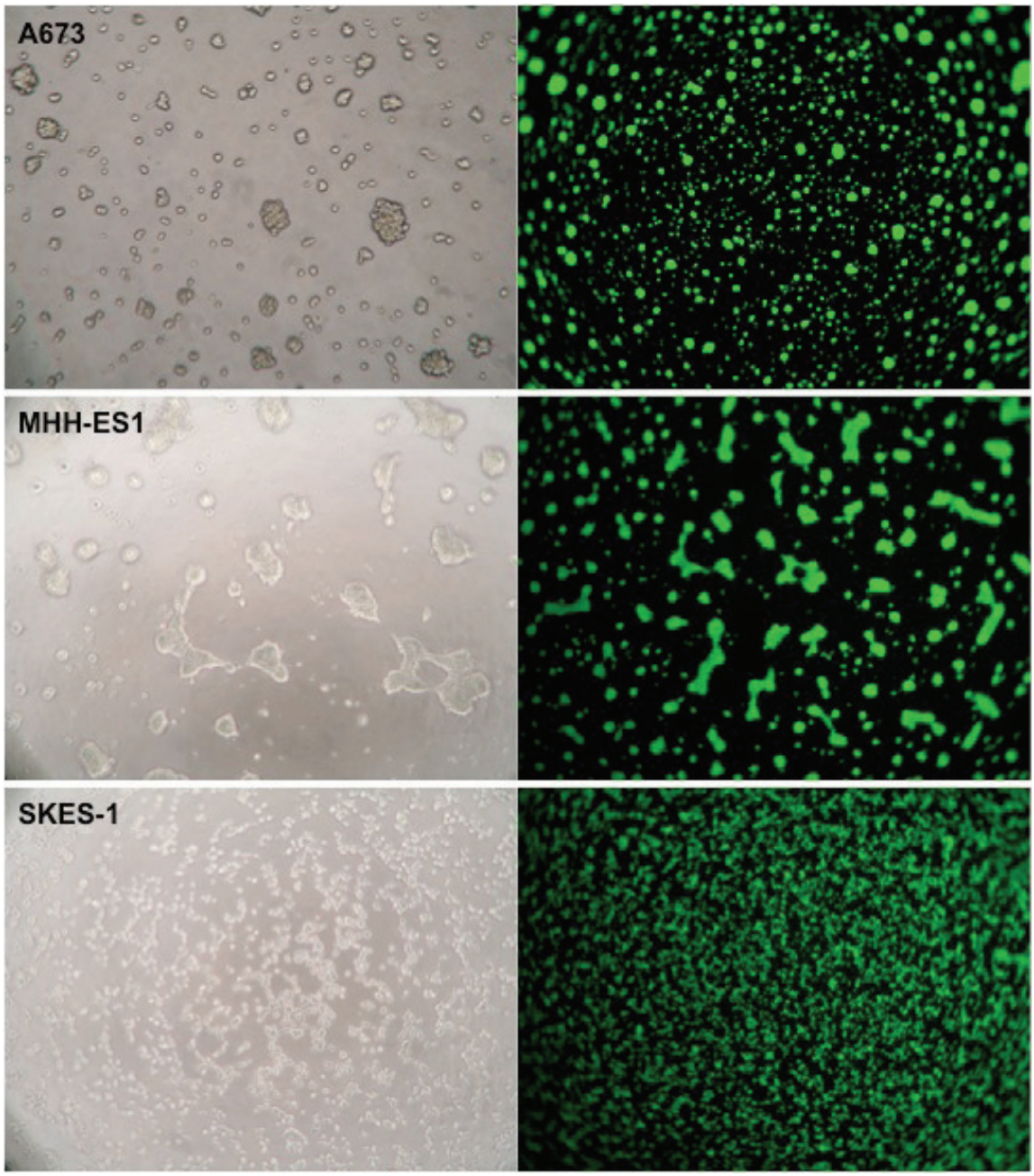

Figure 12: Tube formation assay of parental EFT cell lines with non vasculogenic mimicry phenotype. *Left:* phase contrast microscopy at 10 x magnification. *Right:* Calcein staining, images at 4 x magnification.

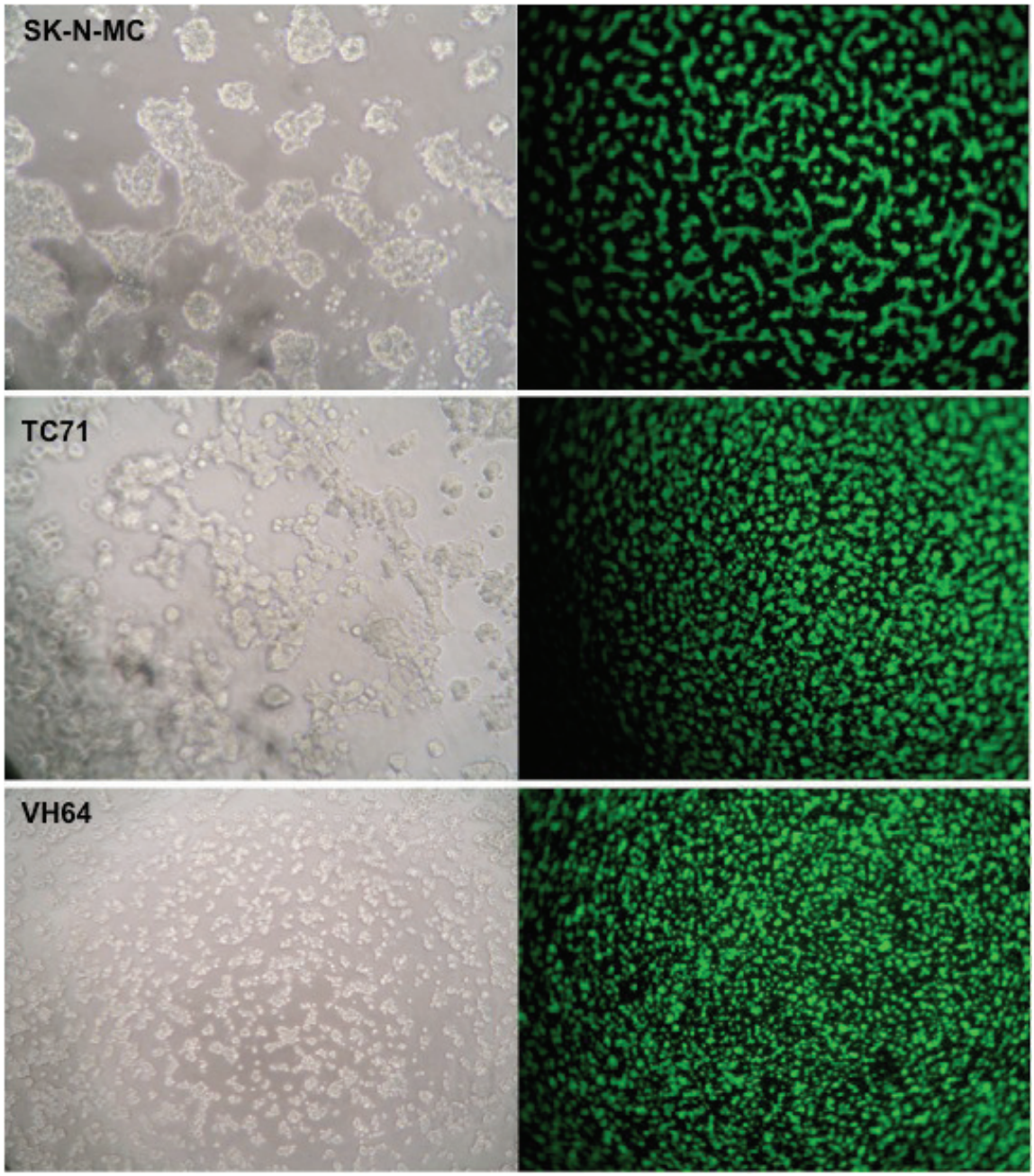

Figure 13: Tube formation assay of parental EFT cell lines with non vasculogenic mimicry phenotype. *Left:* phase contrast microscopy at 10 x magnification. *Right:* Calcein staining, images at 4 x magnification

4.6 Tail Vein Assay of Cancer Metastasis

To evaluate the metastatic potential of different EFT cell lines, I performed tail vein assays of cancer metastasis (see 3.6.2). Therefore I injected 4 x 10^6 cells into the tail vein of $Rag2^{-/-}\gamma_C^{-/-}$ mice and analyzed organ affection after 4 weeks. Results are summarized in table 15.

Table 15: Organ affection of EFT cell lines after i.v. injection. - no affection; + medium affection; ++ strong affection

	A673	SBSR-AKS	TC71	VH64
Liver	++	+	++	+
Lung	++	-	-	+
Kidney	+	+	-	+
Spleen	-	-	+	-
Ovary	-	++	++	++
Soft tissue	+	-	-	+

All tested EFT lines grew to numerous metastases within the liver. This may be due to the site of injection and the ultra-structure of the liver capillaries, which are constituted by so-called liver sinusoidal endothelial cells (LSEC). The liver sinusoids are characterized by the presence of open pores or fenestrae lacking a diaphragm and a basal lamina underneath the endothelium [78]. These fenestrae act as a dynamic filter enabling the exchange of macromolecules, solutes and fluids between the vasculature and surrounding tissues [78]. As the liver sinusoids lack a sustained endothelial lining, tumor cells that were unable to invade lung tissue might pass through this barrier without active extravasation, get trapped in the liver tissue and grow to metastases. Therefore, only differences in lung colonization were considered as relevant. As the EFT cell line A673 induced the strongest metastatic affection of the lung and no tumor colonies within the ovary, I chose to use the stable transfectants of this cell line

and derivates to assess whether down-regulation of the target genes had any influence on metastatic potential of EFT.

4.7 Analysis of CHM1

4.7.1 Influence of EWS/FLI-1 on CHM1 expression

To address the question, whether CHM1 expression is directly induced by EWS/FLI-1, I analyzed CHM1 expression in EWS/FLI-1 cDNA transfected MSC (see 4.4). As shown in **Figure 14**, CHM1 expression was only induced in a minor degree by EWS/FLI-1 in the MSC line V54.2, whereas in MSC line L87, no CHM1 expression could be observed in clone 3 and only negligible expression in clone 5.

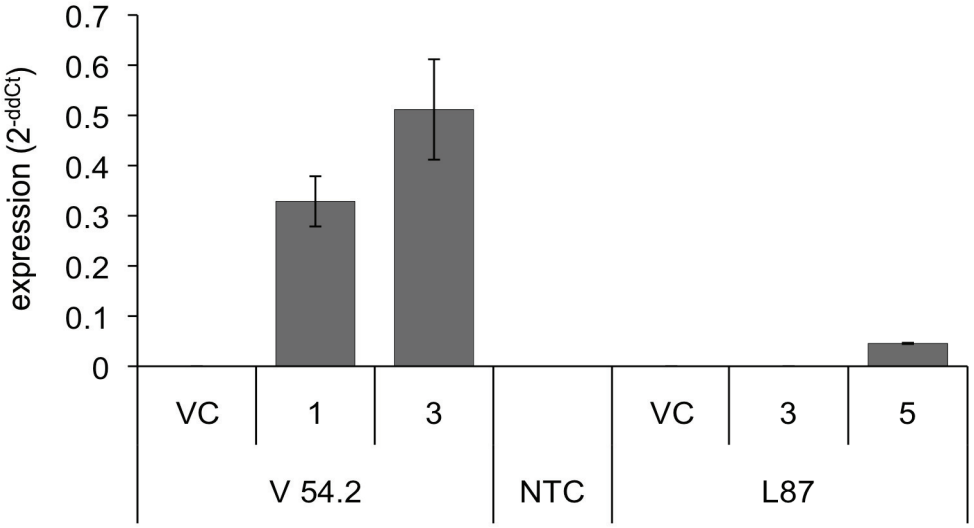

Figure 14: Influence of EWS/FLI-1 induction on CHM1 expression. qRT-PCR of CHM1 mRNA expression in EWS/FLI-1 transfected MSC clones. NTC: non-template control; Error bars represent the mean ± standard deviation of duplicates.

To further investigate, if CHM1 expression is influenced by EWS/FLI-1, I analyzed CHM1 expression after transient EWS/FLI-1 expression knock down in EFT cell lines. As shown in **Figure 15**, EWS/FLI-1 down regulation has no evident influence on CHM1 expression.

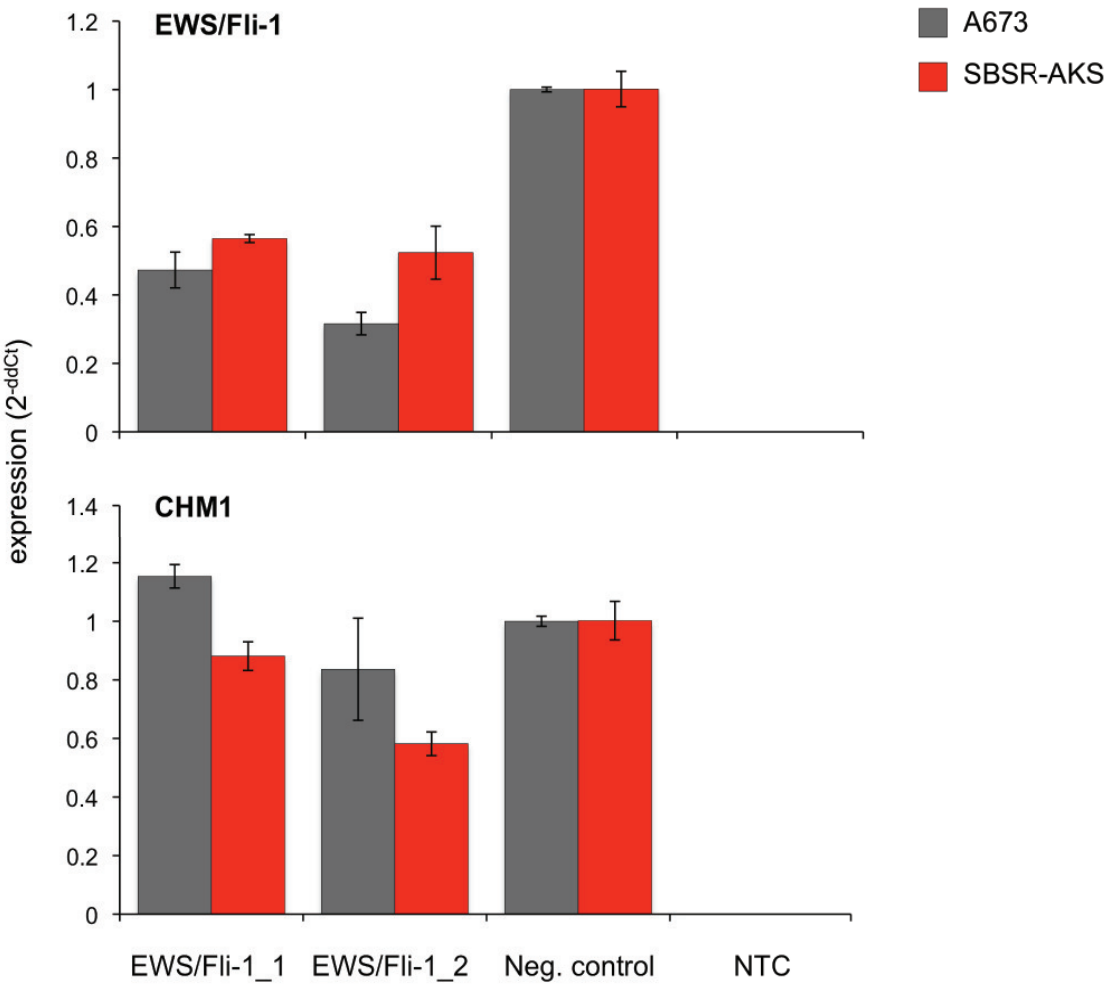

Figure 15: CHM1 expression is not affected by EWS/FLI-1 knock down. mRNA expression analysis (qRT-PCR) 48 hours after transfection. *Upper panel:* EWS/FLI-1 expression; *Lower panel*: CHM1 expression; EWS/FLI-1_1 and EWS/FLI-1_2 are different siRNAs, Neg.siRNA: non-silencing siRNA. NTC: non-template control; Error bars represent the mean ± standard deviation of duplicates.

4.7.2 Influence of CHM1 on in vitro endothelial differentiation potential

Since CHM1 is known to be an angiogenesis inhibitor, I asked, whether down-regulation of CHM1 expression in A673 EFT cells would influence the non-VM phenotype. Therefore, stable pSIREN^{CHM1} infected A673 cells were grown on matrigel. A673 cells, which have no endothelial differentiation potential, show tube formation after constitutive suppression of CHM1 expression (**Figure 16**).

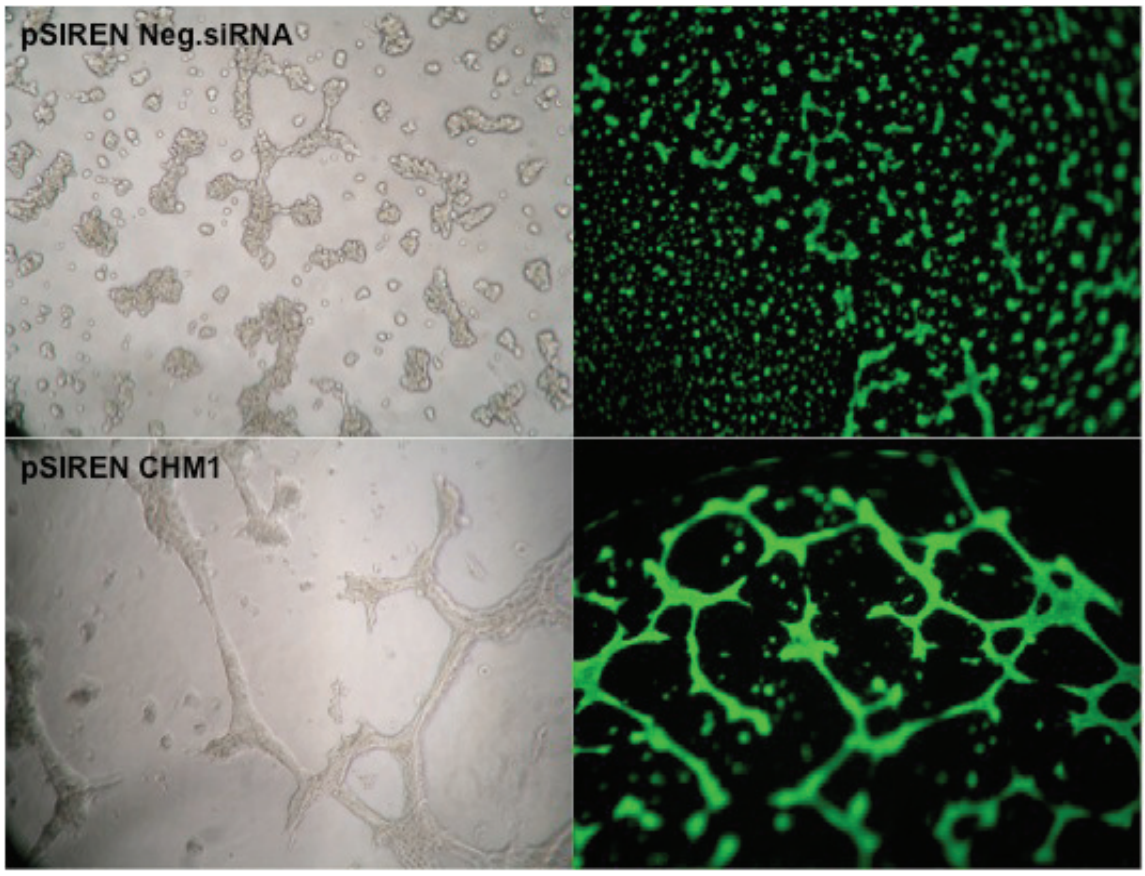

Figure 16: Tube formation assay of constitutive A673 shRNA infectants. *Left:* phase contrast microscopy at 10 x magnification. *Right:* fluorescence microscopy of calcein staining, images at 4 x magnification

To examine the role of CHM1 in endothelial differentiation of SBSR-AKS EFT cells, stable pSIREN^{CHM1} infected SBSR-AKS cells were grown on matrigel. Suppression of CHM1 had no effect on endothelial differentiation potential (**Figure 17**).

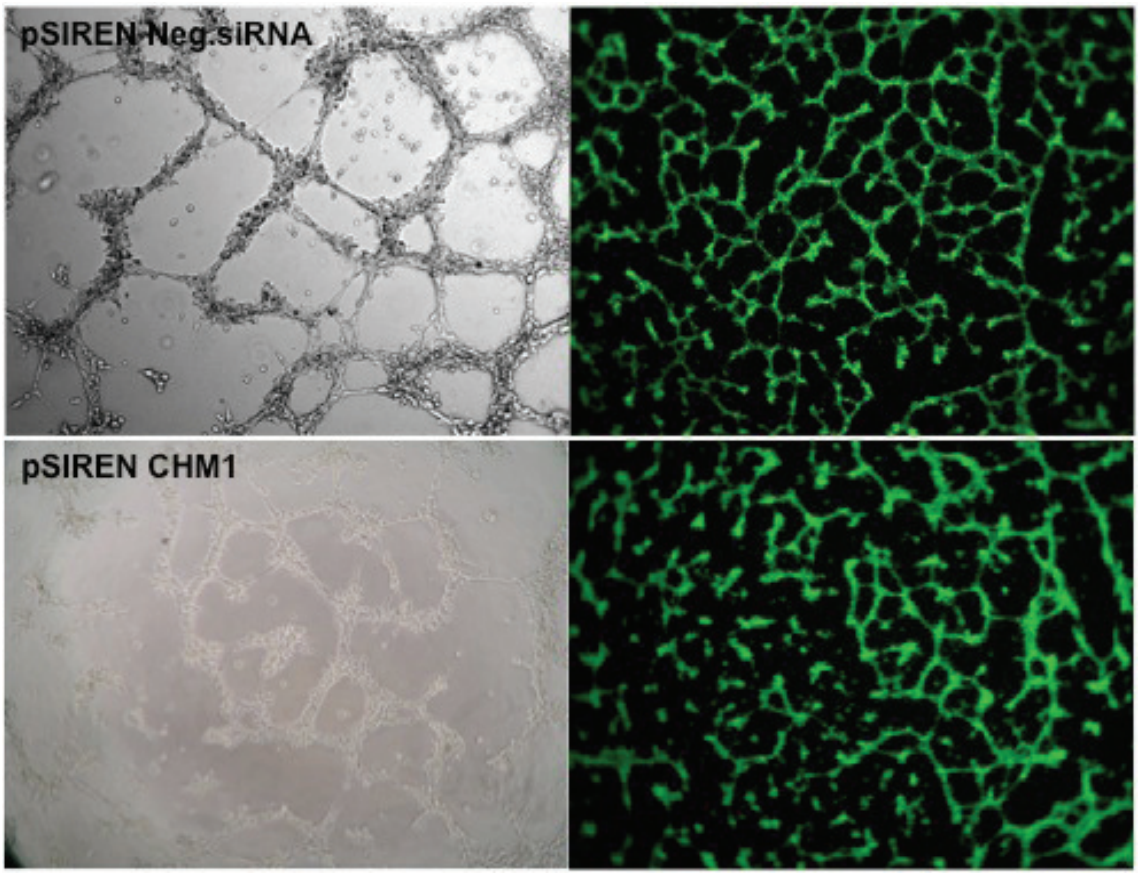

Figure 17: Tube formation assay of constitutive SBSR-AKS shRNA infectants. *Left:* phase contrast microscopy at 10 x magnification. *Right:* fluorescence microscopy of calcein staining, images at 4 x magnification

4.7.3 Influence of CHM1 on local tumor growth

To test whether CHM1 has an effect on tumorigenic growth potential of EFT cells *in vivo*, I injected stable pSIREN^{CHM1} infected SBSR-AKS cells and the respective control subcutaneously in the inguinal of immunodeficient Rag2$^{-/-}\gamma_C^{-/-}$ mice and analyzed tumor growth. As shown in **Figure 18**, suppression of CHM1 expression had no influence on local tumor growth compared to the negative control.

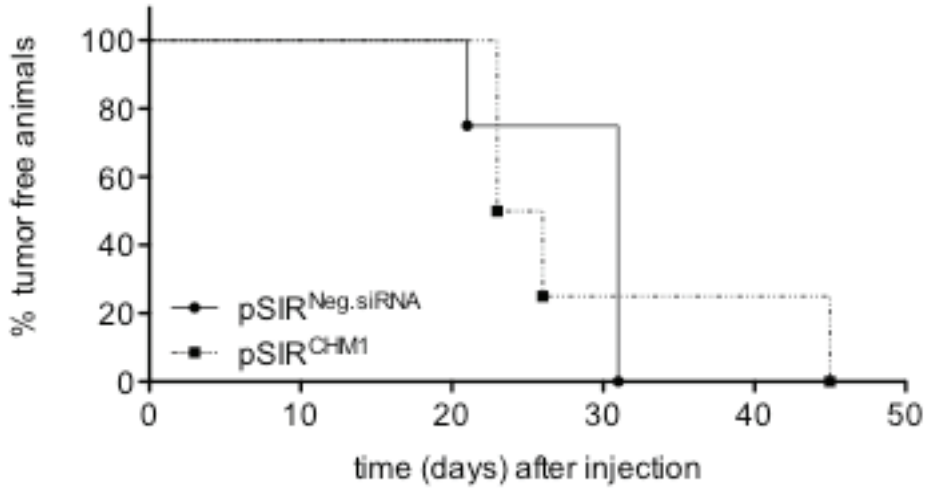

Figure 18: Kaplan-Meier plot of tumor growth experiment. Immunodeficient Rag2$^{-/-}$ ã$_C^{-/-}$ mice were injected s.c. intra-inguinal with SBSR-AKS shRNA infectants (pSIREN$^{Neg.siRNA}$ and pSIREN^{CHM1}). Mice with an average tumor size > 10 mm in diameter were considered as positive and sacrificed. Kaplan-Meier plot of one experiment with 4-5 mice / group is shown

4.7.4 Influence of CHM1 on invasive growth

To investigate the influence of CHM1 on metastatic behavior of EFT cells, I injected stable pSIREN^{CHM1} infected A673 cells and appropriate controls intravenously into the tail vein of Rag2$^{-/-}\gamma_C^{-/-}$ mice. Metastasis was strongly inhibited by suppression of CHM1 expression. While A673 control infectants grew to numerous tumor nodules within the lung, pSIREN^{CHM1} infectants revealed a considerably reduced amount of tumor nodules (**Figure 19**). No difference was observed in liver colonialization.

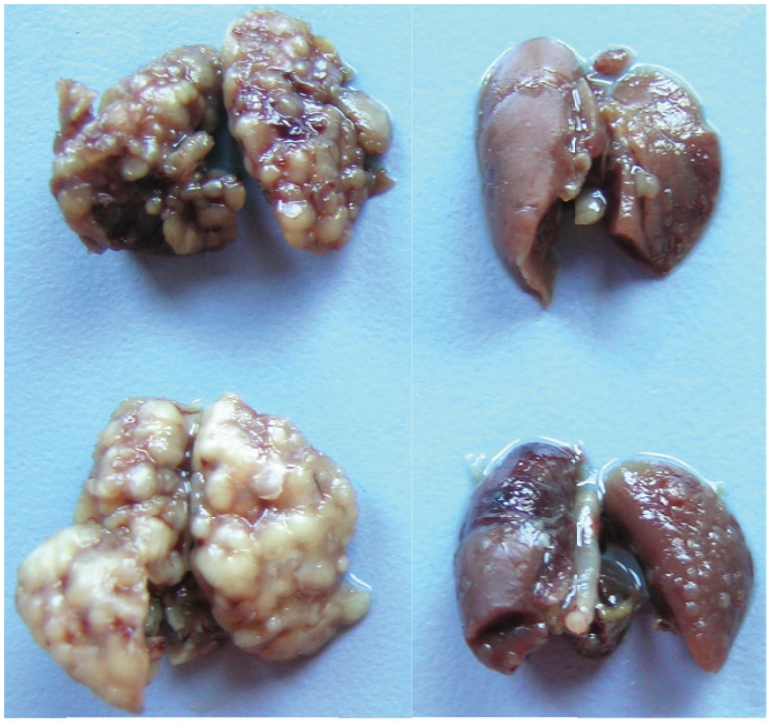

Figure 19: **Metastasized lungs of Rag2$^{-/-}$γc$^{-/-}$ mice after intravenous injection of A673 shRNA Infectants.**

Hematoxylin and Eosin (H&E) staining (**Figure 20**) demonstrated that A673 pSIREN$^{Neg.siRNA}$ affected lungs show multiple tumor nodules (1-2.5 mm) in all lobes with typical histological aspects of Ewing tumors (small-round-blue). Nodules were often confluent with necroses and showed intravascular spreading. A673 pSIREN^{CHM1} affected lungs had considerably less tumor nodules that were mainly non-necrotic with intraparenchymal, subpleural and peribronchial localization without confluence. No difference was observed in liver colonization.

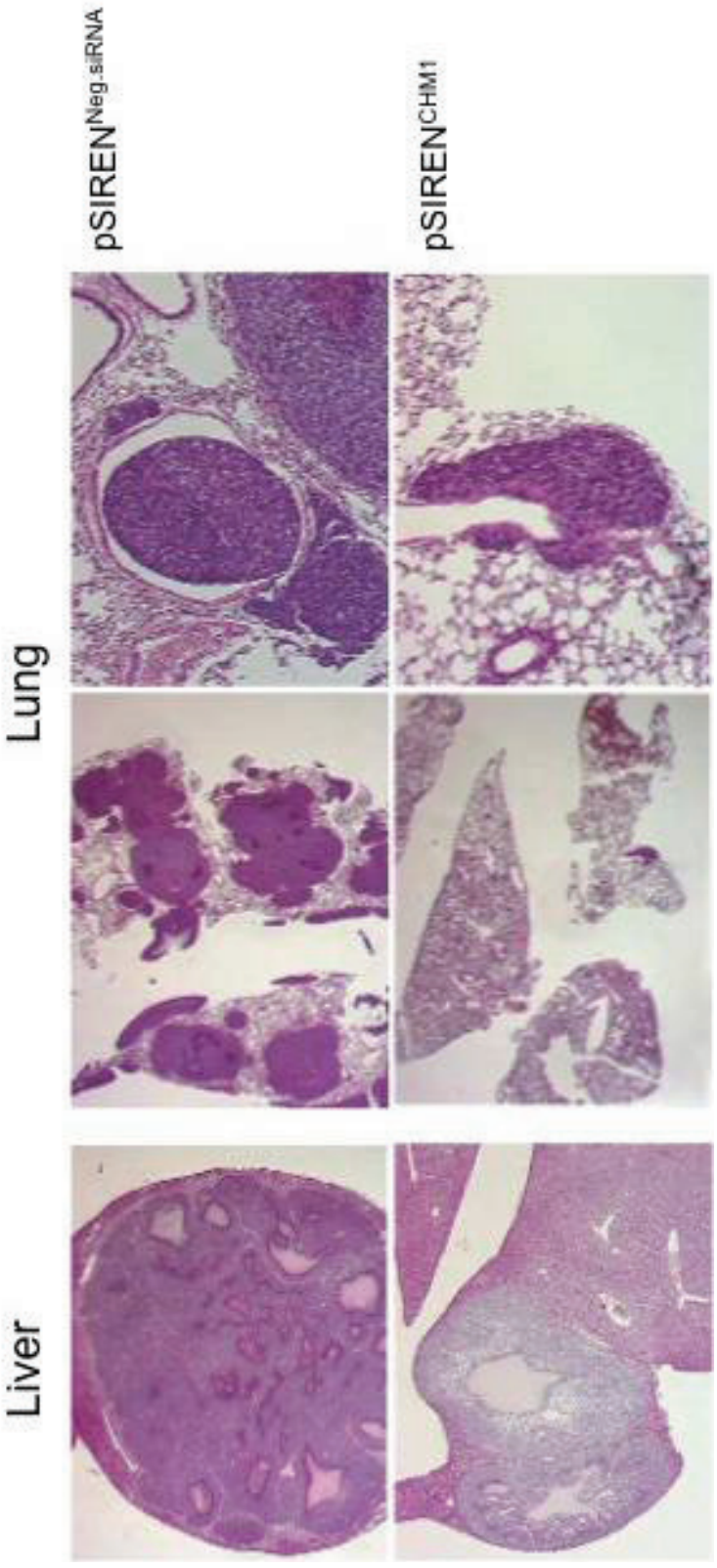

Figure 20: Hematoxylin and Eosin staining of paraffin embedded lung and liver sections from Rag2$^{-/-}$ãc$^{-/-}$ mice after intravenous injection of A673 shRNA infectants. Left panel shows low magnification of liver sections stained with H&E (magnification 2,5 x). Middle panel shows low magnification of lung sections stained with H&E (magnification 2,5 x) Right panel shows a higher magnification of the tumor cells in lung sections (magnification 20 x).

.

4.7.5 Immunohistochemistry

To address the question, whether differences in vascularization or macrophage infiltration are responsible for the reduced metastatic phenotype of CHM1 knock down EFT, immunohistochemistry was performed on sections of pSIREN$^{Neg.siRNA}$ and pSIREN^{CHM1} affected livers and lungs.

Murine CD31 staining was used to analyze blood vessel infiltration (**Figure 21**). CD31, also designated as Platelet-Endothelial Cell Adhesion Molecule (PECAM) is expressed on the membrane of endothelial cells on all murine blood vessels. Thin-walled murine-derived vessels (arrows) were found in all tumor samples. No differences were seen between pSIREN$^{Neg.siRNA}$ and pSIREN^{CHM1} EFT.

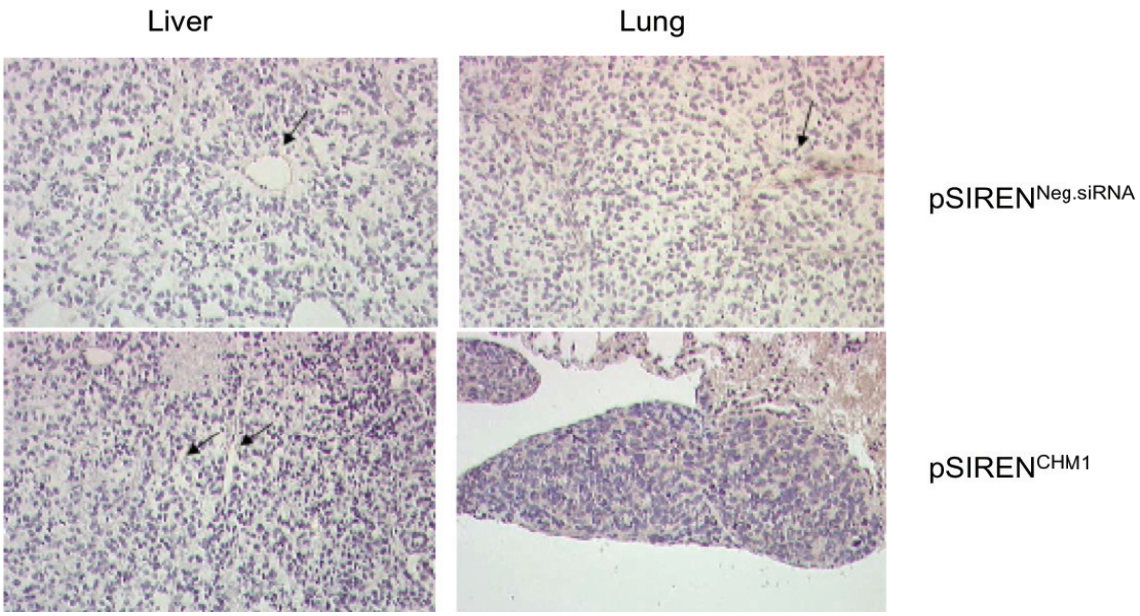

Figure 21: CD31 staining. Immunohistochemistry of paraffin embedded lung and liver sections from Rag2$^{-/-}$ã$_c^{-/-}$ mice after intravenous injection of A673 shRNA infectants. *Left panel:* CD31 staining of liver sections, (magnification 20 x). *Right panel:* CD31 staining of lung sections (magnification 20 x). Arrows indicate thin-walled vessels.

Mac-3 staining was used to investigate macrophage infiltration (**Figure 22**). Mac-3 antibody recognizes the Mac-3 antigen expressed on mouse macrophages. Tumor-infiltrating macrophages were present in both pSIREN^{CHM1} and pSIREN$^{Neg.siRNA}$ affected livers and lungs, without obvious differences. In small tumors macrophages were accumulating at the tumor borders, whereas in larger tumor nodules they were also found within the tumor mass.

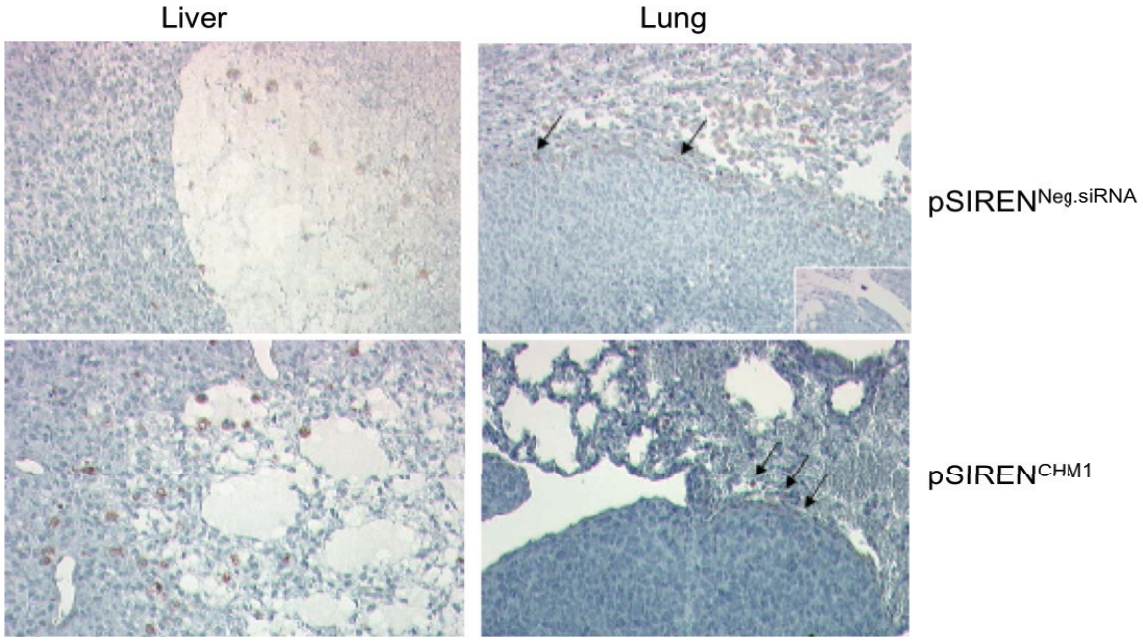

Figure 22: Mac-3 staining. Immunohistochemistry of paraffin embedded lung and liver sections of Rag2$^{-/-}$ã$_c^{-/-}$ after intravenous injection of A673 shRNA infectants. *Left panel:* Mac-3 staining of liver sections, (magnification 10 x). *Right panel:* Mac-3 staining of lung sections (magnification 10 x). Arrows indicate tumor-infiltrating macrophages (brown). Blue background staining due to treatment of H&E stained sections prior to CD31 staining.

4.8 Analysis of GPR64

4.8.1 Influence of EWS/FLI-1 on GPR64 expression

To address the question, if GPR64 expression is directly induced by EWS/FLI-1, I analyzed stable EWS/FLI-1 cDNA transfected MSCs (see 4.4) for GPR64 expression. I observed an increase of GPR64 expression that appeared to be dose dependent on EWS/FLI-1 expression (**Figure 23**). MSC clone L87 #3 however did not show an induction of GPR64 expression.

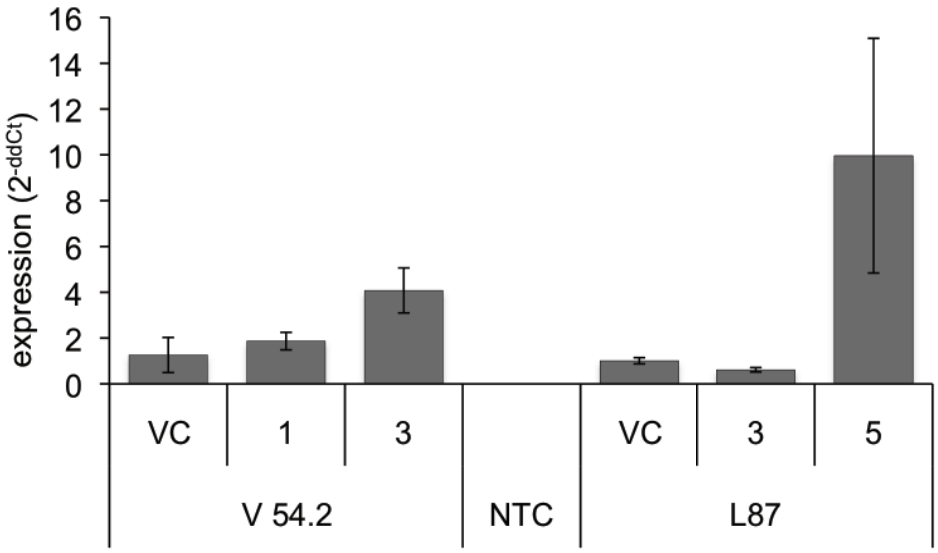

Figure 23: Influence of EWS/FLI-1 fusion protein on GPR64 expression. qRT-PCR of GPR64 mRNA expression in EWS/FLI-1 transfected MSC clones. NTC: non-template control, Error bars represent the mean ± standard deviation of duplicates.

To further evaluate, whether GPR64 expression in EFT is regulated by EWS/FLI-1, I transiently transfected EFT cell lines A673 and SBSR-AKS with EWS/FLI-1 siRNA (see Materials and Methods) and analyzed GPR64 expression 48 hours after transfection. As shown in **Figure 24**, GPR64 expression was not affected in a clear pattern by EWS/FLI-1 knock down. In EWS/FLI-1 siRNA transfected cells, GPR64 expression is induced, whereas EWS/FLI-1 expression knock down in SBSR-AKS has no effect on GPR64 expression.

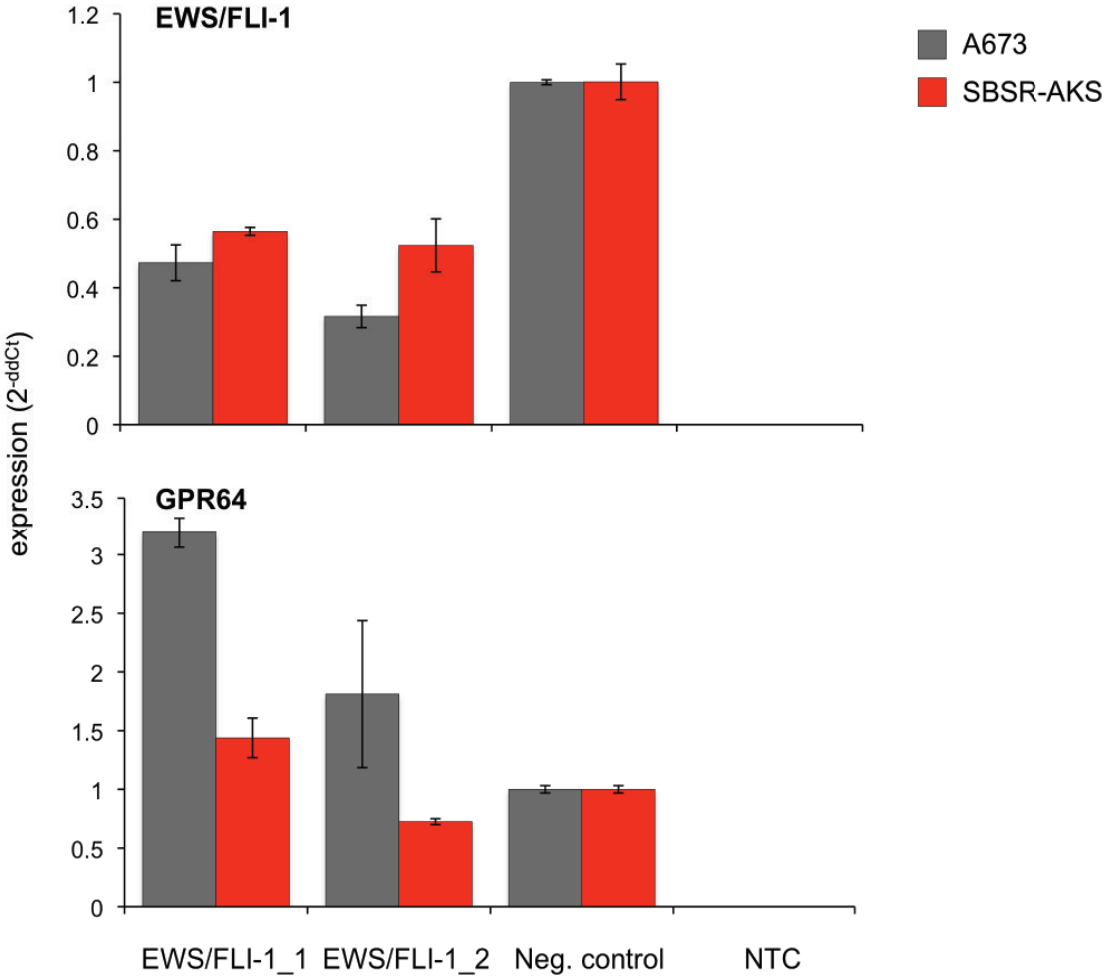

Figure 24: **Affection of GPR64 expression by EWS/FLI-1 knock down.** mRNA expression analysis (qRT-PCR) 48 hours after transfection. *Upper panel:* EWS/FLI-1 expression; *Lower panel:* GPR64 expression; EWS/FLI-1_1 and EWS/FLI-1_2 are different siRNAs, Neg.siRNA: non-silencing siRNA. NTC: non-template control; Error bars represent the mean ± standard deviation of duplicates.

4.8.2 Microarray Analysis of EFT after suppression of GPR64

GPR64 is an orphan receptor with yet unknown ligand. To identify possible downstream targets of GPR64, we performed microarray analysis with transient CHM1 and GPR64 siRNA transfected A673 and SBSR-AKS cells (**Figure 25**). This analysis revealed a GPR64 regulated subset of genes with putative central role in tumor angiogenesis and invasiveness.

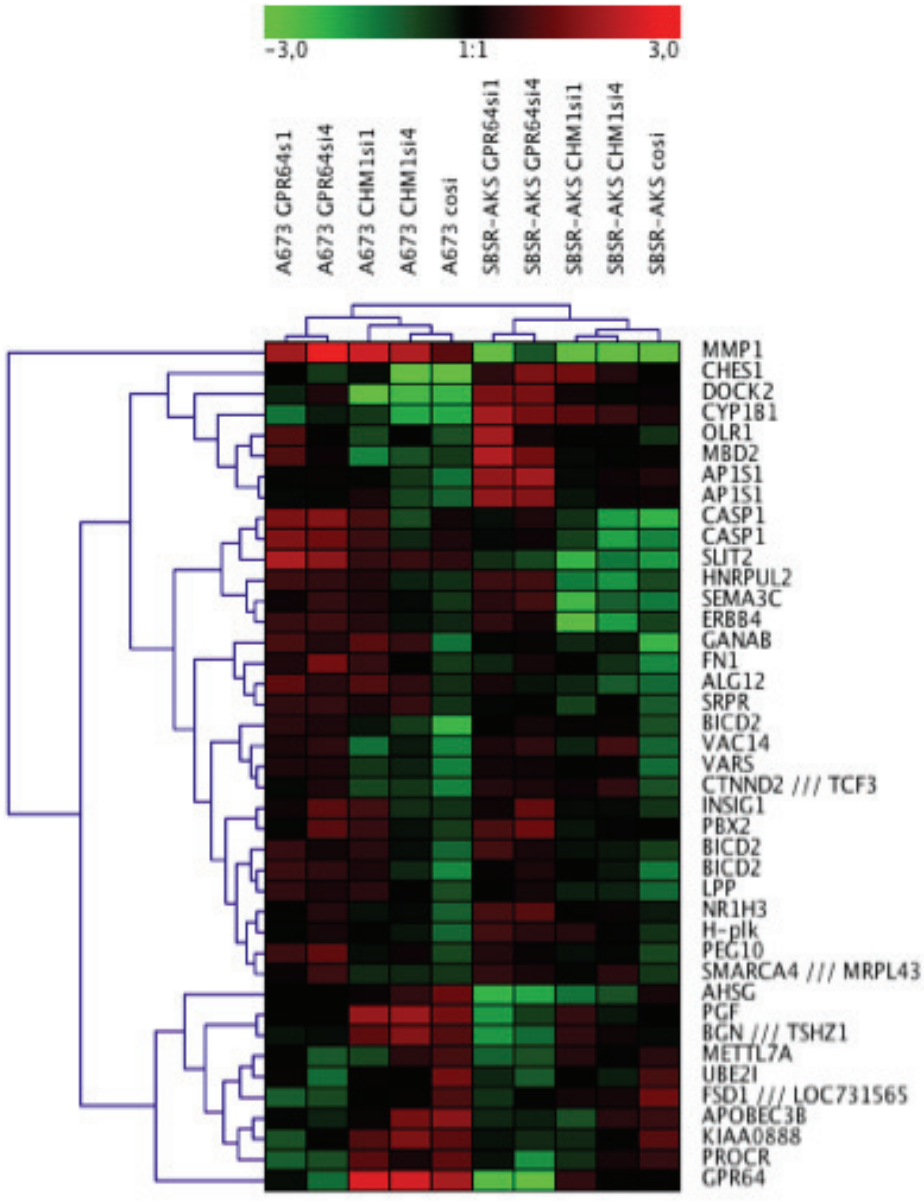

Figure 25: Microarray data of selected genes with their normalized fluorescence signal intensities. Combined results of 2 independent experiments with RNA derived from transient transfection with different siRNAs are shown. Each column represents 1 individual array (Data initially obtained by Sabine Rössler and Colette Zobywalski).

Most prominently, microarray analysis revealed Placental growth factor (PGF) expression to be suppressed upon transient down regulation of GPR64 in A673 and SBSR-AKS EFT cells (**Figure 26**). PGF is a member of the VEGF family of growth factors, which exclusively binds to VEGFR-1. PGF-VEGFR-1 interactions are important in promotion of tumor growth [79] and angiogenesis [80, 81] as described previously. Blocking experiments with a specific PGF antibody proved to inhibit growth and metastasis of various tumors, including those that showed VEGFR-Inhibitor resistance, without affecting healthy vessels [82].

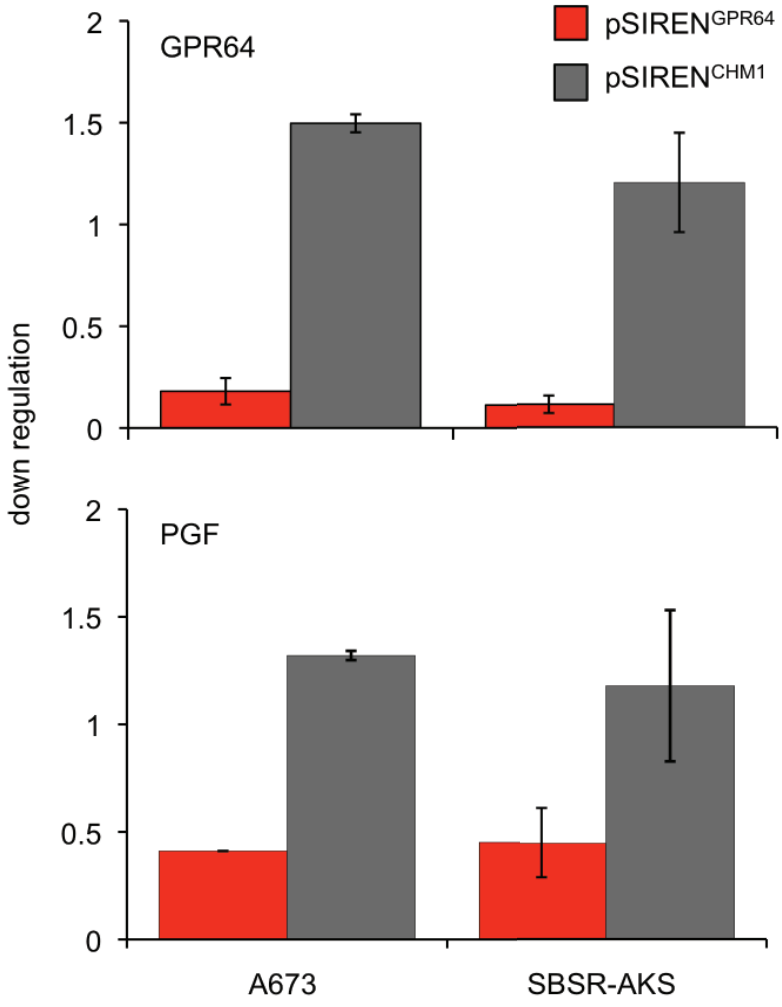

Figure 26: Specific suppression of PGF expression after transient GPR64 knock down. Individual expression profile of selected genes based on microarray analysis of transient GPR64 siRNA transfected cell lines A673 and SBSR-AKS. *Upper panel:* specific GPR64 expression knock down (red) 48 hours after transient GPR64 siRNA transfection compared to CHM1 siRNA transfected cells (gray); *Lower panel:* Down-regulation of GPR64 specifically suppresses PGF expression (red) as compared to CHM1 siRNA (gray).

4.8.3 Influence of EWS/FLI-1on PGF expression

When I analyzed stable EWS/FLI-1 cDNA transfected MSCs (see 4.4) for PGF expression I observed an increase of PGF that appeared dose dependent of EWS/FLI-1 expression (**Figure 27**).

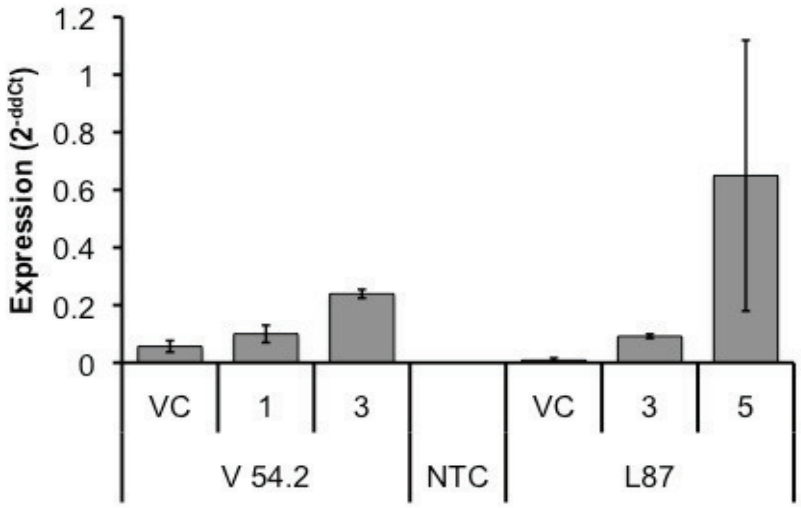

Figure 27: Influence of EWS/FLI-1 fusion protein on PGF expression. qRT-PCR of PGF mRNA expression in EWS/FLI-1 transfected MSC clones; Error bars represent the mean ± standard deviation of duplicates.

To further evaluate, if PGF expression in EFT is regulated via EWS/FLI-1, I transiently transfected EFT cell lines A673 and SBSR-AKS with EWS/FLI-1 siRNA (see Materials and Methods) and analyzed PGF expression 48 hours after transfection. As shown in **Figure 28**, this analysis provided conflicting results, since knock down of EWS/FLI-1 expression in A673 induced PGF expression, whereas in SBSR-AKS EWS/FLI-1 down-regulation caused suppression of PGF expression.

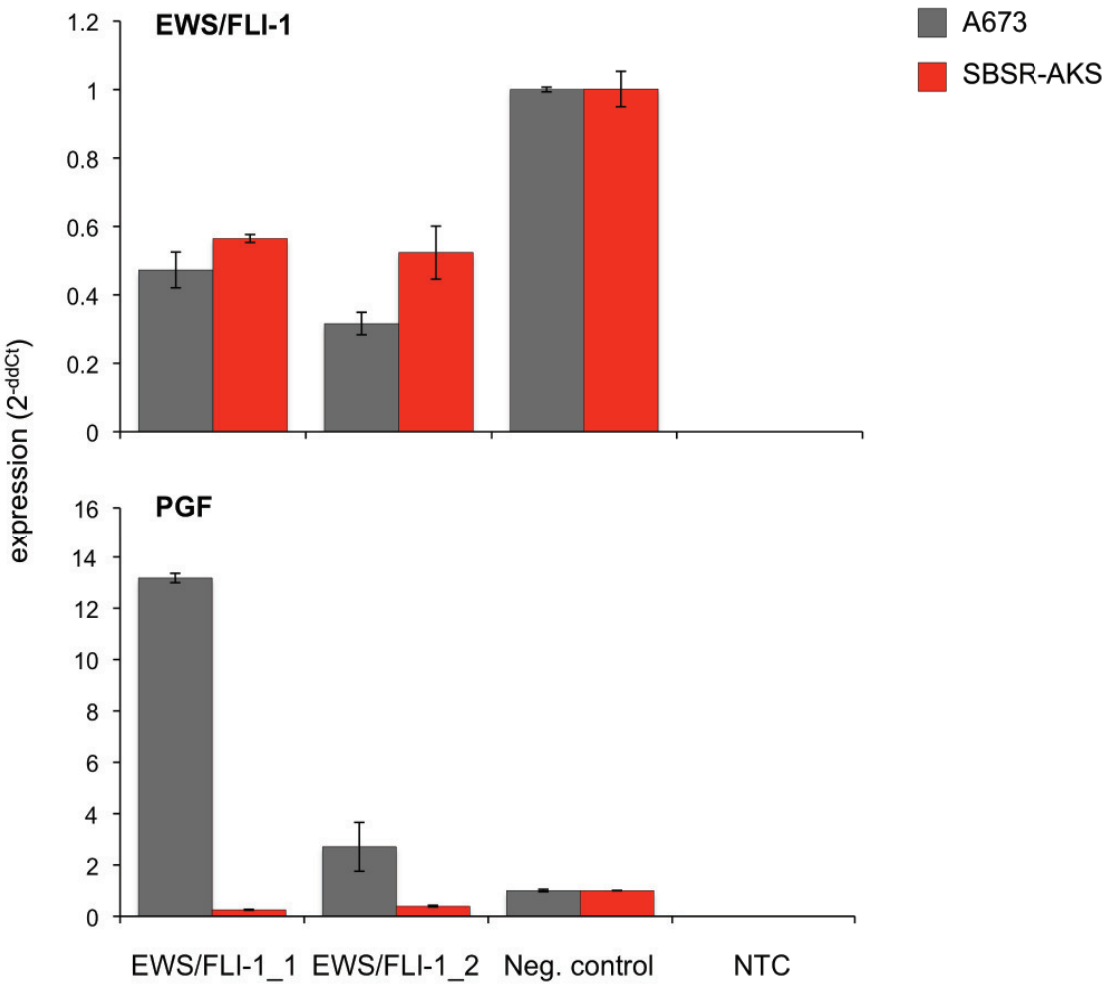

Figure 28: Affection of PGF expression by EWS/FLI-1 knock down. mRNA expression analysis (qRT-PCR) 48 hours after transfection. *Upper panel:* EWS/FLI-1 expression; *Lower panel*: PGF expression; EWS/FLI-1_1 and EWS/FLI-1_2 are different siRNAs, Neg.siRNA: non-silencing siRNA. NTC: non-template control; Error bars represent the mean ± standard deviation of duplicates.

4.8.4 Knock down of PGF gene expression

To further investigate, if PGF is a direct target of GPR64 and if the suppression of PGF expression showed a phenotype of EFT similar to the one observed after GPR64 knock down, I down regulated PGF expression in EFT cells by RNA interference. For expression knock down of PGF, the siRNAs Hs_PGF_1 and Hs_PGF_3 were used (see Materials and Methods). 48 hours after transfection, PGF expression was analyzed by qRT-PCR using specific PGF primer assay (**Figure 29**). PGF expression was validated against the expression of the housekeeping gene *GAPDH*.

The transfection with siRNA PGF_1 resulted in a down-regulation of PGF expression to levels 7-10 % of normal values of siRNA control transfectants in both cell lines. Transfection with siRNA PGF_3 enabled a down regulation of PGF expression to levels 2-5 % of normal values siRNA control transfectants in both cell lines. An unspecific induction of an interferon response was not observed for both siRNAs. The siRNA PGF_3 was used for generation of stable shRNA infectants (see 4.6.1).

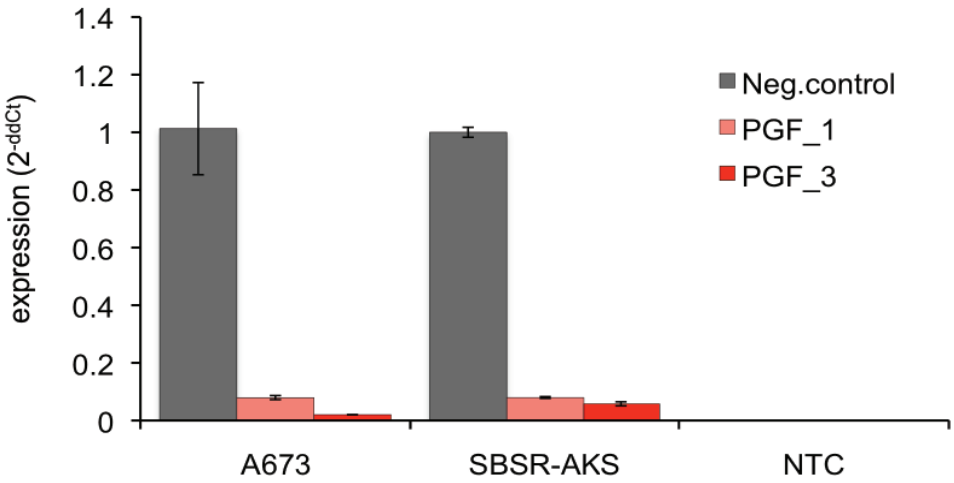

Figure 29: Transient PGF siRNA Transfection. mRNA expression analysis (qRT-PCR) 48 hours after transfection. PGF_1 and PGF_3 are different siRNAs, Neg.control: non-silencing siRNA. NTC: non-template control; Error bars represent the mean ± standard deviation of duplicates.

The oligonucleotide based on siRNA PGF_3 was cloned into the expression vector pSIREN RetroQ and the resulting pSIREN^{PGF} construct introduced into A673 and SBSR-AKS cells by retroviral gene transfer. PGF expression was analyzed by qRT-PCR using a specific PGF primer assay. PGF expression was validated against the expression of the housekeeping gene *GAPDH*.

Stable transfection resulted in a down-regulation of PGF expression to 5-20 % of normal values of siRNA control transfectants in both cell lines (**Figure 30**). An unspecific induction of an interferon response was not observed.

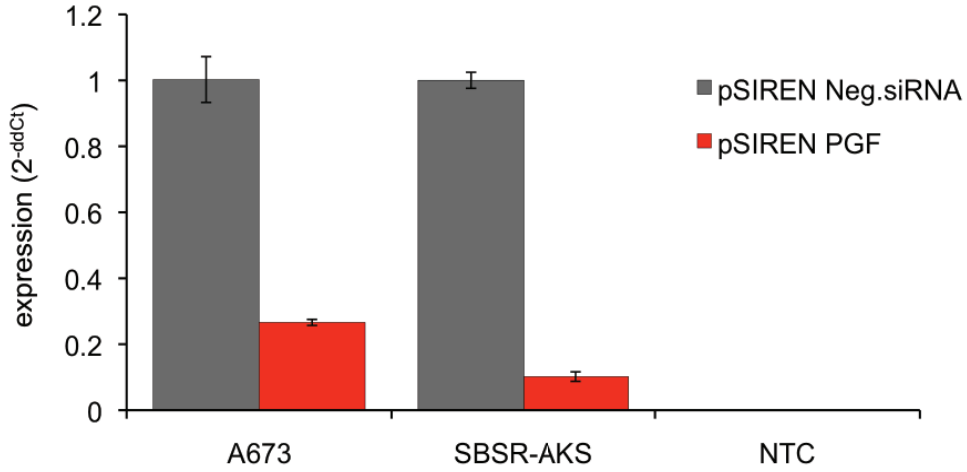

Figure 30: PGF mRNA expression in EFT cell lines after constitutive down-regulation. assessed by qRT-PCR. NTC: non-template control; Error bars represent the mean ± standard deviation of duplicates.

4.8.5 Influence of GPR64 and PGF on endothelial differentiation potential

To examine the role of GPR64 and PGF in endothelial differentiation of SBSR-AKS EFT cells, stable pSIREN^{GPR64} and pSIREN^{PGF} infected SBSR-AKS cells were grown on Matrigel. SBSR-AKS cells were unable to form tubes after suppression of GPR64 and PGF expression (**Figure 31**).

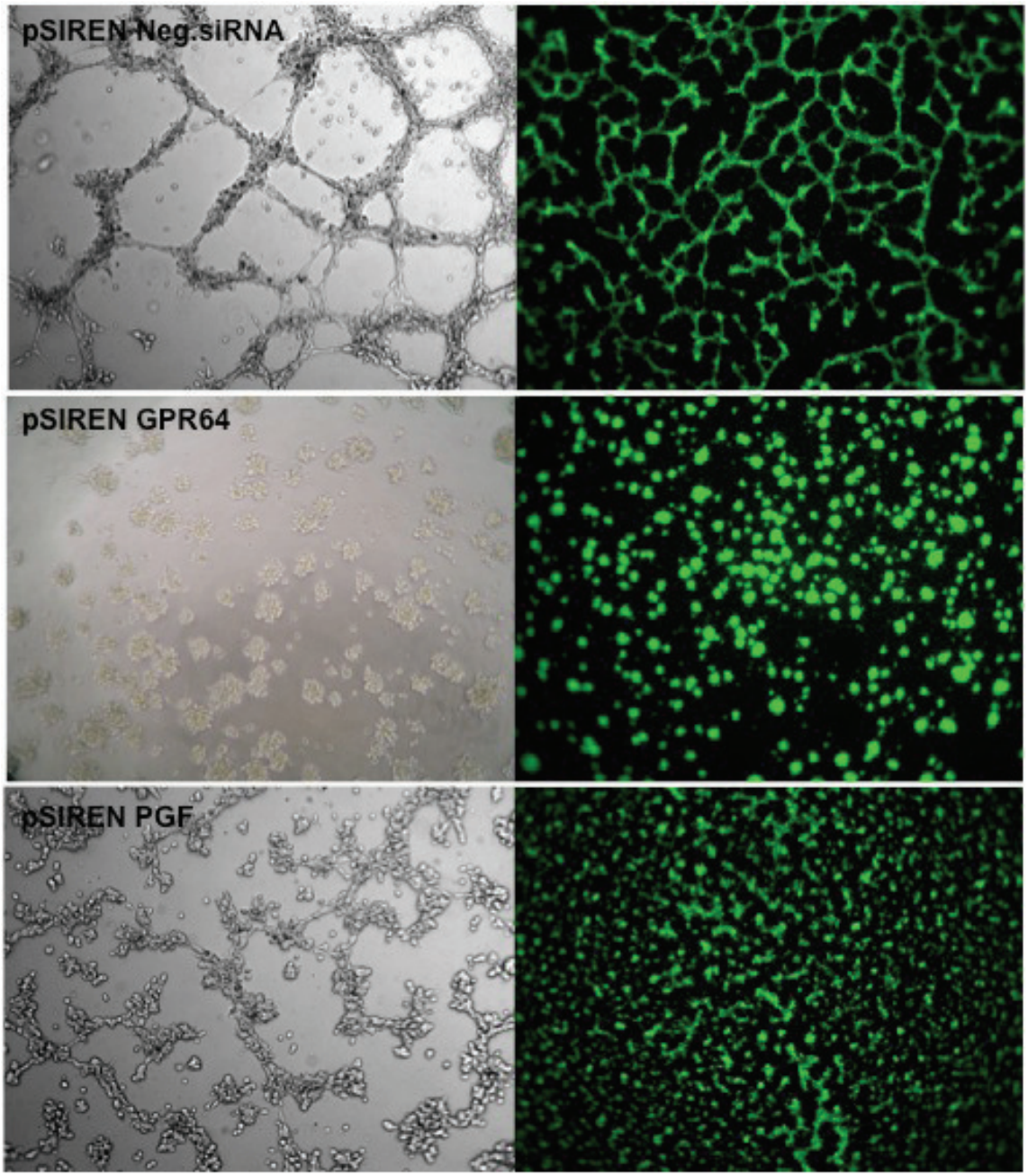

Figure 31: Tube formation assay of constitutive SBSR-AKS shRNA infectants. *Left:* phase contrast microscopy at 10 x magnification. *Right:* fluorescence microscopy of calcein staining, images at 4 x magnification

4.8.6 Influence of GPR64 and PGF on local tumor growth

To test whether GPR64 and PGF had an effect on tumor growth of EFT cells *in vivo*, I injected stable pSIREN^{GPR64} and pSIREN ^{PGF} infected SBSR-AKS cells and the respective controls subcutaneously in the inguinal of immunodeficient Rag2$^{-/-}\gamma_C^{-/-}$ mice and analyzed tumor growth. As shown in **Figure 32**, suppression of GPR64 expression resulted in a complete inhibition of tumor growth up to 50 days, whereas knock down of PGF expression had no prominent effect compared to negative control.

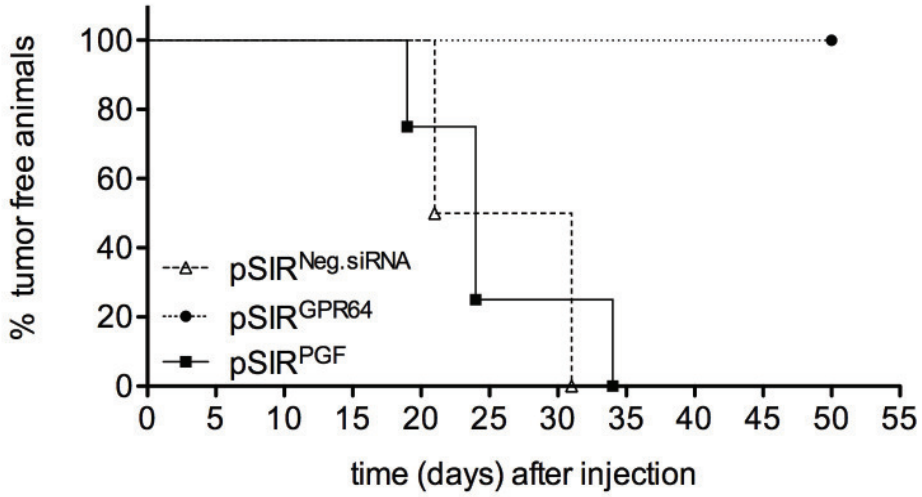

Figure 32: Kaplan-Meier plot of tumor growth experiment. Immunodeficient Rag2$^{-/-}$ ã$_C^{-/-}$ mice were injected s.c. intra-inguinal with SBSR-AKS shRNA infectants (pSIREN$^{Neg.siRNA}$, pSIREN^{GPR64} and pSIREN^{PGF}). Mice with an average tumor size > 10 mm in diameter were considered as positive and sacrificed. Kaplan-Meier plot of one experiment with 4-5 mice / group is shown.

4.8.7 Influence of GPR64 and PGF on invasive growth

To investigate the influence of GPR64 and PGF on metastatic behavior of EFT cells, I injected stable pSIREN^{GPR64} and pSIREN^{PGF} infected A673 cells and appropriate controls intravenously into the tail vein of Rag2$^{-/-}\gamma_C^{-/-}$ mice. Metastasis was strongly inhibited by suppression of GPR64 and PGF expression, as shown in **Figure 33**. While A673 control infectants grew to numerous tumor nodules within the lung, pSIREN^{GPR64} and pSIREN^{PGF} infectants demonstrated a clearly reduced metastatic phenotype. A673 pSIREN^{GPR64} affected lungs were macroscopically normal.

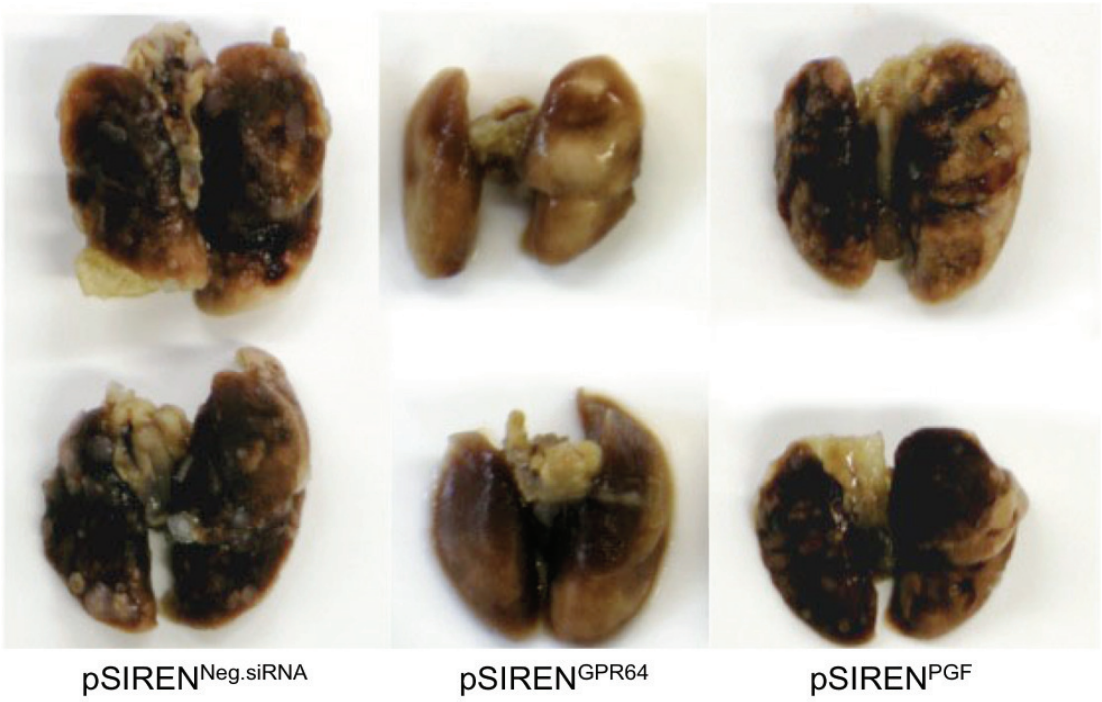

Figure 33: Metastasized lungs of Rag2$^{-/-}\gamma_C^{-/-}$ mice after intravenous injection of A673 shRNA infectants.

H&E staining (**Figure 34**) revealed that A673 pSIREN$^{Neg.siRNA}$ affected lungs show multiple tumor nodules (1-2.5 mm) in all lobes with typical histological aspect of Ewing tumors (small-round-blue). Nodules were often confluent with necroses and showed intravascular spreading. A673 pSIREN^{GPR64} and pSIREN^{PGF} affected lungs revealed only 5-6 small non-necrotic tumor nodules with intraparenchymal, subpleural and peribronchial localization without confluence. No differences were found in liver colonization.

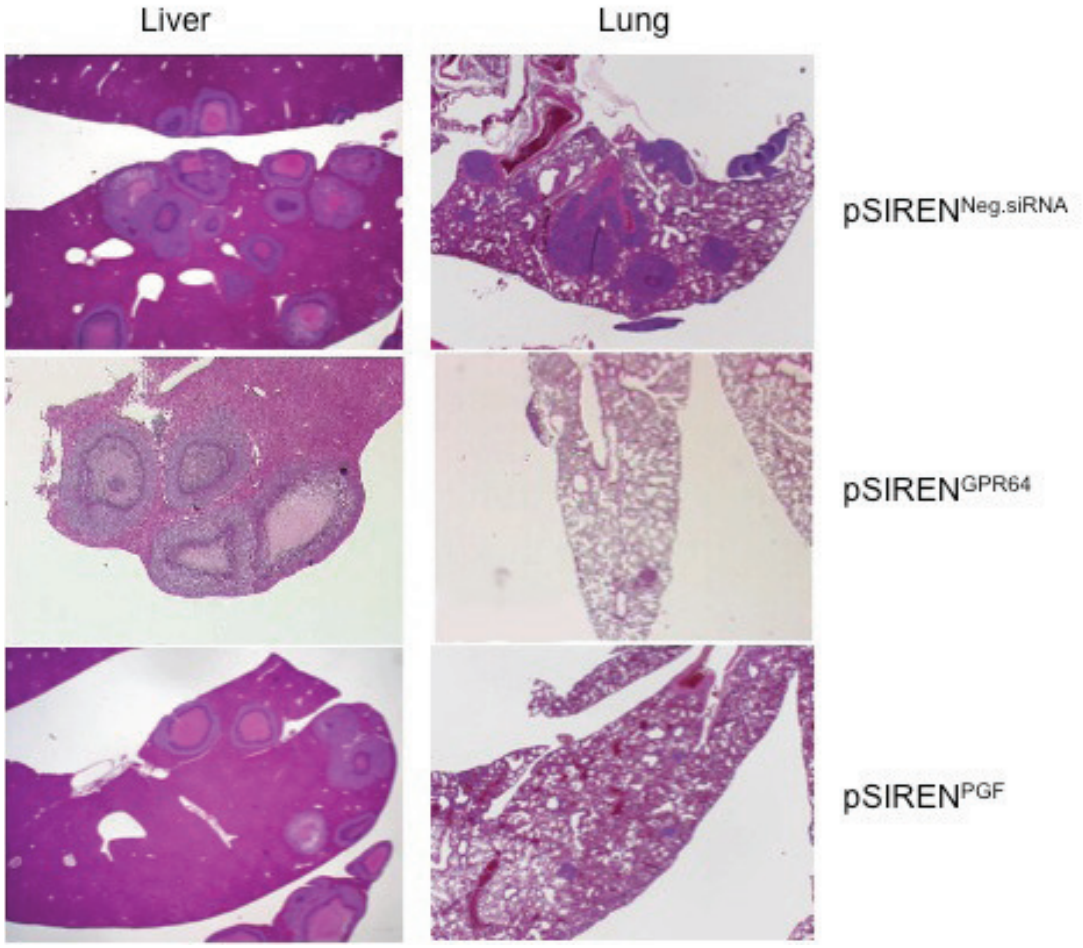

Figure 34: Hematoxylin and Eosin staining of paraffin embedded lung and liver sections of Rag2$^{-/-}\gamma_c^{-/-}$ mice after intravenous injection of A673 shRNA infectants. Left panel shows liver sections stained with Hematoxylin and Eosin (magnification 2,5 x). Right panel shows lung sections stained with Hematoxylin and Eosin (magnification 2,5 x)

4.8.8 Immunohistochemistry

To address the question, whether differences in vascularization or macrophage infiltration are responsible for the reduced metastatic phenotype of GPR64 and PGF knock down cells, immunohistochemistry was performed on sections of pSIREN$^{Neg.siRNA}$ pSIREN^{GPR64} and pSIREN^{PGF} affected organs.

Again, murine CD31 staining was used to analyze blood vessel infiltration. Thin-walled vessels (arrows) were found in all liver sections. No differences were seen between pSIREN$^{Neg.siRNA}$, pSIREN^{GPR64} and pSIREN^{PGF} (**Figure 35**).

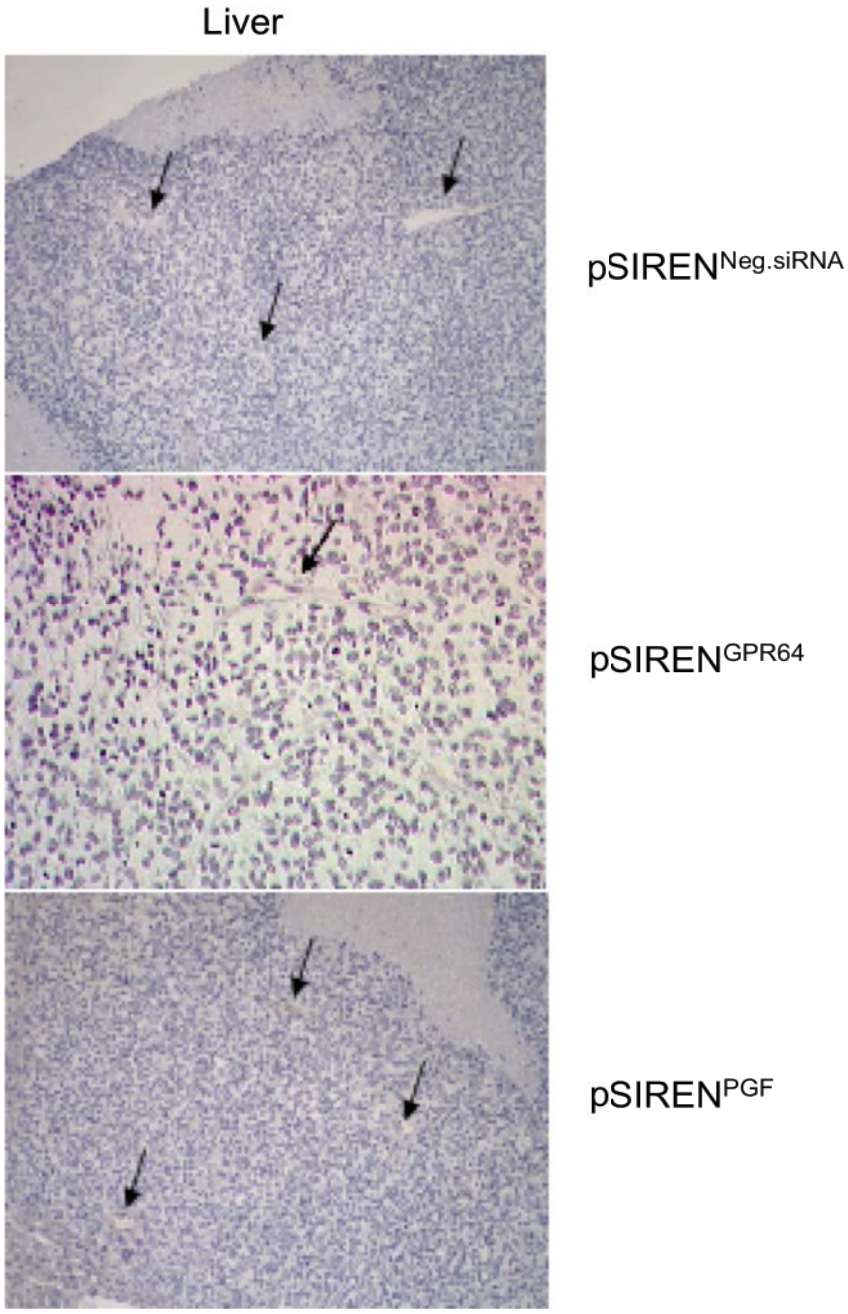

Figure 35: CD31 staining of paraffin embedded liver sections from Rag2$^{-/-}\gamma_c^{-/-}$ mice after intravenous injection of A673 shRNA infectants. pSIREN$^{Neg.siRNA}$: magnification 10 x, pSIREN^{GPR64} : magnification 20 x, pSIREN^{PGF} : magnification 10 x; Arrows indicate thin-walled vessels

Thin-walled vessels (arrows) were also found in all lung sections (**Figure 36**). No differences were seen between pSIREN$^{Neg.siRNA}$ and pSIREN^{PGF}. pSIREN^{GPR64} affected lungs could not be analyzed, since after serial sectioning of pSIREN^{GPR64} affected lungs, no further tumor nodules were detected.

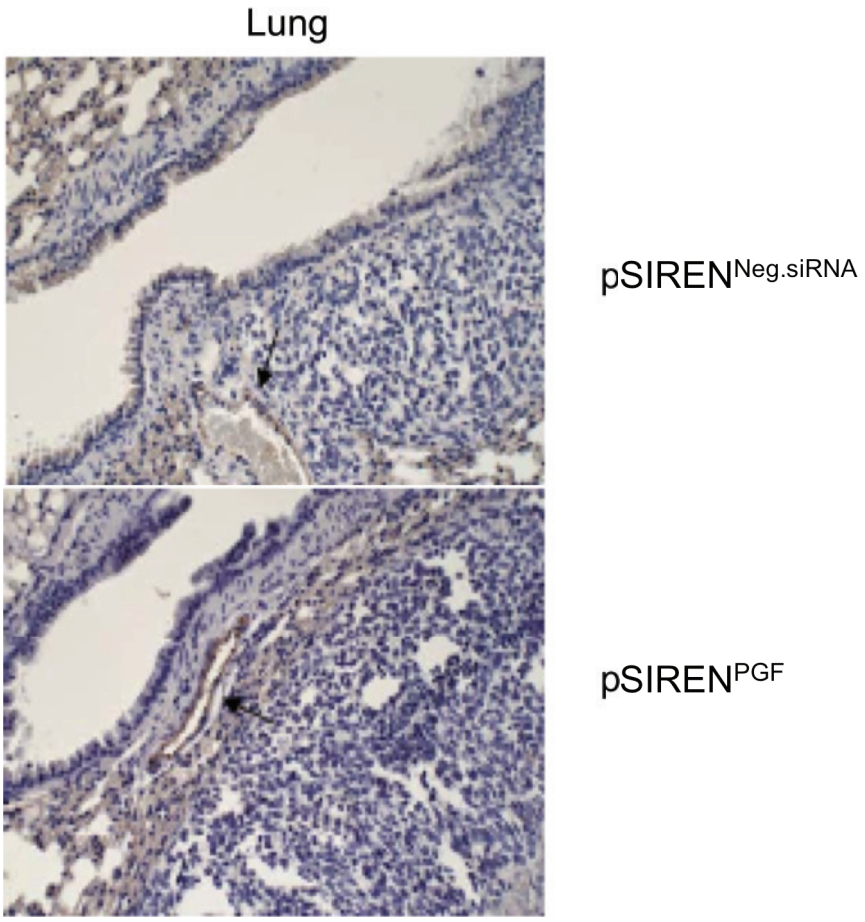

Figure 36: CD31 staining of paraffin embedded lung sections from Rag2$^{-/-}\gamma_c^{-/-}$ mice after intravenous injection of A673 shRNA infectants. Arrows indicate thin-walled vessels (magnification 20 x). Blue background staining due to treatment of H&E stained sections prior to CD31 staining

Mac-3 staining was used to analyze macrophage infiltration. Tumor-infiltrating macrophages were present in all liver sections without obvious differences between pSIREN$^{Neg.siRNA}$, pSIREN^{GPR64} and pSIREN^{PGF} (**Figure 37**). In small tumors macrophages were accumulating at the tumor borders, whereas in larger tumor nodules they were also found within the tumor mass.

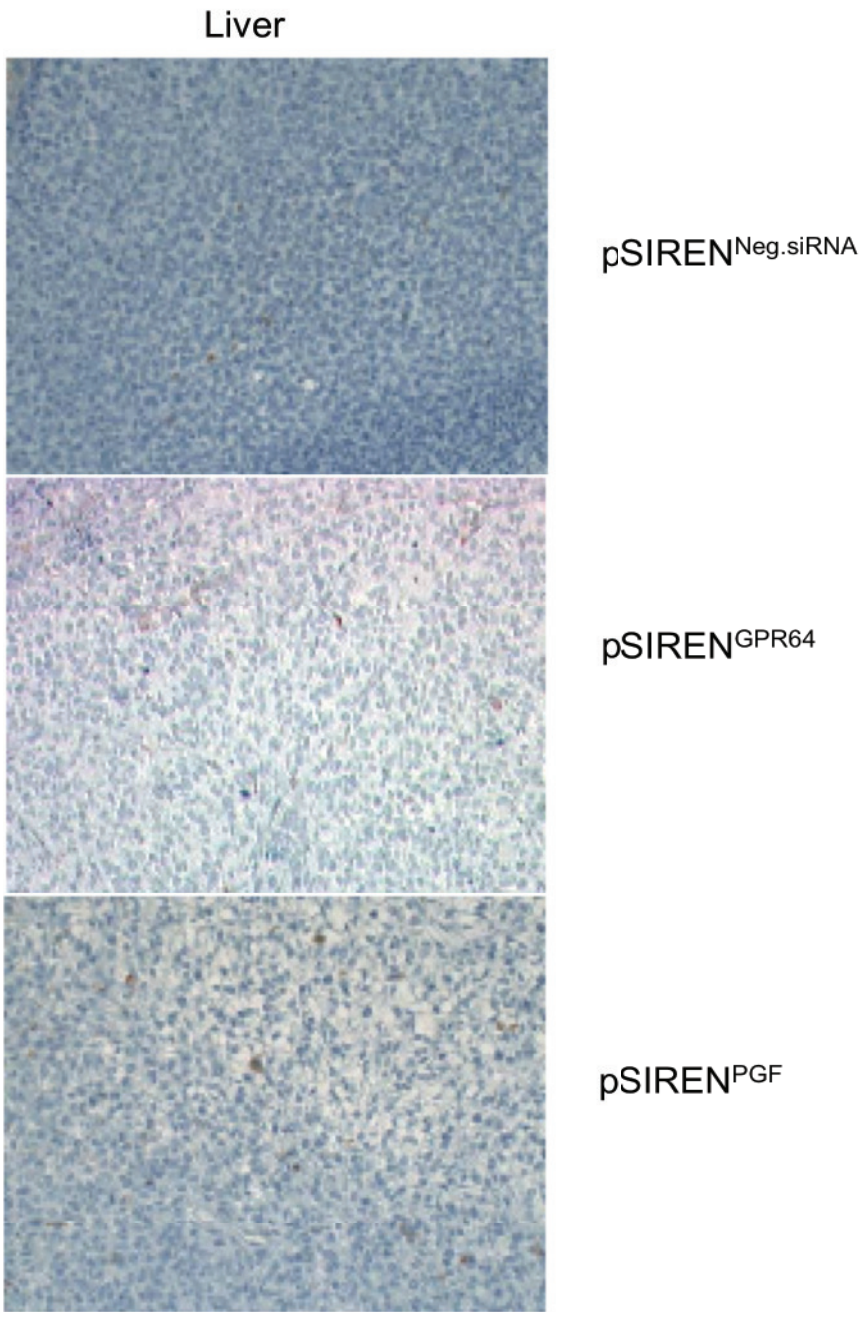

Figure 37: Mac-3 staining of paraffin embedded liver sections of Rag2$^{-/-}\gamma_c^{-/-}$ after intravenous injection of A673 shRNA infectants (magnification 20 x). Blue background staining due to treatment of H&E stained sections prior to CD31 staining.

Tumor infiltrating macrophages were found in all lung sections (**Figure 38**). No differences were seen between pSIREN$^{Neg.siRNA}$ and pSIREN^{PGF}. Again, pSIREN^{GPR64} affected lungs could not be analyzed, since after serial sectioning of pSIREN^{GPR64} affected lungs, no further tumor nodules were detected

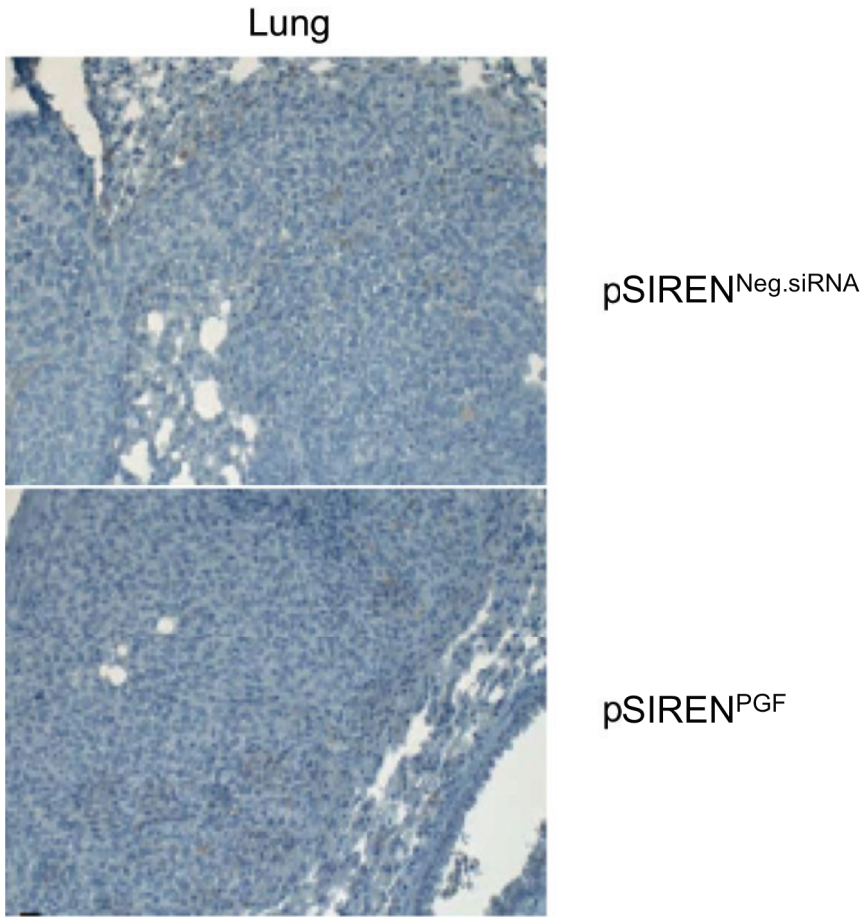

Figure 38: Mac-3 staining of paraffin embedded lung sections of Rag2$^{-/-}\gamma_c^{-/-}$ after intravenous injection of A673 shRNA infectants (magnification 20 x). Blue background staining due to treatment of H&E stained sections prior to CD31 staining.

4.8.9 GPR64 mediated MMP-1 expression

By means of the phenotype of EFT observed after GPR64 knock down, I asked, whether GPR64 could be involved in the regulation of Matrix Metalloproteinases (MMP) or their inhibitors, tissue inhibitors of metalloproteinases (TIMPs). MMPs are a large family of zinc-dependent endopeptidases with crucial roles in cellular processes as angiogenesis, migration and invasion. I analyzed the expression of two MMPs and one TIMP with central roles in invasiveness and angiogenesis in GPR64 knock down EFT cells.

MMP-10 over-expression is associated with anchorage-independent growth and invasiveness of lung cancer cells [83]. Furthermore, it is known to degrade various components of the extracellular matrix and is inducible in lymphoma cells and accelerates the growth of lymphoid tumors *in vivo* [84].

TIMP4 over-expression has been shown to correlate with inhibited invasiveness and tumor growth of human breast cancer cells [85].

MMP-1 has been described to account for the assembly of new tumor blood vessels, the release of tumor cells into the circulation, and the breaching of lung capillaries by circulating tumor cells to seed pulmonary metastasis, when expressed in human breast cancer cells [86]. Furthermore, EWS/FLI-1 has been shown to interact and activate the MMP-1 promoter *in vitro* [87].

The expression analysis of GPR64 knock down in EFT cells revealed MMP-1 expression to be suppressed upon down regulation of GPR64 in A673 and SBSR-AKS EFT cells, whereas the expression of MMP-10 and TIMP-4 followed no clear pattern (**Figure 39**).

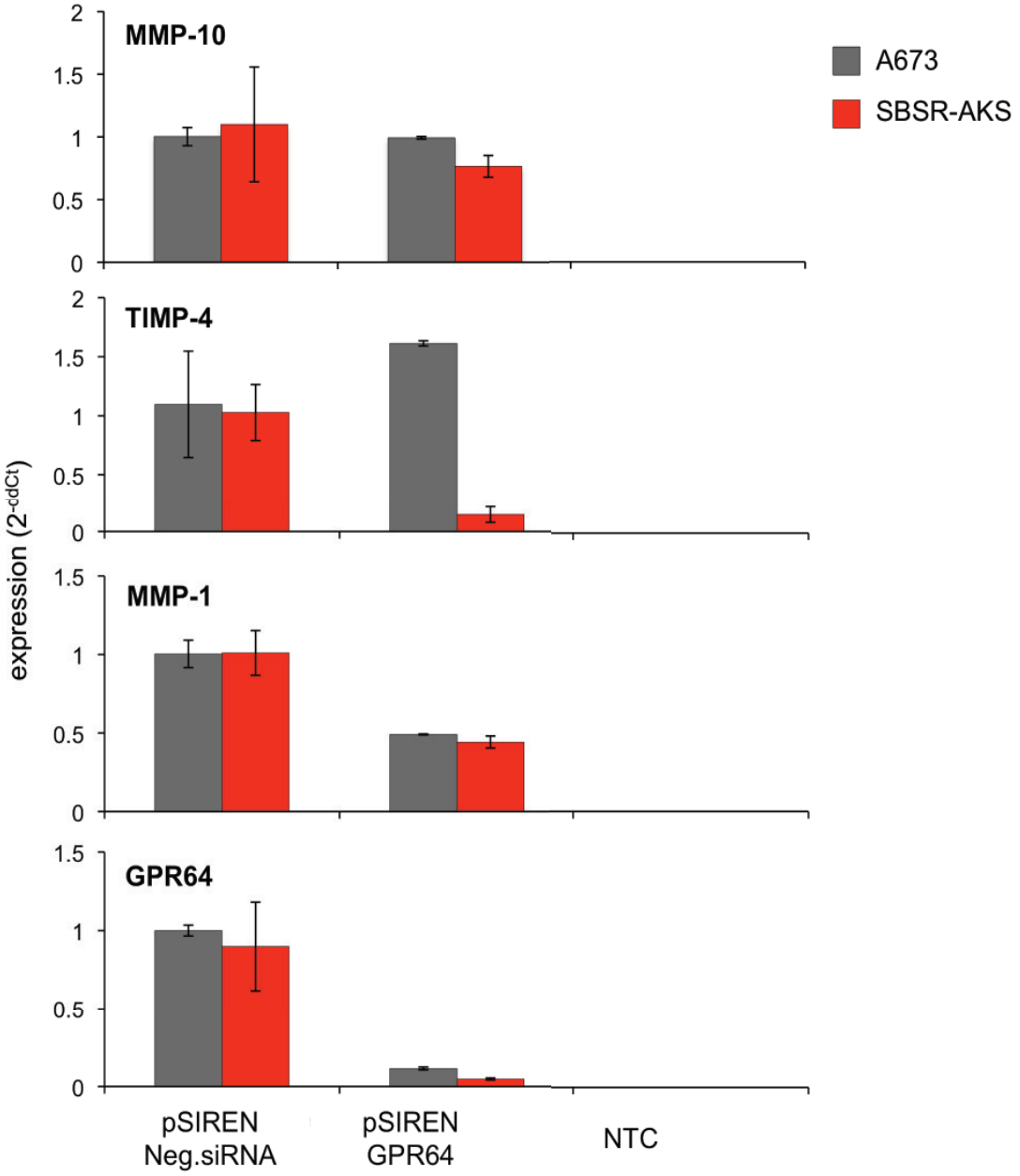

Figure 39: MMP-10, TIMP-4 and MMP-1 mRNA expression in constitutive A673 (gray) and SBSR-AKS (red) GPR64 shRNA infectants assessed by qRT-PCR. GPR64 mRNA expression knock down is shown at the bottom; Error bars represent the mean ± standard deviation of duplicates.

4.8.10 Influence of EWS/FLI-1 on MMP-1 expression

To address the question, if MMP-1 expression is directly induced by EWS/FLI-1, I analyzed stable EWS/FLI-1 cDNA transfected MSCs (see 4.4) for MMP-1 expression. I observed an increase of MMP-1 expression that appeared to be dose dependent on EWS/FLI-1 expression (**Figure 40**). MSC cell clones with lesser EWS/FLI-1 expression (V54.2 #1 and L87 #3) showed a reduced MMP-1 expression compared to negative control, whereas MSC clones with higher EWS/FLI-1 expression (V54.2 #3 and L87 #5) showed an induction of MMP-1 expression.

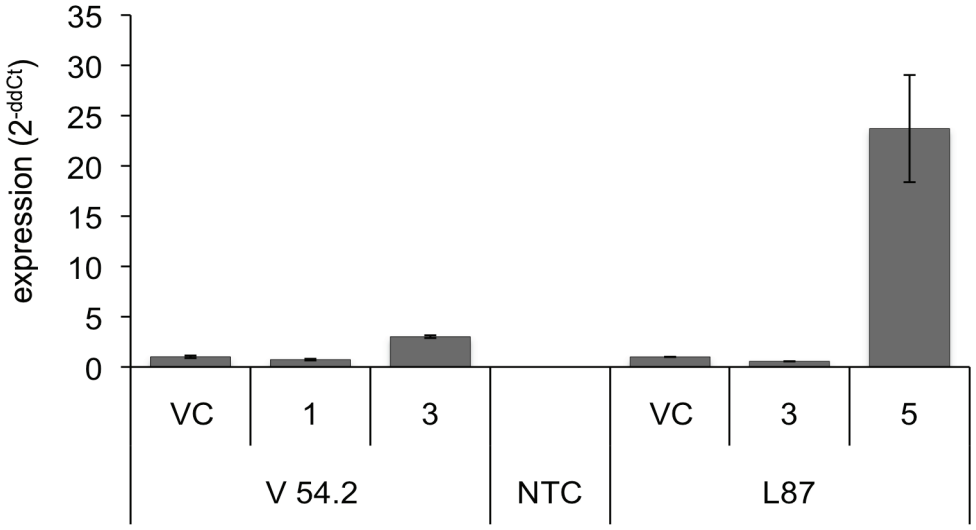

Figure 40: Influence of EWS/FLI-1 fusion protein on MMP-1 expression. qRT-PCR of MMP-1 mRNA expression in EWS/FLI-1 transfected MSC clones; Error bars represent the mean ± standard deviation of duplicates.

To further evaluate, if MMP-1 expression in EFT is correlated to EWS/FLI-1, I transiently transfected EFT cell lines A673 and SBSR-AKS with EWS/FLI-1 siRNA (see Materials and Methods) and analyzed MMP-1 expression 48 hours after transfection. As shown in **Figure 41**, this analysis provided conflicting results, as knock down of EWS/FLI-1 expression in SBSR-AKS induced MMP-1 expression, whereas in A673 EWS/FLI-1 down-regulation caused suppression of MMP-1 expression.

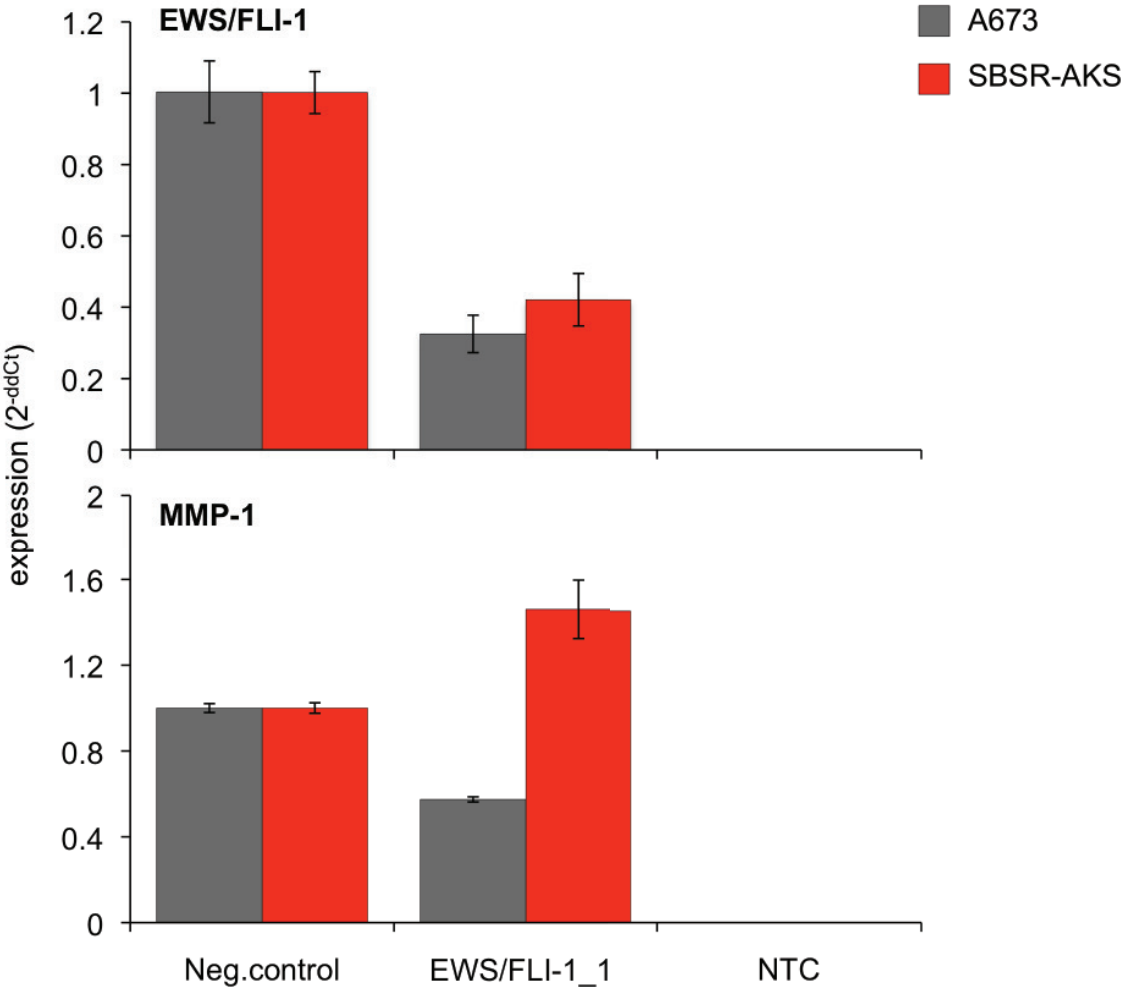

Figure 41: Affection of MMP-1 mRNA expression by EWS/FLI-1 knock down. *Upper panel:* suppression of EWS/FLI-1 mRNA expression by specific siRNA; *Lower panel:* MMP-1 expression; Neg.siRNA: non-silencing siRNA. NTC: non-template control; Error bars represent the mean ± standard deviation of duplicates.

4.8.11 MMP-1 expression knock down

Given that MMP-1 expression seemed to be influenced by GPR64, I decided to study the role of MMP-1 in EFT by RNA-interference. For transient expression knock down of MMP-1, the siRNAs Hs_MMP-1_7 and Hs_MMP-1_12 (see Materials and Methods) were used. 48 hours after transfection, MMP-1 expression was analyzed by qRT-PCR using specific MMP-1 primer assay MMP-1 expression was validated against the expression of the housekeeping gene *GAPDH*.

The transfection with siRNA MMP-1_12 resulted in a down-regulation of MMP-1 expression to levels 20-35 % of normal values of siRNA control infectants in both cell lines. Transfection with siRNA MMP-1_7 only enabled a down regulation of

MMP-1 expression to levels 20 % of normal values of siRNA control infectants in A673, whereas transfection of SBSR-AKS was not effective (**Figure 42**). An unspecific induction of an interferon response was not observed for both siRNAs. The siRNA MMP-1_12 was used for generation of stable shRNA infectants (see 4.6.2).

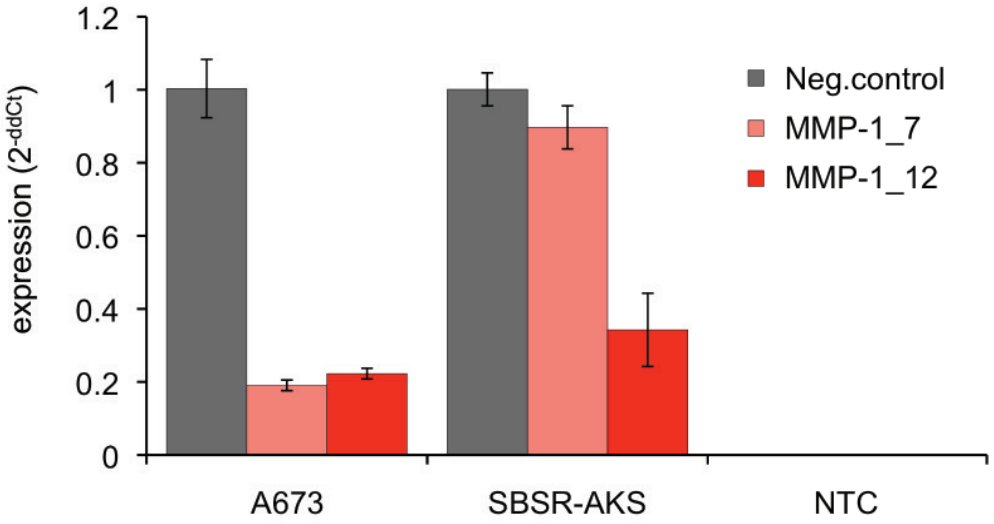

Figure 42: Transient MMP-1 siRNA Transfection. mRNA expression analysis (qRT-PCR) 48 hours after transfection. MMP-1_7 and MMP-1_12 are different siRNAs, Neg.control: non-silencing siRNA; NTC: non-template control; Error bars represent the mean ± standard deviation of duplicates.

The oligonucleotide based on siRNA MMP-1_12 was cloned into the expression vector pSIREN RetroQ and the resulting pSIREN^{MMP-1} construct introduced into A673 and SBSR-AKS cells by retroviral gene transfer. MMP-1 expression was analyzed by qRT-PCR using specific MMP-1 primer assay. MMP-1 expression was validated against the expression of the housekeeping gene *GAPDH*.

Stable transfection resulted in a down-regulation of MMP-1 expression to 5-20 % of normal values of siRNA control infectants in both cell lines (**Figure 43**). An unspecific induction of an interferon response was not observed.

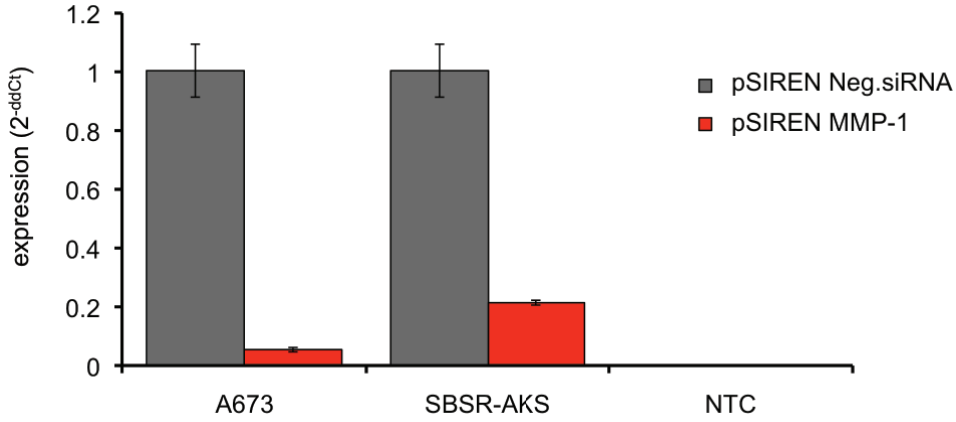

Figure 43: MMP-1 mRNA expression in EFT cell lines after constitutive down-regulation assessed by qRT-PCR. NTC: non-template control; Error bars represent the mean ± standard deviation of duplicates.

4.8.12 Affection of GPR64 expression by MMP-1

To investigate, whether, GPR64 expression is influenced by MMP-1 knock down, I analyzed GPR64 expression in constitutive pSIREN^{MMP-1} shRNA infectants. I found GPR64 expression not influenced by MMP-1 expression knock down in A673, whereas in SBSR-AKS I observed an increase in GPR64 expression after MMP-1 knock down in one clone (**Figure 44**).

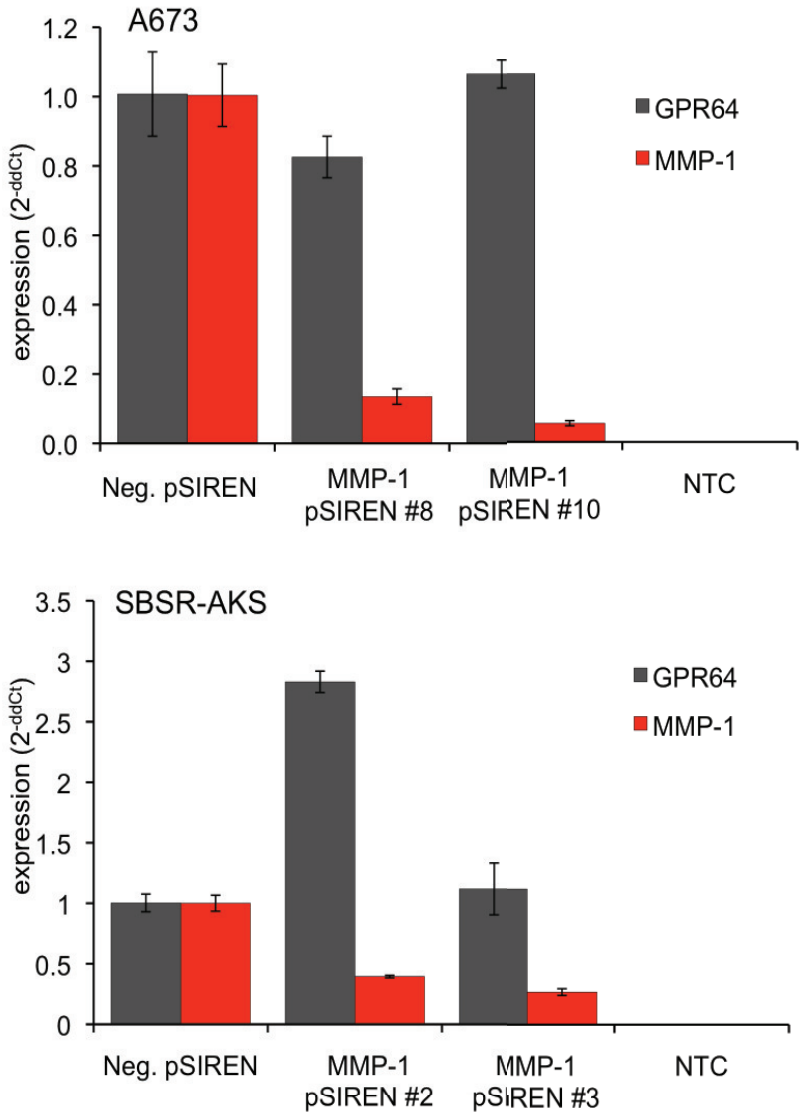

Figure 44: Influence of MMP-1 on GPR64 mRNA expression. Expression analysis of MMP-1 shRNA infectants by qRT-PCR. *Upper panel:* A673 MMP-1 shRNA infectants, MMP-1 specific mRNA expression knock down (red), GPR64 mRNA expression (gray); *lower panel:* SBSR-AKS MMP-1 shRNA infectants, MMP-1 specific expression knock down (red), GPR64 expression (gray); NTC: non-template control; Error bars represent the mean ± standard deviation of duplicates

4.8.13 Influence of MMP-1 on endothelial differentiation potential

To examine the role of MMP-1 in endothelial differentiation of SBSR-AKS EFT cells, stable pSIREN^{MMP-1} infected SBSR-AKS cells were grown on matrigel. SBSR-AKS cells were unable to form tubes after suppression of MMP-1 expression (**Figure 45**).

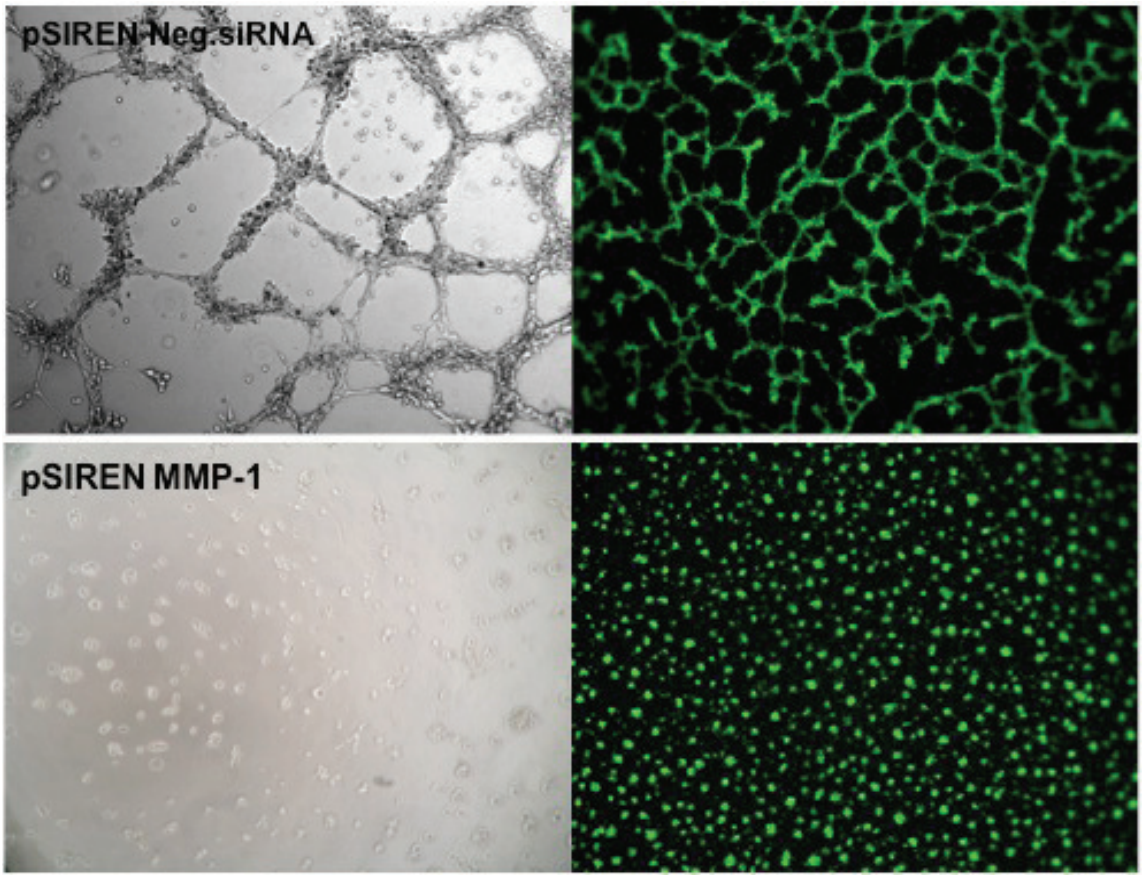

Figure 45: Tube formation assay of constitutive SBSR-AKS shRNA infectants. *Left:* phase contrast microscopy at 10 x magnification. *Right:* fluorescence microscopy of calcein staining, images at 4 x magnification.

4.8.14 Analysis of invasive growth of constitutive shRNA infectants

To further elucidate the reduced metastatic phenotype of EFT cells after GPR64 knockdown, I performed *in vitro* invasion assays using BioCoat™ Angiogenesis System. A673 pSIREN^{GPR64}, pSIREN^{MMP-1} and pSIREN^{PGF} infectants and adequate controls were cultured on BioCoat Invasion plates and cells that have

invaded into the Matrigel and migrated to the other side of the membrane were monitored after 48 hours. As shown in **Figure 46**, A673 pSIREN^{GPR64}, pSIREN^{MMP-1} and pSIREN^{PGF} exhibited clearly reduced invasive capability to cross the Matrigel barrier compared to negative control.

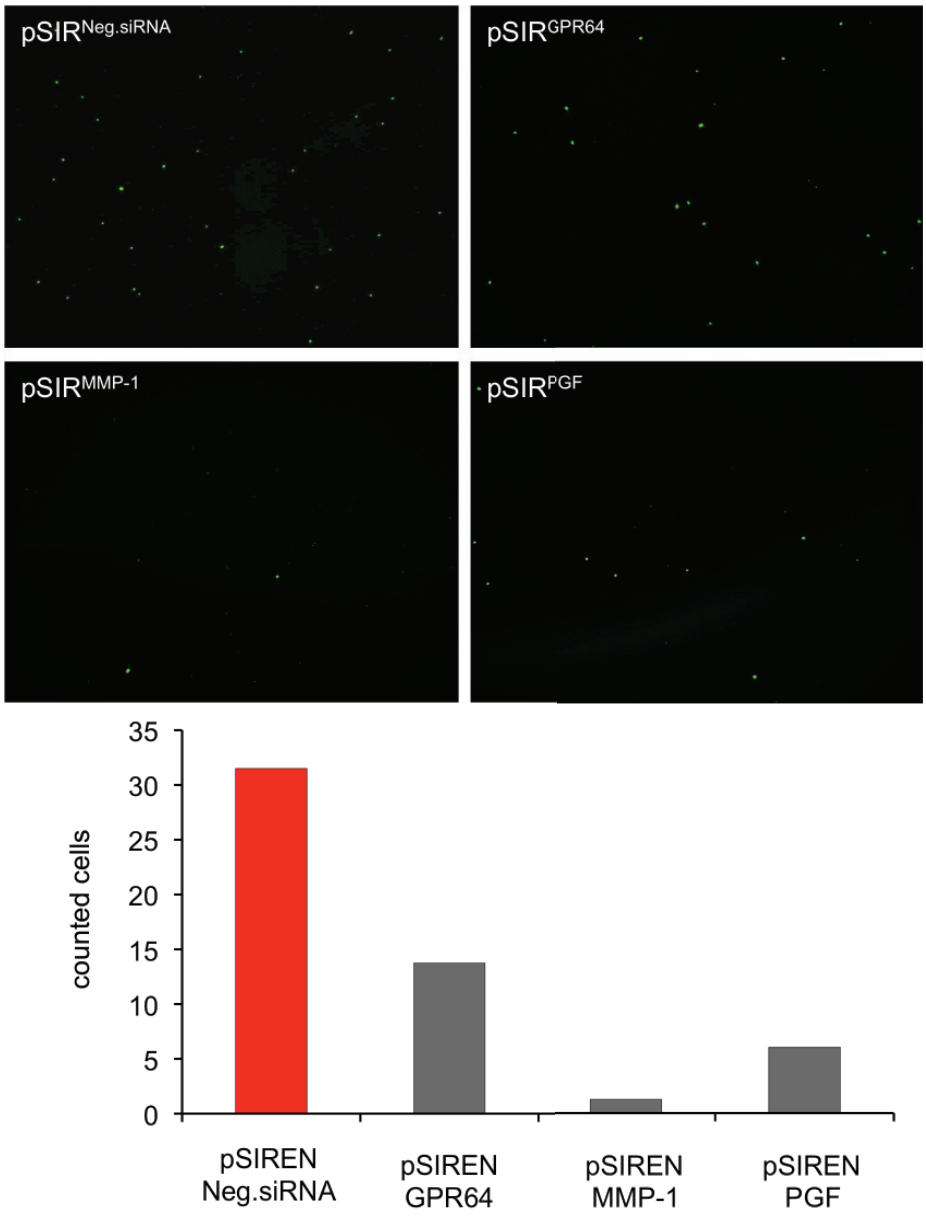

Figure 46: Invasion Assay of constitutive A673 shRNA Infectants. *Top:* Fluorescence Microscopy of invaded cells at the lower side of the invasion chamber; one representative image of calcein stained cells is shown. Images at 4x magnification. *Bottom:* Graphic shows the average amount of cells counted in four images of one experiment.

5 Discussion

Metastatic spread in EFT is hematogenous and malignant features have been shown to correlate with hypoxia and angiogenesis. We found CHM1 and GPR64 to be highly expressed in EFT. An over-expression of CHM1 or GPR64 has not yet been described for other tumor entities.

5.1 CHM1

5.1.1 Overview

Chondromodulin-1 (CHM1) is a cartilage-specific glycoprotein that stimulates the growth of chondrocytes and inhibits the tube formation of endothelial cells [88]. The over-expression of CHM1 in a malignant tumor is surprising and the role in EFT is still unclear. As EFT are characterized by the presence of blood lakes and a low microvessel density, we hypothesized that the over-expression of CHM1 in EFT might be associated with the reduced microvessel density and thus advance the process of vasculogenic mimicry. Furthermore we assumed that CHM1 might promote the aggressive phenotype of EFT, as hypoxic tumor cells are discussed to correlate with increased metastasis and inferior prognosis [23].

5.1.2 Function

In this study I observed that CHM1 expression is only weakly induced by EWS/FLI-1 in MSC and that the repression of EWS/FLI-1 expression has no influence on CHM1. This indicates that the CHM1 over-expression in EFT is regulated via mechanisms independent of EWS/FLI-1. One group was able to show that the expression of the *CHM1* gene in osteosarcoma is regulated by epigenetic mechanisms [89]. Furthermore, it was demonstrated that CHM1 was positively regulated by the transcription factor Sp3 and that the binding of Sp3 was regulated by the methylation status in the core-promoter region of the *CHM1* gene. CHM1 over-expression in EFT may be caused via similar mechanisms.
Furthermore it was observed in the present work that CHM1 influences *in vitro* endothelial differentiation in EFT cell lines. Down-regulation of CHM1 was

demonstrated to induce tube formation in the EFT cell line A673, which originally displayed no endothelial differentiation potential as ascertained by a tube formation assay. The inhibiting effect of CHM1 on tube formation capacity was also observed by others [88]. However, this observation contradicts the working hypothesis of this study that CHM1 over-expression contributes to vasculogenic mimicry of EFT cells, which would imply an abrogation of endothelial differentiation potential after CHM1 down-regulation. The obtained results rather reinforce the known anti-angiogenic function of CHM1, as EFT cells with CHM1 expression knockdown are able to form better tubes on Matrigel. *In vivo* experiments of EFT cells with CHM1 expression knock down did not reveal a difference in tumor development compared to negative control EFT cells after local injection. This result conflicts with CHM1 being an angiogenesis inhibitor, according to that, a CHM1 down-regulation would result in enhanced tumor growth due to a better endothelial differentiation potential of EFT cells, as seen in *in vitro* assays. The resuls rather indicate that CHM1 has no direct role in tumor-growth. In line with these findings, another study analyzed the CHM1 expression profile in chondrosarcomas (CS) by quantitative RT-PCR [90]. The analysis revealed mixed expression of CHM1. CS positive for CHM1 shared expression profiles of cartilage-related genes and articular cartilage cells. Neither the histological grade nor the rate of recurrence showed clear association with the level of CHM1 gene expression. These results suggested that the expression of CHM1 gene in CS has no direct role in tumorigenesis but rather reflects the site of tumor development and therefore precursor of tumor cells.

Interestingly, intravenous application of EFT cells with CHM1 expression knock down lead to a dramatic reduction in tumor cell extravasation and metastases in lungs of injected mice. This indicates that CHM1 is not involved in primary tumor growth, but is vital for the metastatic capability of EFT cells, a rather surprising result, since CHM1 expression is known to prevent blood vessel tube formation in cartilage [91].

Analysis of tumor-induced vascularization and tumor infiltrating macrophages did not reveal any differences between CHM1 knock down in EFT cells and controls, indicating that CHM1 is not likely to be involved in these processes.

5.1.3 Future perspectives

There is a growing body of evidence that CHM1 has various functions for different cell types. Besides its anti-angiogenic properties, CHM1 also has a growth stimulating activity for chondrocytes [74]. One study demonstrated that CHM1 is highly expressed in chondrocytes of the immature articular cartilage, which have a high mitotic activity. CHM1 expression decreased in chondrocytes of the mature cartilage, which has a lower proliferative activity. The authors conclude that the abundance of CHM1 expression in the immature articular cartilage and the decrease in the mature one correlates with the difference in proliferative activity between the immature and mature articular cartilage [92]. CHM1 could therefore act as a stimulator for proliferation in EFT and thus contribute to the progression of this disease.

A well-known strategy that tumors use to escape from immune-system mediated rejection is the expression of immunosuppressive factors. These factors may be expressed by the malignant cells themselves or by noncancerous cells present at the tumor site, such as immune, epithelial, or stromal cells. The most prominent of these factors is transforming growth factor β (TGF-β). TGF-β is a cytokine that affects proliferation, activation and differentiation of cells of innate and adaptive immunity and thus inhibits the anti-tumor immune response. In this context, another study found CHM1 expression not only in cartilage but also in the cortex of the thymus, suggesting a correlation of CHM1 with T cell function. They were able to show that CHM1 is able to suppress the proliferative response of mouse splenic T-cells and human peripheral blood T cells [93]. Furthermore, they were able to show that recombinant human CHM1 is able to suppress antigen specific immune response *in vivo*, suggesting a possible role for CHM1 as immunosuppressive factor.

Another striking feature of the CHM1 protein is that it contains a conserved domain of approx. 100 amino acids called the BRICHOS domain [94]. This domain has been identified in several previously unrelated proteins that are linked to major diseases. It is located in the propeptide region that is removed after proteolytic processing. Experimental data suggest that the role of this domain could be related to the complex post-translational processing of these proteins [94]. Recent studies revealed that in addition to CHM1 Integral membrane protein 2A (ITM2A) belongs to the BRICHOS domain containing

protein family [95]. Furthermore, ITM2A was also highly expressed in EFT [64]. This protein is discussed to inhibit early stages of chondrogenic differentiation of mesenchymal stem cells [96]. As CHM1 and ITM2A share this BRICHOS domain, the role of highly expressed CHM1 in EFT might rather involve the suppression of chondrogenic differentiation of EFT that any major effect on angiogenesis. Another tumor entity with induced CHM1 expression is chondroblastic osteosarcoma (CBOS), a highly undifferentiated rare subtype of osteosarcoma. CBOS cells produce immature cartilage in addition to the osteoid bone matrix [97], suggesting that tumor cells in this subtype have the potential to differentiate into both osteogenic and chondrogenic cells. CHM1 was found to be strongly expressed in CBOS but not in tumors of other osteosarcoma subtypes [98] indicating a connection between the undifferentiated phenotype of CBOS and CHM1 expression. As mentioned above, physiological CHM1 expression decreases with ongoing differentiation of cartilage. Against this background, a possible role of CHM1 in EFT could be to maintain an undifferentiated phenotype as substantiated by the results of endothelial tube formation assays.

5.1.4 Conclusion

Taken together the present study revealed interesting results concerning CHM1 overexpression in EFT. CHM1 was shown to be involved in differentiation of EFT cell lines in vitro, as down-regulation of CHM1 expression induced endothelial differentiation in Matrigel assays. Furthermore, CHM1 seems to contribute to invasive growth of EFT, as inhibition of CHM1 expression clearly reduced lung metastasis.

However the present work could so far not affirm our hypothesis of CHM1 being a regulator of vasculogenic mimicry. Further experiments are necessary to further elucidate the function of CHM1 in EFT but are no longer part of this study.

5.2 GPR64

5.2.1 Overview

The G-protein coupled receptor 64 (GPR64) is an orphan receptor, which was found to be highly expressed in the epithelia of *ductulus efferentes* and proximal epididymis, but in no other tissues of the adult [65]. These results were confirmed by an independent study of our group [64]. Furthermore our data indicate that GPR64 signaling is involved in the regulation of target genes essential for invasion and angiogenesis. Therefore we hypothesize it being an interesting target for new anti-angiogenic therapies.

5.2.2 Function

In this study I observed that *GPR64* seems to be an EWS/FLI-1 target gene, as the induction of EWS/FLI-1 in MSC lead to a predominant up-regulation of GPR64 expression. However, in EFT cell lines, no considerable EWS/FLI-1 dependent regulation of GPR64 expression was observed. This indicates that GPR64 expression in EFT might be regulated by more complex mechanisms.
I observed that GPR64 influences *in vitro* endothelial differentiation in EFT cell lines. I showed that down-regulation of GPR64 inhibits tube formation in the cell lines SBSR-AKS and RDES. From these data, I conclude that the effect of GPR64 on tube formation might directly contribute to the metastatic phenotype of EFT cells. Furthermore, I observed a complete inhibition of local tumor growth and a severe limitation of metastatic growth of EFT after GPR64 knock down. This clearly indicates that GPR64 is crucial for local tumor growth and invasiveness in EFT.

5.2.3 GPR64 and PGF

So far little is known about the physiological function of GPR64, and several attempts to identify its ligand failed. Therefore, a starting point for the analysis of its potential function in EFT is hard to find. We performed microarray analysis after GPR64 knock down in EFT cells to identify possible targets of GPR64 and to bring forward a putative role of GPR64 over-expression in EFT. Most

prominently, we found PGF expression to be influenced by GPR64. Since PGF is known to be a critical player in angiogenesis, we further investigated the role of PGF in EFT.

My data indicates that GPR64 regulated PGF is involved in tumor-induced vessel formation, given that EFT cells with PGF expression knock down display obvious deficiencies in endothelial differentiation potential in Matrigel assays. Interestingly, there was no evident change in primary tumor growth between PGF shRNA and shRNA control tumors, indicating sufficient angiogenesis in both groups to sustain an equal growth rate. This may be due to the subcutaneous injection site, which is well vascularized and where tumor cells therefore may easily access and recruit blood vessels.

However, there were obvious differences in the size and the amount of the metastatic tumors in the also highly vascularized lung tissue after intravenous injection. This may also be due to the type of injection, as the cells are applied in the circulatory system and have to invade the endothelial lining of blood vessels and degrade its underlying basement membrane in order to escape into the extravascular tissue and establish metastases. However, after CD31 staining of affected organs, there were no obvious differences in vascularization of tumor nodules of PGF knock down EFT, suggesting that PGF does not play a crucial role in angiogenesis of EFT *in vivo*. Presumably, EFT after PGF knock down may employ other mechanisms to develop a vascular network independent of PGF. Studies of $PGF^{-/-}$ mice revealed that these mice display rather normal vascularization of calluses in a fracture repair model compared to wild type mice [99]. The authors of these studies suggest that angiogenesis during new bone formation may be regulated by other factors, possibly VEGF. This may also be the case in EFT, as VEGF is highly expressed in EFT.

It is known that PGF induces tumor angiogenesis by recruiting circulating hematopoietic progenitor cells and macrophages to the site of the growing tumor [100]. However, Mac-3 staining revealed no differences in macrophage infiltration of PGF knock down in EFT affected organs compared to negative control. Macrophages are recruited to the growing tumor not only by PGF, but also by several other chemoattractants secreted by the tumor cells, including VEGF, CCL2, CCL-5 and CSF-1 among others [101]. Furthermore, necrotic cells within the tumor mass also release multiple mediators of inflammation, including the

high mobility group box 1 protein (HMGB1) which is a potent stimulator of macrophages [102]. Since tumor cells have multiple mechanisms to recruit macrophages, PGF expression might not be essential for attracting macrophages in EFT.

To further investigate the reduced metastatic phenotype of EFT after GPR64 and PGF expression knock down, I performed *in vitro* invasion assays. Cell invasion is a crucial process in tumor metastasis. Tumor cell invasion and metastasis require proteolytic degradation of the basement membrane and extracellular matrix by MMPs [103]. This plays a fundamental role in cancer progression and constitutes an escape route for further dissemination. In this study, I found that the down-regulation of GPR64 and PGF prominently inhibits EFT cell invasion in the matrigel invasion assays, a result that correlates with the *in vivo* metastasis experiments.

5.2.4 GPR64 and MMP-1

Upon further analysis of putative GPR64 signaling mechanisms, I found Matrix Metalloproteinase 1 (MMP-1) expression to be influenced by GPR64. MMP-1, also known as collagenase 1 [104], belongs to the family of zinc-dependent proteases that degrade extracellular matrix.

There is evidence that MMP-1 is a direct target of EWS/ETS proteins, as a previous study has shown that EWS-ER81 and EWs/FLI-11 fusion proteins can interact with the MMP-1 promoter and collaborate with c-Jun and the cofactor p300 to activate MMP-1 gene transcription in vitro [87]. I was able to confirm this hypothesis to some extend, as the induction of EWS/FLI-1 in MSC lead to an up regulation of MMP-1 expression in clones with the highest EWS/FLI-1 expression. However, EWS/FLI-1 down regulation in EFT cell lines lead to conflicting results concerning MMP-1 expression, as in SBSR-AKS a slight induction of MMP-1 was observed, whereas in A673 MMP-1 expression was repressed. One explanation could be that down regulation of EWS/FLI-1 in a transient manner is insufficient to identify possible downstream targets. Due to the complex process of RNA interference, it might take longer than 48 hours to be able to observe EWS/FLI-1 siRNA mediated regulation of EWS/FLI-1 target

gene expression. Studies of stable EWS/FLI-1 shRNA transfected cells remain to be done to further investigate the effect of EWS/FLI-1 on MMP-1 expression.
MMP-1 expression in cancer cells is associated with invasive growth [68], and the inhibition of MMP-1 expression has been shown to correlate with a reduced metastatic phenotype in melanoma cells [105, 106]. Furthermore, MMP-1 is known to be involved in the in vitro tube formation ability of endothelial cells [106]. I was able to confirm these observations for EFT *in vitro*, as MMP-1 expression knock down in EFT cells lead to an inhibition of endothelial differentiation and a reduced invasive growth capacity *in vitro.*
I observed that knock down of GPR64 expression down-regulates MMP-1 expression, whereas MMP-1 down-regulation did not have an effect on GPR64. This suggests that MMP-1 is a downstream target of GPR64. Since MMP-1 expression is known to be induced at a transcriptional level by activation of the ERK1/2 signaling pathway [107], GPR64 might be involved in regulating this pathway. I started investigating the ERK1/2 signaling pathway and the possible involvement of GPR64 by western blot analysis, but to date without significant results. This is due to the lack of a functional specific antibody against GPR64. Commercial antibodies fail to specifically recognize GPR64 in EFT cell lysates and first attempts to synthesize a specific GPR64 antibody out of rat were not successful yet.
As PGF and MMP-1 are both critical mediators of tumor angiogenesis and were identified as potential targets of GPR64 mediated signal transduction in EFT, we find our hypothesis substantiated that GPR64 might be suitable as novel promising target for anti-angiogenic therapies for EFT.

5.2.5 GPR64 as cancer testis antigen

Based on the expression pattern GPR64 may be classified as a typical Cancer/Testis Antigen (CTA). CTA are a group of tumor antigens expressed in normal germ cells, trophoblast tissue and in different types of tumors. The physiological function of most CTA is unknown but it seems that most of these antigens may have a putative role in transcriptional regulation. Their products can also affect many different cellular processes, such as signaling, translation, and chromosomal recombination. However, the underlying reasons for over-

expression of CTA expression in cancer and the relationship between CTA expression and malignancy are still matter of debate.

CTA have high clinical relevance as they encode a class of immunogenic and highly selective tumor antigens. Immunogenicity is provoked only by short peptide sequences of CTA epitopes, which are presented on the tumor cell surface by HLA Class I molecules in the case of cytotoxic T lymphocyte (CTL) mediated immune responses and by HLA Class II molecules on the surface of APC (antigen presenting cells), in the case of T-helper cell (T_H) mediated immune responses. Identification of these epitopes is one of the main goals of CTA research, as the knowledge of epitopes recognized by the immune system allows the creation of tumor-specific vaccines [108]. In our lab, we also work on the establishment of cytotoxic T cell lines specifically directed against HLA-A*0201-restricted peptides derived from EFT associated antigens. As GPR64 expression is highly specific for EFT, the identification of immunogenic GPR64 epitopes could be of therapeutic benefit in EFT treatment.

In addition, these antigens can also be used as biomarkers for early detection of cancers.

5.2.6 GPR64 as diagnostic tool

Transcripts of tumor-specific genes can be amplified and detected by RT-PCR, which is a reliable technique to detect circulating tumor cells (CTC). In 1991, Smith et al first successfully adopted RT-PCR technique to assess tyrosinase messenger RNA (mRNA) as a tumor marker in detecting circulating melanoma cells [109]. Since then, this technique has been applied to the detection of CTC in solid tumors with a much higher sensitivity than conventional cytological analysis, as one tumor cell per one million background cells can be detected by this approach. RT-PCR has already been applied in EFT patients to search for CTC. In one study, tumor cells were detected at diagnosis in bone marrow and peripheral blood of patients with EFT using an RT-PCR assay targeting the EFT-specific *EWS/FLI-1* or *EWS-ERG* fusion transcripts. The study revealed that patients with localized EFT and bone marrow micrometastasis or CTC are comparable to patients with metastases in terms of the localization of the primary tumor, outcome, and relapse pattern [110].

Our data suggest that GPR64 mRNA expression analysis by RT-PCR could be used as a marker for early detection of metastatic EFT. Furthermore, it might be interesting as an additional tool for the diagnosis of EFT, especially in cases where results from the EWS/FLI-1 RT-PCR are uncertain despite typical histology and immunophenotype. In such cases the absence of GPR64 transcripts should draw attention on possible alternative diagnoses. We did not detect GPR64 in neuroblastomas or cALLs examined, suggesting that GPR64 might be suitable for discrimination between these small blue round cell tumors.

5.2.7 GPR64 as therapeutic target

Silencing of gene expression by siRNAs is rapidly becoming a powerful tool for genetic analysis and represents a potential strategy for therapeutic product development (see Introduction). However, delivery of siRNA into specific organs in vivo is a major obstacle for RNAi-based therapy.

A promising approach in EFT siRNA therapy is the systemic delivery of sequence-specific siRNA against the *EWS/FLI-1* gene product by a targeted, nonviral delivery system [111]. This application dramatically inhibited tumor growth in a murine model of metastatic EFT. This nonviral delivery system uses a cyclodextrin-containing polycation to bind and protect siRNA and transferrin as a targeting ligand for delivery to transferrin receptor–expressing tumor cells. Additionally, no abnormalities in interleukin-12 and IFN-A, liver and kidney function tests, complete blood counts, or pathology of major organs are observed from long-term, low-pressure, low- volume tail-vein administrations. These data provide strong evidence for the safety and efficacy of this targeted, nonviral siRNA delivery system.

In the present study it was demonstrated that the reduction of the GPR64 protein in EFT cells *in vitro* or in xenograft tumors by siRNA results in decreased local and invasive growth, suggesting a potential therapeutic intervention directed at this EFT-specific gene. We therefore hypothesize that systemically delivered siRNA against GPR64 would inhibit growth and dissemination of EFT cells *in vivo.*

5.2.8 Conclusion

Taken together, within this study it was possible to gain substantial insight in the function of GPR64 in EFT. It was demonstrated in Matrigel assays that GPR64 is essential for endothelial differentiation and furthermore has a central role in local and invasive growth as seen in *in vivo* experiments. Functional studies revealed the GPR64 targets PGF and MMP-1 and a possible involvement of GPR64 in the ERK1 signaling pathway. The results of this study open the way for new therapeutic strategies in EFT treatment.

6 Summary

Metastatic spread in Ewing Tumors (EFT) is hematogenous and malignant features have been shown to correlate with hypoxia and angiogenesis. Previously, we confirmed the endothelial signature of EFT by microarray analysis comparing EFT with a normal body map. This analysis revealed 37 genes that are highly up-regulated or even specifically expressed in EFT including genes that may play a central role in angiogenesis: Chondromodulin 1 (CHM1), a cartilage-specific glycoprotein with anti-angiogenic activity is believed to be involved in vasculogenic mimicry of tumor cells. G-protein coupled receptor-64 (GPR64), an orphan receptor with physiological expression restricted to human epididymis, is aberrantly induced in EFT by oncogenic EWS/ETS transcription factors. In this study the role of CHM1 and GPR64 expression in tumorigenicity and malignant phenotype of EFT was analyzed using RNA interference. Here I show that inhibition of CHM1 expression in EFT cell lines induces endothelial differentiation potential in tube formation assays. Furthermore, CHM1 seems to be involved in invasive growth of EFT cell lines, since CHM1 knock down results in reduced metastatic spread in immunodeficient $Rag2^{-/-}\gamma_C^{-/-}$ mice.

Inhibition of GPR64 expression in EFT cell lines resulted in impaired endothelial differentiation in tube formation assays. Furthermore, GPR64 suppression substantially inhibited tumor growth and metastatic spread in immunodeficient $Rag2^{-/-}\gamma_C^{-/-}$ mice, which correlated with reduced proteolytic activity and invasiveness *in vitro*. Subsequent microarray analysis of EFT after GPR64 knock down identified a GPR64-mediated induction of placental growth factor (PGF) and subsequent experiments revealed MMP-1 as a potential target of GPR64-mediated signal transduction in EFT. Repression of PGF and MMP-1 expression in EFT cell lines resulted in a phenotype similar to the one observed after GPR64 knockdown.

To conclude, the explicit function of CHM1 in EFT was not elucidated within this study but its critical contribution to invasive growth of EFT was established. In contrast for GPR64 a critical function in EFT angiogenesis and pathogenesis was identified what substantiates it being a novel promising therapeutic target for this disease.

7 Zusammenfassung

Die Familie der Ewing Tumore (EFT) ist durch ein hohes Metastasierungspotential charakterisiert. In vorangegangenen Studien, in denen das Transkriptom von EFT mit einer normal body map verglichen wurde, konnten wir die nahe Verwandtschaft zu endothelialem Gewebe zeigen. Im Rahmen dieser Analysen konnten 37 Gene identifiziert werden, die in EFT hoch-reguliert oder sogar EFT-spezifisch exprimiert sind. Zu diesen Genen gehören solche, denen eine zentrale Rolle bei der Angiogenese und der Metastasierung von EFT zugeschrieben wird. Chondromodulin-1 (CHM1) ist ein erstmals im Knorpel nachgewiesener Angiogenese-Inibitor der möglicherweise am vaskulären Mimikry von Tumorzellen beteiligt ist. GPR64 ist ein 7-transmembraner G-Protein-gekoppelter Rezeptor mit bisher unbekanntem Liganden, der spezifisch auf Epithelzellen des Nebenhodens exprimiert wird. Die Expression von GPR64 wird in EFT aberrant durch onkogene EWS/ETS Transkriptionsfaktoren induziert.

In dieser Studie wurde die Relevanz der aberrant exprimierten Gene *CHM1* und *GPR64* für das Tumorwachstum und den malignen Phänotyp von EFT durch RNA-Interferenz untersucht. Ich konnte zeigen, dass die Inhibition der CHM1 Expression *in vitro* endotheliales Differenzierungspotential in EFT Zelllinien induziert. Des Weiteren scheint CHM1 in Mechanismen des invasiven Wachstums von EFT verwickelt zu sein, da eine Suppression der CHM1 Expression in EFT Zelllinien mit einem verringerten metastatischen Potential *in vivo* korreliert.

Die Suppression der GPR64 Expression in EFT Zelllinien bewirkte ein vermindertes endotheliales Differenzierungspotential *in vitro* und führte darüber hinaus zu verringertem Wachstum und Metastasierungspotential von EFT *in vivo.* Diese Ergebnisse korrelieren mit einer verminderten proteolytischen Aktivität und geringerer Invasivität dieser Zellen *in vitro*. Eine anschließende Microarray Analyse zeigte eine GPR64 vermittelte Induktion von Placental Growth Factor (PGF) und weitere Analysen identifizierten die Matrix Metalloporoteinase 1 (MMP-1) als potentielles Target einer GPR64-vermittelten Signal-Transduktion in EFT. Die Repression der PGF und MMP-1 Expression in EFT resultierte in einem Phänotyp der vergleichbar war mit dem, der nach GPR64 Suppression beobachtet wurde.

Zusammenfassend war es im Rahmen dieser Studie nicht möglich, die genaue Funktion von CHM1 in EFT eindeutig zu klären. Jedoch konnte eine wichtige Funktion beim invasiven Wachstum von EFT herausgearbeitet werden. Dagegen konnten wir zeigen, dass GPR64 eine zentrale Rolle in der Angiogenese und Pathogenese von EFT spielt und sich somit als vielversprechendes therapeutisches Target für diese Erkrankung eignet.

8 Danksagung

Ich möchte mich bei Herrn Prof. Dr. Stefan Burdach und Herrn Dr. Günther Richter für die Möglichkeit bedanken, hier im Labor Funktionelle Genomik und Transplantationsbiologie der Klinik und Poliklinik für Kinder- und Jugendmedizin des Klinikums rechts der Isar an diesem interessanten Thema zu arbeiten.

Auch Herrn Prof. Dr. Dirk Haller möchte ich herzlich für die Betreuung meiner Doktorarbeit als Doktorvater danken.

Herrn Prof. Dr. Scherer gilt ebenso ein großes Dankeschön für die Übernahme des Prüfungsvorsitzes.

Danke auch an Dr. Irene Esposito aus dem Institut für Pathologie des Helmholtz Zentrums München, die viel Zeit und Mühe in die Färbung, die Auswertung und die Interpretation meiner zahlreichen Tumorproben gesteckt hat.

Alex Wechselberger aus dem Labor von Frau Dr. Irene Teichert von Lüttichau möchte ich danken, dass sie mich in die hohe Kunst der Angiogenese-Assays eingewiesen hat!

Sabine Rössler danke ich herzlich für die kompetente Einarbeitung im Labor und dafür, dass sie mir stets mit Rat und Tat zur Seite stand.

Vielen Dank auch an Andreas Mollweide, der mit seiner Hilfe viel zum Erfolg der Mausexperimente, vor allem der Tail Vein Metastasis Assays, beigetragen hat.

Ein ganz besonderes Dankeschön an meine lieben Arbeitskollegen Steffi Plehm, Uwe Thiel, Kristina Hauer und Colette Zobywalski. Vielen Dank für die zahlreichen Diskussionen, Hilfen, Tipps und Wegweisungen aus diversen Sackgassen. Ein großer Trost: ich lasse euch zwar schweren Herzens als Kollegen zurück, behalte euch aber als Freunde!

Stefan, dir danke ich für die Mühe und die Zeit, die du ins Korrektur lesen gesteckt hat, für die konstruktive Kritik und dafür, dass du auf meine Computerfragen immer eine Antwort hattest.

All meinen Freunden möchte ich danken, dass sie immer an mich geglaubt haben, selbst, wenn ich am Verzweifeln war und dass sie nicht von meiner Seite gewichen sind trotz meiner unberechenbaren Launen und wochenlanger Funkstille. Danke, dass ihr immer noch anruft!

Zu guter Letzt geht noch ein riesiges Dankeschön an meine Familie, an meinen Bruder fürs auf andere Gedanken bringen und an meinen lieben Vater, der mir

ermöglicht hat, bis hierher zu kommen und der den Glauben an den Erfolg dieser Arbeit nie verloren hat.

9 References

1. Hanahan, D. and R. Weinberg, *The hallmarks of cancer.* Cell, 2000. **100**: p. 57-70.
2. Folkman, J., *Tumor angiogenesis: therapeutic implications.* N Engl J Med, 1971. **285**(21): p. 1182-6.
3. Hillen, F. and A.W. Griffioen, *Tumour vascularization: sprouting angiogenesis and beyond.* Cancer Metastasis Rev, 2007. **26**(3-4): p. 489-502.
4. Carmeliet, P. and R.K. Jain, *Angiogenesis in cancer and other diseases.* Nature, 2000. **407**(6801): p. 249-57.
5. Bergers, G. and L.E. Benjamin, *Tumorigenesis and the angiogenic switch.* Nat Rev Cancer, 2003. **3**(6): p. 401-10.
6. Rafii, S., et al., *Vascular and haematopoietic stem cells: novel targets for anti-angiogenesis therapy?* Nat Rev Cancer, 2002. **2**(11): p. 826-35.
7. Folberg, R., M.J. Hendrix, and A.J. Maniotis, *Vasculogenic mimicry and tumor angiogenesis.* Am J Pathol, 2000. **156**(2): p. 361-81.
8. Maniotis, A.J., et al., *Vascular channel formation by human melanoma cells in vivo and in vitro: vasculogenic mimicry.* Am J Pathol, 1999. **155**(3): p. 739-52.
9. Shirakawa, K., et al., *Hemodynamics in vasculogenic mimicry and angiogenesis of inflammatory breast cancer xenograft.* Cancer Res, 2002. **62**(2): p. 560-6.
10. Sood, A.K., et al., *Molecular determinants of ovarian cancer plasticity.* Am J Pathol, 2001. **158**(4): p. 1279-88.
11. Sharma, N., et al., *Prostatic tumor cell plasticity involves cooperative interactions of distinct phenotypic subpopulations: role in vasculogenic mimicry.* Prostate, 2002. **50**(3): p. 189-201.
12. Cai, X.S., et al., *Tumor blood vessels formation in osteosarcoma: vasculogenesis mimicry.* Chin Med J (Engl), 2004. **117**(1): p. 94-8.
13. van der Schaft, D.W., et al., *Tumor cell plasticity in Ewing sarcoma, an alternative circulatory system stimulated by hypoxia.* Cancer Res, 2005. **65**(24): p. 11520-8.
14. Cavallaro, U. and G. Christofori, *Molecular mechanisms of tumor angiogenesis and tumor progression.* J Neurooncol, 2000. **50**(1-2): p. 63-70.
15. Vaupel, P. and A. Mayer, *Hypoxia in cancer: significance and impact on clinical outcome.* Cancer Metastasis Rev, 2007. **26**(2): p. 225-39.
16. Vaupel, P. and L. Harrison, *Tumor hypoxia: causative factors, compensatory mechanisms, and cellular response.* Oncologist, 2004. **9 Suppl 5**: p. 4-9.
17. Vaupel, P., *The role of hypoxia-induced factors in tumor progression.* Oncologist, 2004. **9 Suppl 5**: p. 10-7.
18. Hockel, M. and P. Vaupel, *Tumor hypoxia: definitions and current clinical, biologic, and molecular aspects.* J Natl Cancer Inst, 2001. **93**(4): p. 266-76.
19. Graeber, T.G., et al., *Hypoxia-mediated selection of cells with diminished apoptotic potential in solid tumours.* Nature, 1996. **379**(6560): p. 88-91.

20. Nordsmark, M., M. Overgaard, and J. Overgaard, *Pretreatment oxygenation predicts radiation response in advanced squamous cell carcinoma of the head and neck.* Radiother Oncol, 1996. **41**(1): p. 31-9.
21. Hockel, M., et al., *Association between tumor hypoxia and malignant progression in advanced cancer of the uterine cervix.* Cancer Res, 1996. **56**(19): p. 4509-15.
22. Knocke, T.H., et al., *Intratumoral pO2-measurements as predictive assay in the treatment of carcinoma of the uterine cervix.* Radiother Oncol, 1999. **53**(2): p. 99-104.
23. Dunst, J., et al., *Prognostic impact of tumor perfusion in MR-imaging studies in Ewing tumors.* Strahlenther Onkol, 2001. **177**(3): p. 153-9.
24. Harrison, L. and K. Blackwell, *Hypoxia and anemia: factors in decreased sensitivity to radiation therapy and chemotherapy?* Oncologist, 2004. **9 Suppl 5**: p. 31-40.
25. Riggi, N. and I. Stamenkovic, *The Biology of Ewing sarcoma.* Cancer Lett, 2007. **254**(1): p. 1-10.
26. Delattre, O., et al., *The Ewing family of tumors--a subgroup of small-round-cell tumors defined by specific chimeric transcripts.* N Engl J Med, 1994. **331**(5): p. 294-9.
27. Ewing, J., *Classics in oncology. Diffuse endothelioma of bone. James Ewing. Proceedings of the New York Pathological Society, 1921.* CA Cancer J Clin, 1972. **22**(2): p. 95-8.
28. Turc-Carel, C., et al., *Chromosomes in Ewing's sarcoma. I. An evaluation of 85 cases of remarkable consistency of t(11;22)(q24;q12).* Cancer Genet Cytogenet, 1988. **32**(2): p. 229-38.
29. Aurias, A., et al., *Translocation involving chromosome 22 in Ewing's sarcoma. A cytogenetic study of four fresh tumors.* Cancer Genet Cytogenet, 1984. **12**(1): p. 21-5.
30. Zucman, J., *Combinatorial generation of variable fusion proteins in the Ewing family of tumors.* Embo Journal, 1993. **12**.
31. Paulussen, M., B. Fröhlich, and H. Jürgens, *Ewing tumour: incidence, prognosis and treatment options.* Paediatr Drugs, 2001. **3**(12): p. 899-913.
32. Zhou, Z., et al., *VEGF(165), but not VEGF(189), stimulates vasculogenesis and bone marrow cell migration into Ewing's sarcoma tumors in vivo.* Mol Cancer Res, 2007. **5**(11): p. 1125-32.
33. Reddy, K., et al., *VEGF165 expression in the tumor microenvironment influences the differentiation of bone marrow-derived pericytes that contribute to the Ewing's sarcoma vasculature.* Angiogenesis, 2008. **11**(3): p. 257-67.
34. Zhou, Z., et al., *Suppression of Ewing's sarcoma tumor growth, tumor vessel formation, and vasculogenesis following anti vascular endothelial growth factor receptor-2 therapy.* Clin Cancer Res, 2007. **13**(16): p. 4867-73.
35. Fuchs, B., C.Y. Inwards, and R. Janknecht, *Vascular endothelial growth factor expression is up-regulated by EWS-ETS oncoproteins and Sp1 and may represent an independent predictor of survival in Ewing's sarcoma.* Clin Cancer Res, 2004. **10**(4): p. 1344-53.
36. Nagano, A., et al., *EWS/Fli-1 chimeric fusion gene upregulates vascular endothelial growth factor-A.* Int J Cancer, 2010. **126**(12): p. 2790-8.

37. Simpson, A., et al., *MVD predicts disease-free and overall survival in tumors of the ewing's sarcoma family (ESFT).* Br J Cancer, 2002. **86 (suppl 1)**: p. S 95.
38. Kreuter, M., et al., *Clinical significance of Vascular Endothelial Growth Factor-A expression in Ewing's sarcoma.* Eur J Cancer, 2006. **42**(12): p. 1904-11.
39. Mikulic, D., et al., *Angiogenesis and Ewing sarcoma--relationship to pulmonary metastasis and survival.* J Pediatr Surg, 2006. **41**(3): p. 524-9.
40. Holzer, G., et al., *Concentration of vascular endothelial growth factor (VEGF) in the serum of patients with malignant bone tumors.* Med Pediatr Oncol, 2001. **36**(6): p. 601-4.
41. Pavlakovic, H., et al., *Quantification of angiogenesis stimulators in children with solid malignancies.* Int J Cancer, 2001. **92**(5): p. 756-60.
42. Tabone, M.D., et al., *Are basic fibroblast growth factor and vascular endothelial growth factor prognostic indicators in pediatric patients with malignant solid tumors?* Clin Cancer Res, 2001. **7**(3): p. 538-43.
43. Brizel, D.M., et al., *Tumor oxygenation predicts for the likelihood of distant metastases in human soft tissue sarcoma.* Cancer Res, 1996. **56**(5): p. 941-3.
44. Fyles, A.W., et al., *Oxygenation predicts radiation response and survival in patients with cervix cancer.* Radiother Oncol, 1998. **48**(2): p. 149-56.
45. Dalal, S., et al., *Vascular endothelial growth factor: a therapeutic target for tumors of the Ewing's sarcoma family.* Clin Cancer Res, 2005. **11**(6): p. 2364-78.
46. Holash, J., et al., *VEGF-Trap: a VEGF blocker with potent antitumor effects.* Proc Natl Acad Sci U S A, 2002. **99**(17): p. 11393-8.
47. Zhou, Z., et al., *E1A gene therapy inhibits angiogenesis in a Ewing's sarcoma animal model.* Mol Cancer Ther, 2003. **2**(12): p. 1313-9.
48. Fong, T.A., et al., *SU5416 is a potent and selective inhibitor of the vascular endothelial growth factor receptor (Flk-1/KDR) that inhibits tyrosine kinase catalysis, tumor vascularization, and growth of multiple tumor types.* Cancer Res, 1999. **59**(1): p. 99-106.
49. Maris, J.M., et al., *Initial testing of the VEGFR inhibitor AZD2171 by the pediatric preclinical testing program.* Pediatr Blood Cancer, 2008. **50**(3): p. 581-7.
50. Maris, J.M., et al., *Initial testing (stage 1) of sunitinib by the pediatric preclinical testing program.* Pediatr Blood Cancer, 2008. **51**(1): p. 42-8.
51. Potikyan, G., et al., *EWS/FLI1 regulates tumor angiogenesis in Ewing's sarcoma via suppression of thrombospondins.* Cancer Res, 2007. **67**(14): p. 6675-84.
52. Rennel, E.S., et al., *Recombinant human VEGF165b protein is an effective anti-cancer agent in mice.* Eur J Cancer, 2008. **44**(13): p. 1883-94.
53. Chaplin, D.J., et al., *Antivascular approaches to solid tumour therapy: evaluation of tubulin binding agents.* Br J Cancer Suppl, 1996(27): p. S86-88.
54. Dalal, S. and S.A. Burchill, *Preclinical evaluation of vascular-disrupting agents in Ewing's sarcoma family of tumours.* Eur J Cancer, 2009. **45**: p. 713-722.

55. Guan, H., et al., *A small interfering RNA targeting vascular endothelial growth factor inhibits Ewing's sarcoma growth in a xenograft mouse model.* Clin Cancer Res, 2005. **11**(7): p. 2662-9.
56. Hannon, G.J., *RNA interference.* Nature, 2002 **418**: p. 244-251.
57. Elbashir, S.M., et al., *Duplexes of 21-nucleotide RNAs mediate RNA interference in cultured mammalian*
cells. Nature, 2001. **411**: p. 494-498.
58. Brummelkamp, T.R., R. Bernards, and R. Agami, *A system for stable expression of short interfering RNAs in mammalian cells.* Science, 2002. **296**: p. 550-553.
59. Elbashir, S.M., et al., *Analysis of gene function in somatic mammalian cells using small interfering RNAs.* Methods, 2002. **26**: p. 199-213.
60. Paddison, P.J., et al., *Short hairpin RNAs (shRNAs) induce sequence-specific silencing in mammalian cells.* Genes Dev, 2002. **16**: p. 948-958.
61. Toudjarska, I., et al., *Development of ALN-VSP: an RNAi Therapeutic for Liver Malignancies.* 2009.
62. Aleku, M., et al., *Atu027, a liposomal small interfering RNA formulation targeting protein kinase N3, inhibits cancer progression.* Cancer Res, 2008. **68**(23): p. 9788-98.
63. Halder, J., et al., *Focal adhesion kinase targeting using in vivo short interfering RNA delivery in neutral liposomes for ovarian carcinoma therapy.* Clin Cancer Res, 2006. **12**(16): p. 4916-24.
64. Staege, M.S., et al., *DNA microarrays reveal relationship of Ewing family tumors to both endothelial and fetal neural crest-derived cells and define novel targets.* Cancer Res, 2004. **64**(22): p. 8213-21.
65. Osterhoff, C., R. Ivell, and C. Kirchhoff, *Cloning of a human epididymis-specific mRNA, HE6, encoding a novel member of the seven transmembrane-domain receptor superfamily.* DNA Cell Biol, 1997. **16**(4): p. 379-89.
66. Tomeczkowski, J., et al., *Absence of G-CSF receptors and absent response to G-CSF in childhood Burkitt's lymphoma and B-ALL cells.* Br J Haematol, 1995. **89**(4): p. 771-9.
67. Giard, D.J., et al., *In vitro cultivation of human tumors: establishment of cell lines derived from a series of solid tumors.* J Natl Cancer Inst, 1973. **51**(5): p. 1417-23.
68. Goldman, J.P., et al., *Enhanced human cell engraftment in mice deficient in RAG2 and the common cytokine receptor gamma chain.* Br J Haematol, 1998. **103**(2): p. 335-42.
69. Chambers, A.F., A.C. Groom, and I.C. MacDonald, *Dissemination and growth of cancer cells in metastatic sites.* Nat Rev Cancer, 2002. **2**(8): p. 563-72.
70. Fidler, I.J., *The relationship of embolic homogeneity, number, size and viability to the incidence of experimental metastasis.* Eur J Cancer, 1973. **9**(3): p. 223-7.
71. Karrer, H.E., *The ultrastructure of mouse lung fine structure of the capillary endothelium.* Exp Cell Res, 1956. **11**(3): p. 542-7.
72. Hiraki, Y., et al., *Molecular cloning of a new class of cartilage-specific matrix, chondromodulin-I, which stimulates growth of cultured chondrocytes.* Biochem Biophys Res Commun, 1991. **175**(3): p. 971-7.

73. Hiraki, Y., et al., *Identification of chondromodulin I as a novel endothelial cell growth inhibitor. Purification and its localization in the avascular zone of epiphyseal cartilage.* J Biol Chem, 1997. **272**(51): p. 32419-26.
74. Inoue, H., et al., *Identification of an autocrine chondrocyte colony-stimulating factor: chondromodulin-I stimulates the colony formation of growth plate chondrocytes in agarose culture.* Biochem Biophys Res Commun, 1997. **241**(2): p. 395-400.
75. Hayami, T., et al., *Specific loss of chondromodulin-I gene expression in chondrosarcoma and the suppression of tumor angiogenesis and growth by its recombinant protein in vivo.* FEBS Lett, 1999. **458**(3): p. 436-40.
76. Davies, B., et al., *Targeted deletion of the epididymal receptor HE6 results in fluid dysregulation and male infertility.* Mol Cell Biol, 2004. **24**(19): p. 8642-8.
77. Richter, G.H., et al., *EZH2 is a mediator of EWS/FLI1 driven tumor growth and metastasis blocking endothelial and neuro-ectodermal differentiation.* Proc Natl Acad Sci U S A, 2009. **106**(13): p. 5324-9.
78. Braet, F. and E. Wisse, *Structural and functional aspects of liver sinusoidal endothelial cell fenestrae: a review.* Comp Hepatol, 2002. **1**(1): p. 1.
79. Adini, A., et al., *Placental growth factor is a survival factor for tumor endothelial cells and macrophages.* Cancer Res, 2002. **62**(10): p. 2749-52.
80. Odorisio, T., et al., *Mice overexpressing placenta growth factor exhibit increased vascularization and vessel permeability.* J Cell Sci, 2002. **115**(Pt 12): p. 2559-67.
81. Luttun, A., M. Tjwa, and P. Carmeliet, *Placental growth factor (PlGF) and its receptor Flt-1 (VEGFR-1): novel therapeutic targets for angiogenic disorders.* Ann N Y Acad Sci, 2002. **979**: p. 80-93.
82. Fischer, C., et al., *Anti-PlGF inhibits growth of VEGF(R)-inhibitor-resistant tumors without affecting healthy vessels.* Cell, 2007. **131**(3): p. 463-75.
83. Frederick, L.A., et al., *Matrix metalloproteinase-10 is a critical effector of protein kinase Ciota-Par6alpha-mediated lung cancer.* Oncogene, 2008. **27**(35): p. 4841-53.
84. Van Themsche, C., et al., *Stromelysin-2 (matrix metalloproteinase 10) is inducible in lymphoma cells and accelerates the growth of lymphoid tumors in vivo.* J Immunol, 2004. **173**(6): p. 3605-11.
85. Wang, M., et al., *Inhibition of tumor growth and metastasis of human breast cancer cells transfected with tissue inhibitor of metalloproteinase 4.* Oncogene, 1997. **14**(23): p. 2767-74.
86. Gupta, G.P., et al., *Mediators of vascular remodelling co-opted for sequential steps in lung metastasis.* Nature, 2007. **446**(7137): p. 765-70.
87. Fuchs, B., C.Y. Inwards, and R. Janknecht, *Upregulation of the matrix metalloproteinase-1 gene by the Ewing's sarcoma associated EWS-ER81 and EWS-Fli-1 oncoproteins, c-Jun and p300.* FEBS Lett, 2003. **553**(1-2): p. 104-8.
88. Hiraki, Y., et al., *Molecular cloning of human chondromodulin-I, a cartilage-derived growth modulating factor, and its expression in Chinese hamster ovary cells.* Eur J Biochem, 1999. **260**(3): p. 869-78.
89. Aoyama, T., et al., *Methylation in the core-promoter region of the chondromodulin-I gene determines the cell-specific expression by regulating the binding of transcriptional activator Sp3.* J Biol Chem, 2004. **279**(27): p. 28789-97.

90. Aoyama, T., et al., *Expression of the chondromodulin-I gene in chondrosarcomas.* Cancer Lett, 2004. **204**(1): p. 61-8.
91. Shukunami, C. and Y. Hiraki, *Chondromodulin-I and tenomodulin: the negative control of angiogenesis in connective tissue.* Curr Pharm Des, 2007. **13**(20): p. 2101-12.
92. Kitahara, H., et al., *Chondromodulin-I expression in rat articular cartilage.* Arch Histol Cytol, 2003. **66**(3): p. 221-8.
93. Setoguchi, K., et al., *Suppression of T Cell Responses by Chondromodulin I, a Cartilage-Derived Angiogenesis Inhibitory Factor.* Arthritis & Rheumatism, 2004. **50**(3): p. 828-839.
94. Sanchez-Pulido, L., D. Devos, and A. Valencia, *BRICHOS: a conserved domain in proteins associated with dementia, respiratory distress and cancer.* Trends Biochem Sci, 2002. **27**(7): p. 329-32.
95. Hedlund, J., J. Johansson, and B. Persson, *BRICHOS - a superfamily of multidomain proteins with diverse functions.* BMC Res Notes, 2009. **2**: p. 180.
96. Boeuf, S., et al., *Enhanced ITM2A expression inhibits chondrogenic differentiation of mesenchymal stem cells.* Differentiation, 2009. **78**(2-3): p. 108-15.
97. Dorfman, H.D. and B. Czerniak, *Bone Tumors.* Cancer, 1995. **75**: p. 203-210.
98. Aoyama, T., et al., *Methylation in the Core-promoter Region of the Chondromodulin-I Gene Determines the Cell-specific Expression by Regulating the Binding of Transcriptional Activator Sp3*.* Journal of Biological Chemistry, 2004. **279**(27): p. 28789-28797.
99. Maes, C., et al., *Placental growth factor mediates mesenchymal cell development, cartilage turnover, and bone remodeling during fracture repair.* J Clin Invest, 2006. **116**(5): p. 1230-42.
100. Carmeliet, P., et al., *Synergism between vascular endothelial growth factor and placental growth factor contributes to angiogenesis and plasma extravasation in pathological conditions.* Nat Med, 2001. **7**(5): p. 575-83.
101. Murdoch, C., A. Giannoudis, and C.E. Lewis, *Mechanisms regulating the recruitment of macrophages into hypoxic areas of tumors and other ischemic tissues.* Blood, 2004. **104**(8): p. 2224-34.
102. Chen, K., et al., *Toll-like receptors in inflammation, infection and cancer.* Int Immunopharmacol, 2007. **7**(10): p. 1271-85.
103. McCawley, L.J. and L.M. Matrisian, *Matrix metalloproteinases: they're not just for matrix anymore!* Curr Opin Cell Biol, 2001. **13**(5): p. 534-40.
104. Nagase, H., A.J. Barrett, and J.F. Woessner, Jr., *Nomenclature and glossary of the matrix metalloproteinases.* Matrix Suppl, 1992. **1**: p. 421-4.
105. Blackburn, J.S., et al., *A matrix metalloproteinase-1/protease activated receptor-1 signaling axis promotes melanoma invasion and metastasis.* Oncogene, 2009. **28**(48): p. 4237-48.
106. Blackburn, J.S., et al., *RNA interference inhibition of matrix metalloproteinase-1 prevents melanoma metastasis by reducing tumor collagenase activity and angiogenesis.* Cancer Res, 2007. **67**(22): p. 10849-58.
107. Westermarck, J., et al., *p38 mitogen-activated protein kinase-dependent activation of protein phosphatases 1 and 2A inhibits MEK1 and MEK2 activity and collagenase 1 (MMP-1) gene expression.* Mol Cell Biol, 2001. **21**(7): p. 2373-83.

108. Stevanovic, S., *Identification of tumour-associated T-cell epitopes for vaccine development.* Nat Rev Cancer, 2002. **2**: p. 514-520.
109. Smith, B., et al., *Detection of melanoma cells in peripheral blood by means of reverse transcriptase and polymerase chain reaction.* Lancet, 1991. **338**(8777): p. 1227-9.
110. Schleiermacher, S., et al., *Increased Risk of Systemic Relapses Associated With Bone Marrow Micrometastasis and Circulating Tumor Cells in Localized Ewing Tumor.* J Clin Oncol, 2003. **21**: p. 85-91.
111. Hu-Lieskovan, S., et al., *Sequence-specific knockdown of EWS-FLI1 by targeted, nonviral delivery of small interfering RNA inhibits tumor growth in a murine model of metastatic Ewing's sarcoma.* Cancer Res, 2005. **65**(19): p. 8984-92.

10 Appendices

10.1 List of Figures

10.2 List of Tables

10.3 List of Abbreviations

aa	Amino acids
BCP	Bromochloropropane
bFGF	Basic fibroblast growth factor
BSA	Bovine serum albumin
cALL	common acute lymphoblasic leukemia
CEP	Circulating endothelial progenitors
CTA	Cancer/Testis Antigen
DEPC	Diethylpyrocarbonate
DMSO	Dimetylsulfoxide
DNA	Desoxyribonucleic acid
dNTP	Deoxyribonucleotide triphosphate
DSMZ	Deutsche Sammlung für Mikroorganismen und Zellkulturen
EDTA	ethane-1,2-diyldinitrilo tetraacetic acid
EFS	Event free survival
EFT	Ewing Family of Tumors
EphA2	Ephrin receptor A2
EWS	Ewing's Sarcoma oncogene
FAM	6-carboxy-fluorescein
FLI1	Friend leukemia integration
FBS	Fetal bovine serum
FCS	Fetal calf serum
GAPDH	Glyceraldehyde 3-phosphate dehydrogenase
HBSS	Hank's buffered salt solution
HIF-1α	Hypoxia inducible factor 1 α
HRP	Horse raddish peroxidase
i.v.	intravenously
kb	Kilo bases
MPNT	Malignant peripheral neuroectodermal tumor
MR	Magnetic resonance
mRNA	Messenger RNA
MSC	Mesenchymal stem cell

MVD	Microvessel density
NTC	Non template control
PAS	Periodic acid schiff
PBS	phosphate buffered saline
PCR	Polymerase chain reaction
RNA	Ribonucleic acid
RT	Room temperature
s.c.	subcutaneously
siRNA	Short interfering RNA
TEMED	N,N,N′,N′-Tetramethylethan-1,2-diamin
TFPI	Tissue pathway inhibitor
VEGF	Vascular endothelial growth factor
VE-cadherin	Vascular endothelial cadherin